EVALUATING AND PREDICTING THE RESPIRATORY HAZARD OF PARTICLES USED IN LI-ION BATTERIES FOR A SAFE AND SUSTAINABLE DEVELOPMENT

Violaine Sironval

President
Pr. Charles PILETTE
Université catholique de Louvain, Institut de Recherche Expérimentale et Clinique (IREC), Pôle de Pneumologie, ORL et Dermatologie (PNEU), Brussels.

Promoter
Pr. Dominique LISON
Université catholique de Louvain, Institut de Recherche Expérimentale et Clinique (IREC), Louvain Centre for Toxicology and Applied Pharmacology (LTAP), Brussels.

Co-promoter
Dr. Sybille VAN DEN BRULE
Université catholique de Louvain, Institut de Recherche Expérimentale et Clinique (IREC), Louvain Centre for Toxicology and Applied Pharmacology (LTAP), Brussels.

External jury members
Pr. Benoît NEMERY DE BELLEVAUX
Katholieke Universiteit Leuven, Unit of Environment and Health, Department of Public Health and Primary Care, Laboratory of Toxicology, Leuven.

Pr. Roel SCHINS
Leibniz Research Institute for Environmental Medicine, Düsseldorf, Germany.

Dr. Steven VERBERCKMOES
Umicore, Brussels.

Internal jury member
Pr. François HUAUX
Université catholique de Louvain, Institut de Recherche Expérimentale et Clinique (IREC), Louvain Centre for Toxicology and Applied Pharmacology (LTAP), Brussels.

Une page ne sera certainement pas suffisante pour contenir les remerciements que je voudrais adresser à toutes les personnes m'ayant accompagnée et épaulée durant ce doctorat.

Avant tout, je voudrais remercier mon mentor, la Dr Sybille van den Brule, qui a toujours cru en moi. Ses conseils au quotidien, son esprit critique, son perfectionnisme et son soutien ont largement contribué au succès de cette thèse. Bien plus qu'un mentor, Sybille est aussi une personne qui m'est chère et avec qui passer du temps et discuter a été, et restera, un réel plaisir.

Ensuite, je voudrais remercier le Pr Dominique Lison, mon promoteur, pour ses conseils avisés et sa sagesse. Avoir un promoteur me permettant et m'encourageant à dépasser mes limites, que ce soit dans mes recherches ou dans mes présentations à l'étranger, a été un réel atout. Je voudrais également le remercier pour sa compagnie attentionnée et teintée d'humour.

Mes collègues, qu'elles soient techniciennes ou doctorantes méritent aussi largement d'être remerciées. Francine, alias « ma petite maman du labo », Nadtha, ma partenaire d'organisation d'after-works, Saloua, ma collègue directe de projet, Audrey, ma copine de toujours, Micaela et Eleonora mes deux acolytes de doctorat, ont toutes contribué, par l'entremise d'un sourire, de conversations animées ou de fous rires à ce que cette thèse s'accomplisse dans la bonne humeur, la gaieté et la légèreté.

Je tiens aussi à chaleureusement remercier les membres de mon comité d'accompagnement de thèse, le Pr François Huaux, le Pr Charles Pilette et le Pr Benoît Nemery qui m'ont guidée et challengée durant chacune de ces quatre années de doctorat. Je remercie également les membres externes de mon jury, le Pr Roel Schins et le Dr Steven Verberckmoes pour leurs questions et suggestions qui ont permis de parfaire ce travail.

Ce travail n'aurait pas été possible sans le soutien du Fonds de la Recherche Scientifique (FNRS), qui m'a permise, grâce à l'attribution d'une bourse Fonds pour la Formation à la Recherche dans l'Industrie et dans l'Agriculture (FRIA) de me consacrer pleinement à mes recherches.

Plus que tout, je voudrais exprimer ma gratitude à mes proches. Tout d'abord, merci à mon papa, ma maman et ma sœur, Anaïs, de m'avoir toujours poussée à aller au bout de mes rêves, d'avoir cru en moi et de m'avoir entourée de tant d'encouragements et d'attentions durant la réalisation de cette thèse. Ils ont rendu tous les obstacles franchissables, et les moments de doute en force. Ensuite, je voudrais remercier une personne ayant une place très spéciale dans mon cœur, Loup, mon compagnon de (et pour) toujours. Merci à lui d'avoir été fier de moi à chaque étape de mon doctorat, me donnant envie d'aller plus loin et de toujours faire mieux.

Enfin, je consacre ces dernières lignes pour remercier toutes les autres personnes qui ont contribué, de près ou de loin à la réalisation de cette thèse, qui ont rendu mon quotidien de doctorante agréable, ou qui me sont simplement chères, notamment Cristina Pavan, Riccardo Leinardi, Marie Dallemagne, Inès Gaussin, Sophie Vandercam, Elisabeth Casagrande et ma belle-famille.

De tout cœur, merci.

LIST OF ABBREVIATIONS

µ-XRF, x-ray micro fluorescence
8-OHdG, 8-hydroxy-2'-deoxyguanosine
ABA, abscisic acid
ACGIH, American Conference of Governmental Industrial Hygienists
ANOVA, analysis of variance
AO, adverse outcome
AOP, adverse outcome pathway
AP-1, activator protein-1
AT-II, alveolar type II epithelial cells
BAL, broncho-alveolar lavage
BALF, BAL fluid
BBB, blood brain barrier
CBP, cAMP-response element-binding protein
CBPI, cytokinesis-block proliferation index
CH1, Zn^{2+}-binding cysteine/histidine rich 1
CLS, centrifugal liquid sedimentation
CNS, central nervous system
CNT, carbon nanotubes
COPD, chronic obstructive pulmonary disease
CTGF, connective tissue growth factor
Cul2, cullin 2
d_{50}, mass median geometric particle diameter
DEP, diesel exhaust particles
DMPO, 5,5-dimethyl-l-pyrroline-N-oxide
DMSO, dimethylsulfoxide
DMT, divalent metal transporter
ECM, extracellular matrix
EDX, energy-dispersive X-ray spectroscopy
ELISA, enzyme-linked immunosorbent assay

EMT, epithelial-mesenchymal transition
EPO, erythropoietin
EPR, electron paramagnetic resonance
FB, ferruginous bodies
FIH-1, factor inhibiting HIF-1
FPF, fine particle fraction
FPG, *E. Coli* formamidopyrimidine-DNA glycosylase
HE, hematoxylin and eosin
HIF, hypoxia-inducible factor
HMGB1, high mobility group box 1
HO, heme oxygenase
hOGG1, human 8- oxoguanine DNA glycosylase 1
HRE, hypoxia responsive elements
IARC, International Agency for Research on Cancer
ICP-MS, inductively coupled plasma mass spectrometry
IKK, IκB kinase
IL, interleukin
iNOS, inducible NO synthase
KE, key event
KER, KE relationship
LCO, $LiCoO_2$
LDH, lactate dehydrogenase
LFP, $LiFePO_4$
LIB, lithium-ion battery
LMO, $LiMn_2O_4$
LOD, limit of detection
LPS, lipopolysaccharide
LRR, C-terminal leucine-rich repeat
LTO, $Li_4Ti_5O_{12}$
MIE, molecular initiating event
MMADe, experimental mass median aerodynamic diameter
MN, micronucleus
NADP, nicotinamide adenine dinucleotide phosphate

NCA, $LiNiCoAlO_2$
NF-κB, nuclear factor kappa B
NMC, $LiNiMnCoO_2$
NOAEL, no adverse effect level
NRAMP 2, natural resistance-associated macrophage protein 2
Nrf2, nuclear factor erythroid-2-related factor 2
OECD, Organization for Economic Cooperation and Development
p300, histone acetyltransferase p300
PAH, polycyclic aromatic hydrocarbon
PAI-1, plasminogen activator inhibitor-1
PBS, phosphate buffered saline
PHD, prolyl hydroxylase domain
PM, particulate matters
PRR, pattern recognition receptor
pVHL, von Hippel-Lindau tumor suppressor protein
PX-478, S-2-amino-3-[4'-N,N,-bis(2-chloroethyl)amino]phenyl propionic acid N-oxide dihydrochloride
PYD, N-terminal pyrin domain
Rbx1, ring box protein 1
REACH, Registration, Evaluation, Authorization and Restriction of Chemicals
RLE, rat lung epithelial cells
RNS, reactive nitrogen species
ROS, reactive oxygen species
SDH, succinate dehydrogenase
SEM, scanning electron microscopy
SEM, standard error on the mean
Sil, silica
SN, supernatant
SSAT2, spermidine/spermine N-acetyltransferase-2
TA, terephthalate
TfR, transferrin receptor
TGF, transforming growth factor
Th, T helper

TIMP; tissue inhibitor of metalloproteinases
TLR, Toll-like receptor
TLV, threshold-limit value
TNF, tumor necrosis factor
ToF-SIMS, time-of-flight secondary ion mass spectrometry
TWA, time weighted average
UQ, ubiquitin
VEGF, vascular endothelial growth factor
WC-Co, tungsten carbide cobalt (cemented carbide)
WST, water soluble tetrazolium salt
WT, wild-type

TABLE OF CONTENT

ABSTRACT

Li-ion batteries (LIB) are invading the market and their production and use dramatically increase. LIB are made of relatively insoluble particles, respirable in size and containing toxicologically relevant metal ions such as cobalt or nickel. Workers, and possibly the general population, can be exposed to these particles via inhalation. Information about their respiratory toxicity is, however, very limited. Here, we identified the respiratory toxicity of particles used in LIB in a mouse bioassay, and conclude that they represent a differential respiratory hazard (lung inflammation and fibrosis). Given that a large range of LIB particles with different composition, metal content and synthesis processes are developed by the industry, we investigated the mechanisms of toxicity of these LIB particles. We identified Co and Ni content/bioaccessibility and *in vitro/in vivo* hypoxia-inducible factor-1 α as determinants and key mediator, respectively, of the inflammatory lung responses induced by LIB particles. These parameters can be monitored *in vitro* in cell culture to predict the lung inflammatory potential of LIB particles and possibly categorize them. Additionally, we showed that one of the most inflammatory particles, $LiCoO_2$, exerts genotoxic and mutagenic activities *in vitro* and *in vivo* with, at least, a primary mechanism and in association with the production of reactive oxygen species. This work provides, for LIB particles, the first toxicological information, and contributes to support stakeholders from academia and industry, in their efforts for a safer and sustainable development of LIB.

INTRODUCTION

1.1 Li-ION BATTERIES: BASICS AND APPLICATIONS

The major sources of energy are currently fossil fuel and nuclear power but both are associated with important concerns: fossil fuel is finite and nuclear energy sources and wastes are radioactive [1]. Global warming and pollution, in conjunction with these concerns about energy production make citizens and authorities around the world more sensitive to the importance of developing green energy technologies (photovoltaic and photoelectrochemical cells, wind turbines, etc.). Renewable energy sources thus represent unavoidable alternatives but require energy storage devices. There is, therefore, a need to develop storage technologies [1-3], and batteries represent the key solution.

Two types of batteries exist. Primary batteries (zinc-carbon, alkaline batteries, etc.) are disposable, simple to use but they cannot be recharged. Secondary batteries (lead-acid, nickel-cadmium, nickel-zinc, lithium batteries, etc.) can be recharged and reused, and have higher power density[1] and discharge rate [1]. Lithium batteries represent the best promising systems thanks to the high reducing capacity of Li, its small atomic radius that allows a high diffusion coefficient, high theoretical specific capacity and high electropositivity combined with a high power energy density [3-5]. In the first generation of Li batteries (Li-metal batteries), the anode was composed of metallic Li. However, this type of battery presented an explosion hazard. This problem was solved by replacing the anode by a Li ion intercalation material forming Li-ion batteries [6, 7].

Li-ion batteries (LIB) are composed of electrochemical cells interconnected together. Each cell contains a negative reductant electrode (anode), a positive oxidant electrode (cathode), an electrolyte, a separator and current collectors around the electrodes [1, 8] (**Figure 1**). Electrodes are active porous materials where electrochemical reactions occur [8]. During the charge and the discharge of the battery, reversible atom intercalations occur in the electrodes. During the

[1] The power density is the power that can be derived per unit mass of the cell (W/kg).

charge, the cathode releases Li ions in the electrolyte and an external field forces the transfer of electrons to the anode. The separator is a microporous membrane allowing the electronic segregation between the two electrodes and the transport of Li-ion between them [1, 9]. Li ions, with their compensatory charge, are attracted by the anode. During the discharge, the reverse reaction occurs. An electron flow results in the external circuit [1, 10].

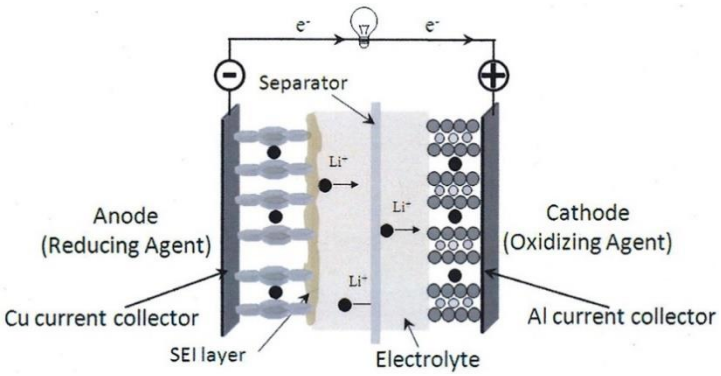

Figure 1: **Representation of a C/$LiCoO_2$ cell during the discharge of the battery.** The anode is in graphitic carbon and the cathode is composed of $LiCoO_2$. SEI: solid electrolyte interphase. Reproduced from Goodenough J.B., 2013 [10].

LIB generally use graphite at the anode side and lithium metal oxide particles such as $LiFePO_4$ (LFP), $LiCoO_2$ (LCO), $LiMn_2O_4$ (LMO), $Li_4Ti_5O_{12}$ (LTO), $LiNiCoAlO_2$ (NCA) or $LiNiMnCoO_2$ (NMC) at the cathode side [11]. LCO was the first particle successfully commercialized in LIB with a layered structure allowing Li insertion between CoO_2 planes [12, 13]. The composition of the electrode material determines electrode voltage and capacity[2]. On the other hand, the microstructure of the material strongly influences the performance, the rate capability (long-term performance level) of the battery, the contact surface area between the particles and the electrolyte and the energy density of the battery [14]. The size of the particles used

[2] The theoretical capacity of a battery is the quantity of electricity involved in the electrochemical reaction (Ah/g).

in LIB is, therefore, an important parameter. Currently, micro-sized electrode materials are used in commercialized batteries but nano-sized materials can also be used and are under strong development to improve rate performance and electronic transport in LIB [1].

The first LIB was commercialized by the Sony Company in 1991 and rapidly invaded the market of portable electronics [3, 8]. Since then, research interest exploded in this field [3]. Indeed, thanks to their high efficiency, LIB are useful for various electric applications (green energy storage), and for electric vehicles [5, 8]. Conventional LIB have a fixed shape and size, which limits their applications [15]. New generation of LIB should be flexible, lightweight, thin and customizable [16]. Efforts are made in the development of such batteries and new types of batteries are emerging, such as printable solid-state, 3D printed, sprayed or multi-step spray painted batteries [15-22]. These flexible multi-layered LIB could be easily integrated into an object or on a surface (**Figure 2**), for example directly connected with the harvesting energy device structure [17].

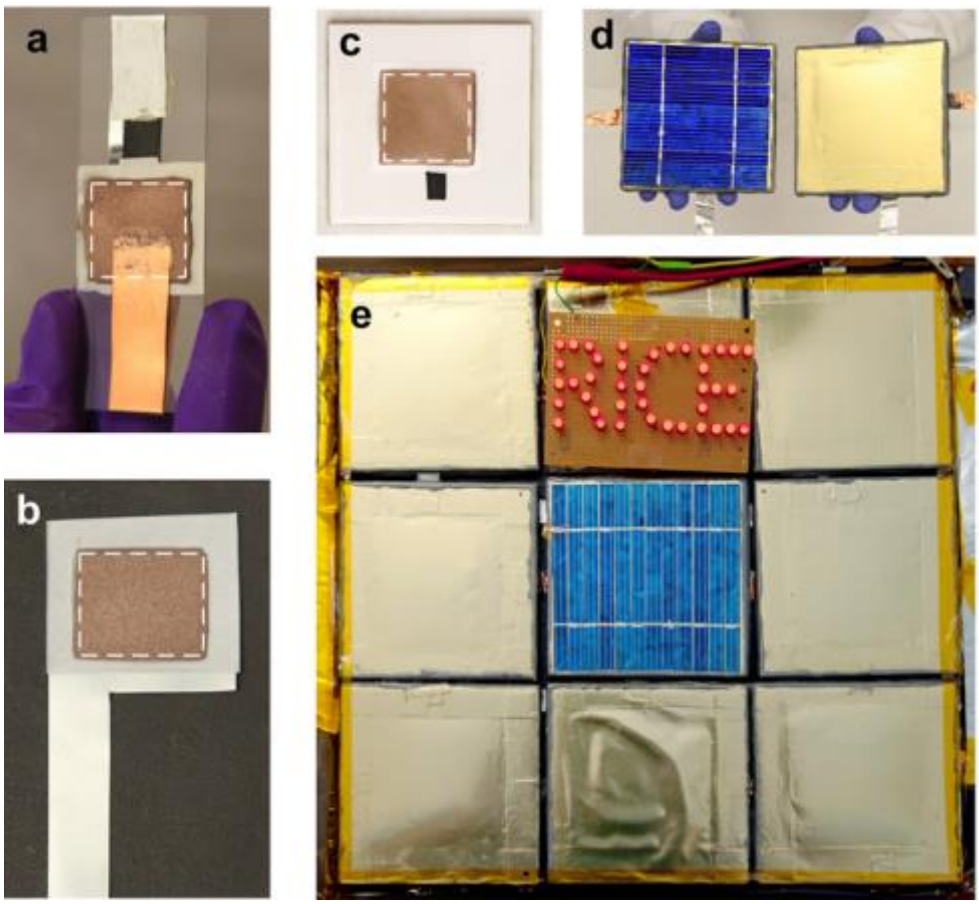

Figure 2: **Sprayed/painted batteries on different surfaces.** Li-ion cells on **(a)** glass slide; **(b)** stainless steel sheet; **(c)** glazed ceramic tile. **(d)** (Left) A packaged and charged tile cell and (right) a similar tile cell charged with a photovoltaic panel mounted on the tile. **(e)** Fully charged battery of 9 parallely connected powering 40 red LEDs spelling 'RICE'. Original figure in Singh et al. 2012 [17].

The *Service Public de Wallonie* financed the BATWAL project (2013-2020, [23]) that developed this type of multi-layered LIB with the objective to spray/paint each part of the battery (cathode, electrolyte and anode) on flexible surfaces. This innovative approach could easily be integrated for the local storage of energy in public and private applications. This interdisciplinary project also aimed to develop sustainable and safe batteries and thus integrated toxicity studies of LIB components in the

project. In this context, the Louvain centre for Toxicology and Applied Pharmacology (LTAP) was responsible of the evaluation of the toxicity of LIB particles via inhalation. This exposure route was considered because of the likely presence of LIB particles in the ambient air during production and manipulation.

1.2 Li-ION BATTERY HAZARDS

1.2.1 Environmental hazards

Lithium used in LIB is mostly extracted from continental brines in desert areas [24]. The mining practices have an impact on the environment as the extraction of lithium consumes a large amount of water (water is evaporated to recover lithium) and produces a lot of wastes (all salts other than lithium) [24].

Once produced, LIB generate less waste than primary batteries due to their longer life. LIB contain, however, metals that could be harmful for the environment if improperly disposed [25]. The high rate of use and disposal of consumer portable electronics suggests such an impact on the environment [26]. The Directive 2006/66/EC on batteries, accumulators and waste batteries and accumulators targets a minimal recycling of 50 % of LIB mass [27]. With the recycling process, nickel, cobalt, copper and iron are recovered but aluminum, lithium and manganese are not [27].

Researchers have investigated the impact of LIB components on the environment. LCO and NMC nanoparticles used in LIB were tested on different environmental models. In *Daphnia Magna* (a critical planktonic crustacean of freshwater) a dose-dependent reduction of survival and reproduction was recorded due to NMC and LCO accumulation in the digestive tract and adhesion on carapace [28]. In *Shewanella oneidensis* (a soil and sediment bacterium) growth and respiration were also affected by NMC nanoparticles due to Ni and Co dissolution [29]. Another work using a model of biological membranes (synthetic lipid bilayer membranes) concluded that NMC did not affect compositional symmetry of the membrane but LCO did [30].

These findings show the possible impact of LIB particles on the environment and the importance to steer a sustainable development and use of LIB.

1.2.2 Human health hazards

Fires or explosions have been observed with devices equipped with LIB, such as the Samsung Note 7, a NASA robot, a Boeing airplane or a Chevrolet car [31]. Short circuit, overcharging, external heating or many other reasons can cause irreversible thermal events in LIB, leading to fire or explosion and release of LIB components [31]. In case of accidental exposure, the heat itself, produced by the fire, represents an issue but gas emissions and smoke are also hazardous [31]. The electrolytes of LIB contain flammable and volatile substances and are generally composed of organic carbonates and Li-salts containing fluorine which can generate hydrogen fluoride, a very toxic gas [31, 32].

Non-accidental scenarios can also cause exposure to LIB components. Indeed, inhalation of LIB materials can occur during production or recycling [26, 33, 34]. Organic carbonates used in electrolytes, such as dimethyl carbonate, ethyl methyl carbonate, diethyl carbonate and propylene carbonate, can induce neurotoxicity [32]. LIB electrodes contain particles. These materials are also a source of concern because they are micro- or nanometric in size and poorly soluble, suggesting that they might be respirable and biopersistent in the human respiratory tract. During the course of this PhD work, the inhalation hazard of LCO micro- and nanoparticles was investigated *in vitro* by another team using an air-liquid interface model co-culturing human alveolar epithelial cells (A549), human monocyte-derived macrophages (MDM) and monocyte-derived dendritic cells (MDDC) [33]. Twenty-four h after exposure to 238, 1428 or 2619 µg/cm^2 by using a dry powder insufflator, low cytotoxicity was observed while pro-inflammatory markers (tumor necrosis factor (TNF) -α and interleukin (IL) -8) were dose-dependently increased by LCO microparticles but not by nanoparticles. This study was the first published on the possible lung toxicity of particles used in LIB. No other study has been carried out since then. There are no data on the levels of airborne exposure to LIB components in the workplace. However, Yokota et al. have measured the total dust concentration of cobalt and nickel in the air of a battery plant using microparticles containing 97.2 % of nickel hydroxide and 2.8 % of cobalt hydroxide, and calculated a time weighted average (TWA) of 0.481 mg/m^3 (mean) for nickel and of 0.067 mg/m^3 (mean) for cobalt in air [34]. In comparison, the threshold-limit values (TLV)-

TWA recommended by the American Conference of Governmental Industrial Hygienists (ACGIH) for inhalable Ni or Co compounds are lower: 1.5 mg Ni/m^3 for metallic Ni, 0.1 mg Ni/m^3 for soluble inorganic Ni compounds and 0.2 mg Ni/m^3 for insoluble inorganic Ni compounds and 0.02 mg Co/m^3 for Co compounds.

The new applications of sprayed or paintable batteries increase the potential for exposure to LIB particles via inhalation. In view of their physico-chemical properties, their content in potentially toxic metals (see section 2.4) and the large variety of existing and future LIB materials, the increasing production, use and disposal of LIB, it appears essential to better identify their health hazards and to generate information about their mechanisms of toxicity. During this PhD thesis, we focused on the pulmonary toxicity of LIB particles, as inhalation appears the most worrying route of exposure to these components.

1.3 TOXICITY OF INHALED PARTICLES

Humans are daily exposed to inhaled particles via the environment or via their work. The health risks of particles are a function of exposure and hazard (toxicity). Effects of particles on health can differ if exposure is acute or chronic, continuous or intermittent [35, 36]. Toxicologists use different methods (*in silico*, *in vitro*, *in vivo*, epidemiological studies, …) to evaluate the hazard of inhaled particles. Guidance values can be proposed as limits of particle concentrations in workplace or ambient air. To prevent worker exposure to hazardous particles, controls and safety measures are implemented including substitution for a less hazardous particle, containment of the production process, isolation of the worker, ventilation of the workplace, safe work practices and individual protections as last resort [37, 38]. Particle air levels can be measured via personal exposure monitoring with pumped sampling or via indirect measurement of the particle air concentrations at various locations and time spent by workers in each specific environment [38]. TLV for respirable particles are available; e.g the TLV recommended for respirable crystalline silica particles is 0.05 mg/m^3 [39].

Given the micrometric size of LIB particles, the exposure scenarios associated to the manufacture or use of these particles (see section 2.2.2) which suggest inhalation exposure, combined with their content in toxicologically relevant elements (Co, Ni, Al, etc.) (see section 2.4), we suspected that they can induce lung toxicity. We review here below the main knowledge about the toxicity of inhaled particles in general.

As developed later in this section, lung responses to inhaled particles depend on particle exposure/dosimetry and other parameters such as the composition and the physico-chemical properties of the particles (**Figure 3**). Other organs than the lungs can also be affected.

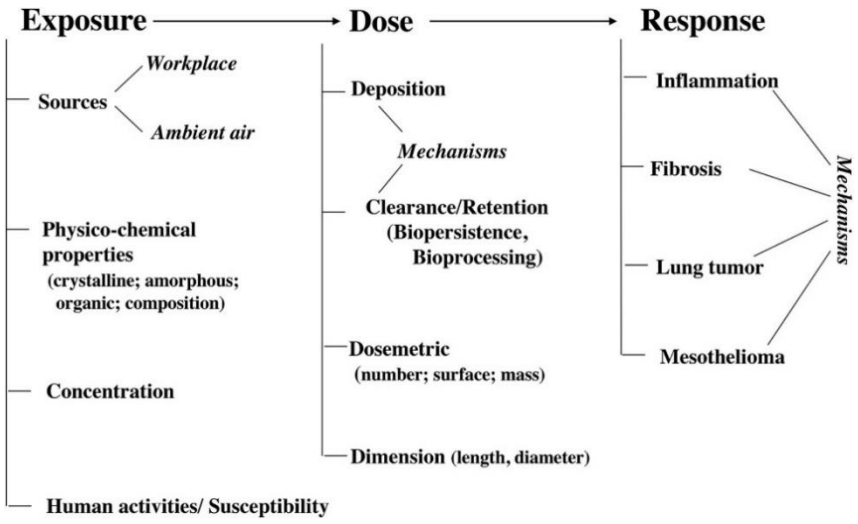

Figure 3: Parameters influencing the lung responses to inhaled particles. Original figure from Oberdörster and Graham, 2018 [40].

1.3.1 Health hazard of inhaled particles

Different particles can contaminate the air. For example, the general population is daily exposed to ambient particulate matter (PM). This exposure induced 2.94 million deaths in 2017 in the world, caused by respiratory infections, tracheal, bronchus and lung cancer, ischemic heart disease, ischemic stroke, intracerebral hemorrhage, subarachnoid hemorrhage, chronic obstructive pulmonary disease (COPD) and type 2 diabetes mellitus [41]. Other toxic particles or fibres can be present in occupational settings such as crystalline silica or asbestos and have induced 230000 and 60000 deaths respectively in 2017. Asbestos can cause larynx cancer, tracheal, bronchus and lung cancer, ovarian cancer, mesothelioma, asbestosis, and occupational exposure to silica can lead to death by inducing lung cancer or silicosis [41]. There is thus ample evidence justifying the need to manage the impact/risk of inhaled particles on human health.

Pulmonary adverse effects caused by inhaled particles

Lung diseases are among the most important occupational diseases [42]. After particle inhalation, the lung activates several mechanisms of defense such as the epithelial barrier and innate immune cells (macrophages, neutrophils, etc.) leading to the secretion of pro-inflammatory mediators, the production of reactive oxygen species (ROS), bronchial hypersecretion and cellular chemotaxis to remove the particles [43, 44]. The initiation of this inflammatory response represents the first defensive reaction but also triggers structural alterations of the lung parenchyma [44].

Several adverse lung effects have been reported epidemiologically as being associated to exposure to particles such as quartz (crystalline silica), asbestos fibres, coal dust, diesel exhaust particles (DEP) or ultrafine particles in general [45, 46]. One of these adverse effects is **pulmonary fibrosis** which refers to lung disorders characterized by an increased accumulation of extracellular matrix and the progressive destruction of the normal lung architecture, leading to scarring of the lung parenchyma [47, 48]. A progressive decline in lung function and gas exchange leads to morbidity and mortality [47]. The particulate materials leading to pulmonary fibrosis are mainly crystalline silica particles, asbestos fibres and coal dusts.

Several studies have also confirmed that exposure to particles has a significant effect on **asthma and allergic rhinitis** [49]. Asthma represents a global health problem with approximately 300 million people affected worldwide [50]. Upon environmental exposure to ambient PM, existing asthma can be exacerbated through oxidative stress and inflammation [49, 51-54]. In addition, some data show that DEP act as adjuvant for allergic sensitization to common environmental allergens [52]. In contrast, only some evidence show that PM can cause new cases of asthma, but this remains controversial [50, 51]. However, in occupational settings, inhalation of particles can exacerbate existing asthma and cause new cases. These new cases can be subdivided into sensitizer- (allergic) and irritant-(non-allergic) induced occupational asthma [55, 56]. Different particles can lead to occupational asthma such as metal dusts containing Ni, Cr, Mn, Co or V [57, 58]. For

example, workers performing welding of metallic alloys produce fumes containing ultrafine particles of these metals [57].
COPD and infections have also been linked to particulate exposure [45, 46]. For example, occupational exposure to respirable crystalline silica is associated with COPD [59].

Some inhaled particles can also induce cancer. Air pollution in general, and PM as a component of air pollution, can lead to **lung cancer** and have been classified as carcinogenic agents (group 1) by the International Agency for research on Cancer (IARC) in 2016 [60]. Exposure to crystalline silica particles can induce lung cancer and the risk of lung cancer appears the greatest in silicosis patients who smoke [61]. IARC classified crystalline silica as carcinogenic for human (group 1) in 1997 [60]. Asbestos fibres can also cause lung cancer with the greatest risk also associated with cigarette smoking [62]. In addition, exposure to asbestos can lead to pleural or peritoneal **mesothelioma** [63]. Asbestos fibres are classified as carcinogenic for humans (group 1) by the IARC [60]. In addition to epidemiological data, experimental research has also identified some engineered nanomaterials as hazardous, with a potential of carcinogenicity. One of the most famous examples are the engineered carbon nanotubes (CNT), named “asbestos-like” due to their fibre-like structure and their potential capacity to induce mesothelioma and lung cancer [64, 65]. One type of multi-walled CNT (Mitsui-7) is classified as possibly carcinogenic for human (group 2B) by the IARC in 2017 [60].

Other target organs
After inhalation, different mechanisms may contribute to particle clearance. These mechanisms can also lead to the translocation of particles to other organs. Secondary organs can also be affected by mediators from the lung acting systematically [66, 67] (**Figure 4**).

The mucociliary escalator contributes to particle clearance and the particles deposited in the mucus are partially pushed by ciliated epithelial cells to the larynx, where they can be swallowed [68]. The particles can then reach the stomach and the gut [69]. Ingested engineered nanomaterials such as silver, titanium dioxide or silica nanoparticles have been shown to interact with the gastro-intestinal tract or

the microbiota [70, 71]. Recently there are growing evidence that inhaled engineered nanomaterials could also impact on **the gastro-intestinal tract** [70]. Other examples can be cited such as the environmental exposure to PM that increases the incidence of inflammatory bowel diseases (Crohn disease and ulcerative colitis) [69, 72]. Some mechanisms are suggested such as the direct effect on epithelial cells of the digestive tract, activation of systemic inflammation and immunity, or modulation of the intestinal microbiota composition [69, 73]. Association between PM and **type 2 diabetes mellitus** has also been investigated [67]. Contribution of DEP to appendicitis is also explored due to the pro-inflammatory cytokine secretion caused by DEP inhalation [74].

Inhaled particles can also directly or indirectly affect other organs such as the heart [46]. A famous example is the episode of air pollution named “great smog on London”, which occurs in 1952, resulting in a large number of deaths from cardiorespiratory diseases [75]. Evidence now shows that exposure to air pollution, especially airborne PM, is associated with acute and chronic **cardiovascular adverse effects** [46, 76]. In systemic circulation, PM can interact with atheromatous plaques and increase the risk of myocardial infarction or can induce cardiac arrhythmias and strokes [77]. PM also induce oxidative stress participating to the deterioration of the cardiovascular system [76]. Iron oxide, silicon oxide, carbon, silver and zinc oxide nanoparticles have also been associated to cardiovascular adverse effects in experimental studies [78]. Some studies investigate the adverse effects of inhaled CNT on the cardiovascular system but this is not fully elucidated yet [79, 80].

The brain and the central nervous system (CNS) can also be affected upon particle exposure. For example, epidemiological and experimental studies show a positive association between long-term exposure to airborne PM and neurodegeneration, such as dementia, Alzheimer’s disease, Parkinson’s disease and general declines in cognition [67]. Exposure to $PM_{0.1}$ (PM with a diameter less than 100 nm) during neurogenesis could lead to **diseases** such as autism disorders, schizophrenia, deficit disorder or periventricular leukomalacia [82]. Some studies also showed deleterious effects of silica [83], titanium dioxide or silver nanoparticles [84] on the

CNS but further studies are needed to demonstrate a sufficient link between occupational exposure to particles and neurodegeneration.

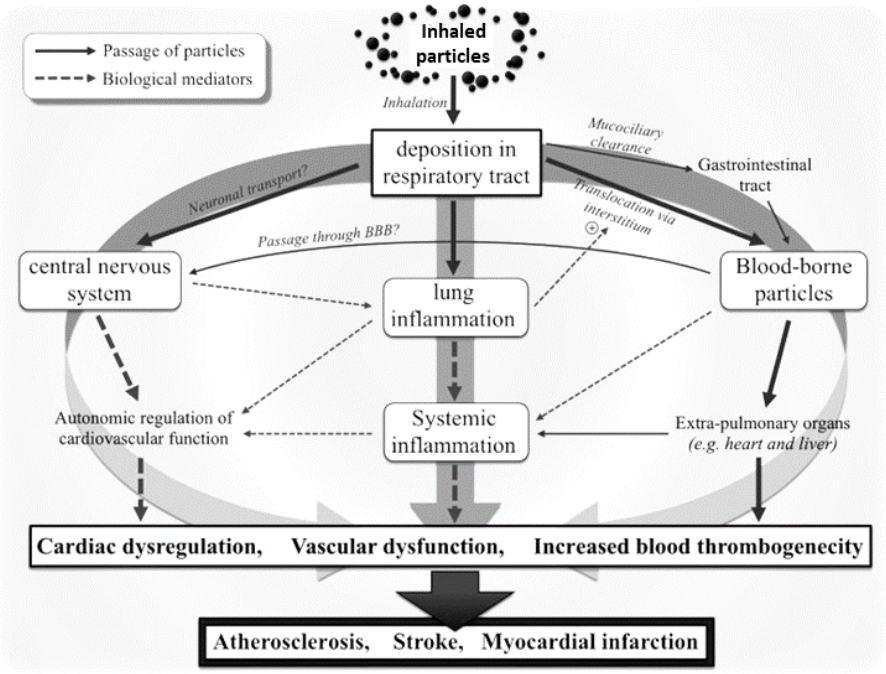

Figure 4: Some of the key mechanisms through which inhaled particles can reach and induce adverse effects on secondary organs. Emphasis is made on the means through which inhaled particles can cause cardiovascular events. Adapted from Stone 2017 [81].

Reproduction can also be affected by particle inhalation. For example, both animal and epidemiological studies support the conclusion that $PM_{2.5}$ (PM with a diameter less than 2.5 µm) can induce qualitative and quantitative alterations of sperm, and induce defects during gametogenesis leading to decrease of reproductive capacities in population [85, 86]. Inhaled $PM_{2.5}$ are also associated to low birth weight [87] and could have an impact on the body development. Some *in vivo* and *in vitro* studies also suggest that TiO_2 nanoparticles could exert **reproductive and developmental toxicity** [88].

Particles can also induce health effects due to the release of their elemental components. For example, metals such as Cd (kidney disorders, chemical

pneumonitis, osteoporosis, itai-itai disease, etc. [89]), Pb (saturnism[90]), Mn or Co (see sections 2.4.2 and 2.4.6) can lead to specific health effects and are present as components of airborne PM [91, 92] or can also be found as inhalable particle in industries.

1.3.2 Determinants of the toxicity of inhaled particles

Upon particle inhalation, pulmonary toxicity depends on the susceptibility of the lungs and on the physico-chemical and functional properties of the particles (**Figure 3**). Other key parameters of toxicity are the dose and duration of exposure [40].

Anatomy, morphology and physiological parameters of the lungs vary within and among individuals. Physiological parameters such as body size, age, sex, growth, ethnic origin, level of physical activity and state of health vary among the population and define the morphology of the lungs. Morphologic characteristics of the lungs influence the pressure, the flow rate, the direction, the humidity as air moves into and out the lungs. These changes determine the rate and sites of penetration and deposition of airborne particles in the lungs. These variations of the respiratory tract influence the susceptibility to airborne particles [93].

The main physico-chemical properties of particles influencing their toxicity are the size, surface area, shape, crystal structure, elemental composition, density and surface properties, and the main functional properties include the solubility rate and the capacity to produce ROS [40].

Firstly, the site and the level of particle deposition in the lung after inhalation are influenced by the size and the geometry (shape, density and surface properties) of the particles [68]. **Figure 5** shows the relationship between the aerodynamic diameter[3] and the pulmonary site of particle deposition. Particles larger than 10 µm mainly deposit in the oropharynx and can be swallowed. Particles smaller than 10

[3] The aerodynamic diameter of a particle is defined as that of a sphere, whose density is 1 g/cm^3, which settles in still air at the same velocity as the particle in question.

µm have the greatest potential to reach the lungs and the alveolar region [94]. The shape of the particles also affects their aerodynamic and diffusive behavior [95].

When deposited in the lungs, particles can persist or be removed. The biopersistence of particles is an important factor of their toxic activity with an impact on their long-term toxicity [40]. The biopersistence of particles is defined as the extent to which they are able to resist chemical, physical, and other physiological clearance mechanisms in the body [96]. The biopersistence is influenced by the solubility of the particles and by the capacity of the lung to clear the particles. The dissolution, defined as the release of molecules or ions from particles, is an important determinant of biodurability (the ability to resist chemical/biochemical alteration) and provides an insight on how particles will interact with cells and induce toxicity [96].

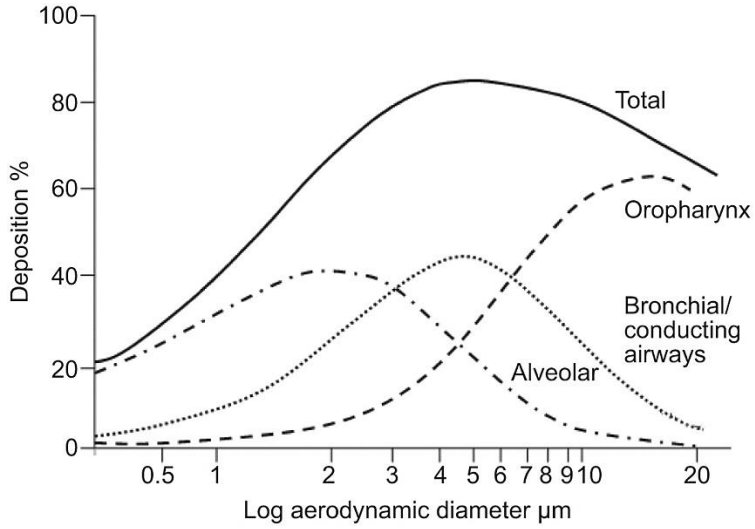

Figure 5: Model of the relationship between aerodynamic diameter and lung deposition. Deposition has been modeled assuming an adult breathing through the nose at 25 l/min (light exercise), and exposed to spherical particles with a density of 1000 kg/m^3. This model was determined by the International Commission on Radiological Protection (ICRP). Original figure from Köbrich et al 1994 [97].

The dissolution of particles depends on their size, composition, shape, crystallinity and surface properties but also on the solvent properties such as the pH, the ionic strength, the temperature and the concentrations of other molecules (sulphides,

chlorides, proteins, enzymes etc.) [96]. By testing the dissolution of particles in artificial fluids mimicking extracellular (neutral pH) or lysosomal (acidic pH) media, we can obtain useful information about their biopersistence [40]. Insoluble particles are mostly cleared in the long-term by phagocytosis [98, 99]. Some factors can influence the phagocytosis of the particles. Particles with a diameter of 1-3 µm are phagocytosed faster than those of a diameter larger than 6 µm. Particles with a diameter smaller than 0.3 µm can escape phagocytosis [68]. The shape also influences phagocytosis. Thin and elongated fibres can lead to frustrated phagocytosis [64, 68]. The physico-chemical properties of the particle surface (charges and hydrophilic properties) influence the interaction of the particles with macrophages or opsonins [100].

Particles can also translocate to the systemic circulation to reach secondary organs. The size of the particles influences their translocation ability [68, 99, 101]. Shorter and thinner fibres and nanoparticles are translocated more efficiently [40]. The ability of particles to translocate from one compartment to another is a key factor in their toxicity [77].

In the lungs, particles can induce different levels of toxicity depending on their physico-chemical properties too. Particles with larger surface areas (dependent on the size and the porosity [102]) are associated with higher lung responses [103]. Nanoparticles are characterized by an excess of energy at the particle surface and are thus thermodynamically less stable. This phenomenon leads to an increase of surface reactivity and to a higher potency to react, implicating an increased toxic activity [101]. A growing number of studies show that smaller (nanosized) particles cause more toxicity than larger particles. However, in some specific cases, toxicity increased with increasing size (e.g. membrane rupture of red blood cells) [101]. The chemical composition and the surface reactivity of the particles also influence their toxicity activity [40]. Metals or other toxic elements composing the particles can be released in cells as ions, via the biodissolution of the particles, and lead to ROS formation or induce specific biological responses [45, 101]. The surface of particles themselves can also be reactive and produce ROS [64].

1.3.3 Main processes involved in inhaled particle toxicity

Inflammation

The innate immune system is the first line of defense against inhaled particles, generating non-specific inflammation to protect the host and maintain homeostasis [104]. It is composed of natural killer cells, granulocytes and phagocyte cells [105]. The phagocyte cells sense the particles to clear them and prevent tissue injury. Acute inflammation is one way to eliminate particles and repair injury. However, if particles are biopersistent and/or if particle phagocytosis is impaired, it can result in a prolonged activation of innate immune responses characterized by inflammatory cell accumulation, pro-inflammatory cytokine release causing tissue damage and chronic diseases [106]. Indeed, inflammation is an early response to inhaled particles. Persistent inflammation is linked to fibrosis, the exacerbation of asthma and COPD, lung cancers and mesothelioma [47].

When particles enter the lungs, they are actively recognized by macrophages or epithelial cells [107]. Multiple types of epithelial cells are present in the respiratory tree: ciliated, mucous and goblet cells in the extra-thoracic and bronchial airways, serous (club cells) in the bronchioles, epithelial cells type I and II in the alveoli [93, 108]. Macrophages play important roles in inflammatory responses [104]. There are different ways of particle recognition leading to inflammation (**Figure 6**). Firstly, particles can be recognized by pattern recognition receptors (PRRs) which are at the cell surface [106]. Scavenger receptor-mediated sensing represents the main PRR system to detect particles and initiate early tissue responses and the production of pro-inflammatory cytokines [106] (**Figure 6 c**). Secondly, particles can lead to inflammation by the release of alarmins (**Figure 6 a**). Indeed, particles and particle phagocytosis can induce cell damage, leading to cytokine and alarmin release [47, 106]. Alarmins such as IL-1α or High Mobility Group Box 1 (HMGB1), have a direct activity on innate immune cell recruitment and stimulation, and can bind to their receptors on adjacent cells and induce the transcription of pro-IL-1β, the pro-form of a crucial pro-inflammatory cytokine [104]. Finally, a simple contact between particles presenting ROS at their surface can lead to inflammation by the release of alarmins and TNF-α secretion [106] (**Figure 6 b**). TNF-α is the first innate

immune signal and is a powerful activator of nuclear factor kappa B (NF-κB) and activator protein (AP)-1 transcription factors leading to the transcription of pro-inflammatory cytokines such as pro-IL-1β [106].

The secretion of IL-1β requires two steps [104]. The first one is the activation of NF-κB and AP-1 leading to the transcription of pro-IL-1β, and the second one implies the NLRP inflammasome to cleave and activate the pro-form in active IL-1β [47]. The NLRP3 inflammasome is the most fully characterized inflammasome. It is composed of an N-terminal pyrin domain (PYD) required for the signal transduction, a central NACHT domain for the oligomerization, and a C-terminal leucine-rich repeat (LRR) for ligand recognition. NLRP3 binds to the adaptor protein, apoptosis speck-like protein, containing a CARD domain (ASC) which in turn recruits and activates caspase-1 (**Figure 7**) [47, 109]. It was recently shown that particles can activate the NLRP3 inflammasome in mesothelial and epithelial cells, in addition to immune cells [47]. Three classic models of NLRP3 activation are described [47]. The first one includes ion flux and modifications of K^+, Ca^{2+} and H^+ cytosolic concentrations that can activate the NLRP3 inflammasome [47]. In the second model, ROS activate NLRP3 inflammasome but the exact mechanism is not fully elucidated [47, 110]. The last model describes NLRP3 inflammasome activation via the lysosome rupture and the release of ROS, Ca^{2+} and cathepsin B. These molecules promote the assembly of inflammasome components and the cleavage of pro-IL-1β in active IL-1β [104]. Beside the cleavage of pro-IL-1β to mature IL-1β, the NLRP3 inflammasome also leads to the maturation and secretion of IL-18 [47]. Among others, IL-1β induces fever, promotes the secretion of transforming growth factor (TGF)-β and mediates the recruitment of leukocytes [47]. IL-1β is a critical mediator of inflammation, promoting fibrosis and tumorigenesis [111-115]. IL-18 can induce interferon-γ production. Activation of the inflammasome also induces gasdermin D cleavage inducing pyroptosis, a mode of cell death, leading to IL-1β, IL-18, cytoplasmic content (including alarmins) and ROS release [116].

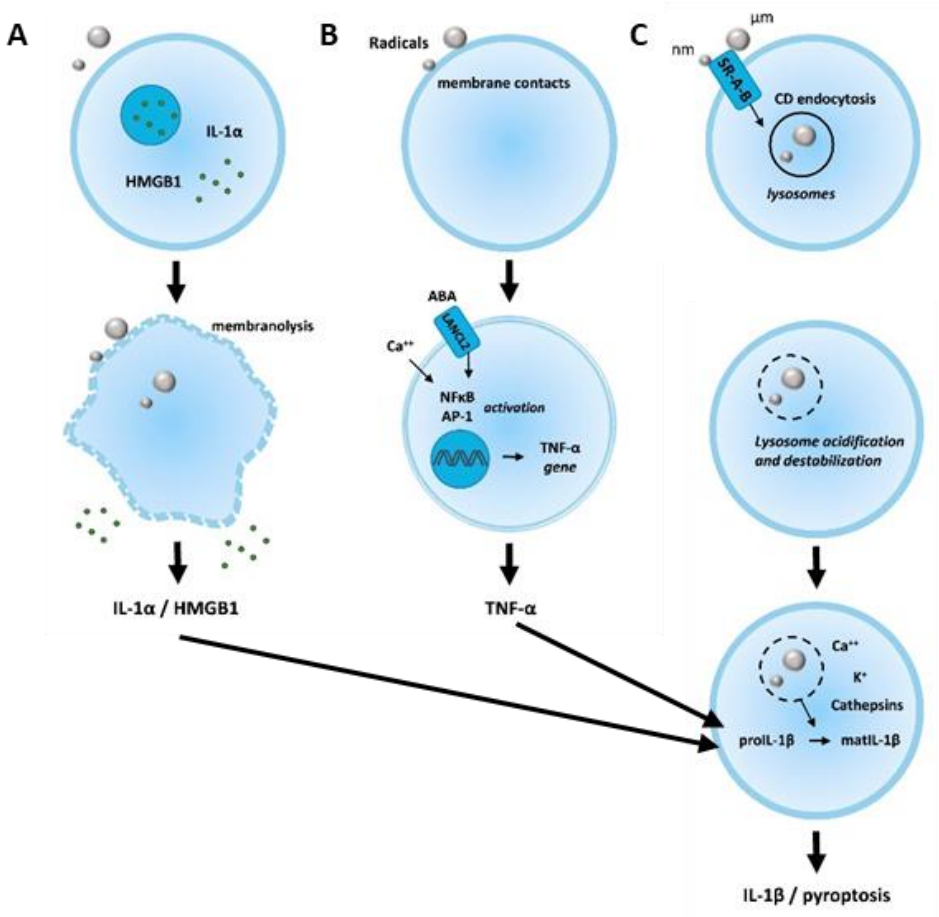

Figure 6: Pathways of particle recognition leading to inflammation. Particle endocytosis can result in cell death leading to the release of alarmins in the tissue environment. Alarmins recruit inflammatory cells and activate the transcription of pro-IL-1β (**a**). ROS on particle surface induce membrane peroxidation, calcium flux perturbation, abscisic acid (ABA) release and LANCL2 receptor activation that results in TNF-α release. TNF-α stimulates the transcription of pro-IL-1β (**b**). Particles are internalized via scavenger receptors (SR) and clathrin-dependent (CD) endocytosis (**c**). Particles can interfere with the cytoplasmic homeostasis (ion concentration modification, lysosome destabilization and release of cathepsins) and activate the intracellular PRR-related inflammasome complex (NLRP) leading to the release of the active form of IL-1β and pyroptosis. Adapted from Huaux 2018 [106].

In addition to the mediators cited above, other master pro-inflammatory cytokines such as type I and II interferons and IL-17 produced by effector T lymphocytes are

essential in the pathogenesis of diseases induced by inhaled particles [107]. During tissue injury-mediated immune responses, naïve CD4+ T helper (Th) cells can also differentiate into Th1 or Th2. Type 2 immune pathways have been recognized as important events for the development of fibrosis. Activated Th2 immune cells and cytokines (IL-4 and IL-13) stimulate over-repair responses, leading to fibrosis [117, 118].

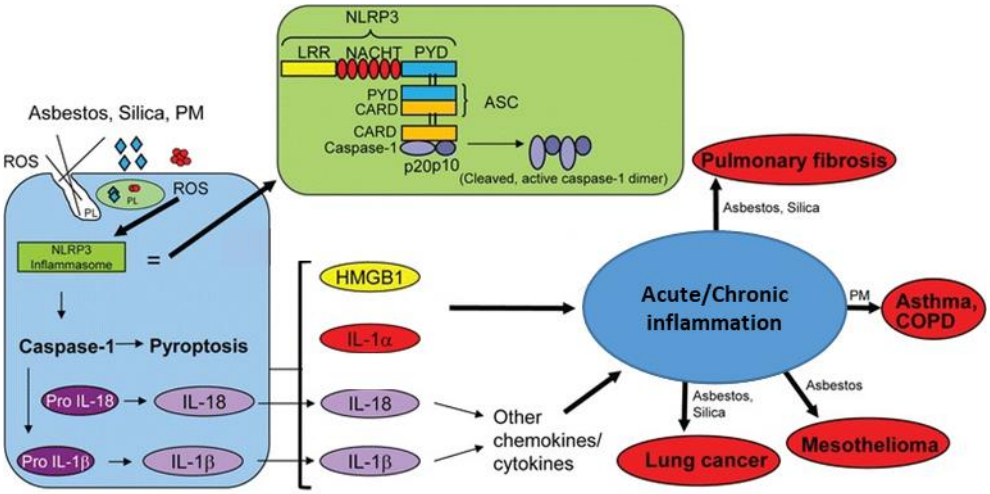

Figure 7: **General view of the biological events linking the inflammasome activation and the particle-associated lung diseases.** Image adapted from Sayan and Mossman 2016 [47].

Thus, when cells are activated, they can release various inflammatory mediators such as cytokines, chemokines, ROS, etc [107]. These mediators induce a marked and persistent recruitment of inflammatory cells and contribute to chronic lung inflammation, resulting in various particle- and fibre-associated lung and pleural diseases. Persistent inflammation can be followed by an exaggerated reparative phase where growth factors stimulate non-controlled fibroblast recruitment, proliferation and extracellular matrix production leading to fibrosis [47].

In addition to these inflammatory events, the role of immunosuppression in diseases induced by inhaled particles emerges, as reviewed in Huaux et al. [107]. Inhaled particles can cause an exaggerated and persistent immunosuppression which is initially established to limit the inflammation but contributes to later diseases [107]. This immunosuppression is characterized by the release of anti-

inflammatory mediators (TGF-β and IL-10) and the recruitment of regulatory immune cells (M2 macrophages, regulatory T and B lymphocytes and myeloid derived suppressive cells) [107]. The main function of TGF-β is immunosuppression [119]. However, TGF-β also induces myofibroblast differentiation, collagen overproduction and scar formation contributing to lung fibrosis, and generates a favorable microenvironment for tumor growth [107]. IL-10 is also an immunosuppressive cytokine and it is admitted that IL-10 limits the inflammation but contributes to the fibrotic responses by stimulating fibroblasts, matrix protein release, increasing the expression of pro-fibrotic mediators by macrophages and limiting the synthesis of anti-fibrotic mediators by epithelial cells [107]. Thus, in addition to inflammation, immunosuppression also contributes to lung disorders induced by inhaled particles.

Reactive oxygen species and oxidative stress

An important mechanism of particle toxicity is the generation of ROS and reactive nitrogen species (RNS). The main radicals produced in cells are the hydroxyl radical ($HO^{\bullet}$), superoxide anion radical ($O_2^{\bullet-}$), peroxyl radical ($ROO^{\bullet}$), alkoxyl radical ($RO^{\bullet}$) and thiyl radical ($RS^{\bullet}$) and nitrogen oxide ($^{\bullet}NO$). Non-radical ROS such as hydrogen peroxide (H_2O_2) and hypochlorite (HOCl) are also implicated in the toxicity induced by particles [120, 121].

Radicals may be (i) generated intrinsically by particles and/or (ii) produced by inflammatory and/or target cells in response to particles [122]. Particles can produce ROS/RNS due to the presence of oxidants or free radicals at their surface. Alternatively, particles may also generate relatively diffusible moieties such as peroxynitrite ($ONOO^-$) and $O_2^{\cdot-}$ [122]. When particles are endocytosed, $O_2^{\bullet-}$ can be generated and its dismutation results in H_2O_2 production [120]. Various transition metals at the surface of particles or released by particles can induce ROS production through Fenton(-like) and Haber-Weiss reactions by reacting with H_2O_2 [121]. In the Fenton-like and Haber-Weiss reactions, a transition metal ion reacts with H_2O_2 to produce $HO^{\bullet}$ and an oxidized metal ion [121]. ROS can also be produced by target cells such as lung epithelial cells and macrophages upon interaction with the particles or their uptake. Particles can damage the mitochondria or interact with

the electron transport chain, can activate nicotinamide adenine dinucleotide phosphate (NADP)H-like systems or disturb the antioxidant defense [123]. Phagocytic cells can produce $O_2^{\bullet-}$, $^{\bullet}NO$, H_2O_2, $HO^{\bullet}$, $ONOO^-$ and HOCl in response to phagocytosed particles [124]. The persistent production of ROS/RNS can lead to cellular damage [122]. Some insoluble particles or fibres can lead to repeated frustrated phagocytosis and cytoplasmic release (containing cellular ROS) and to the activation of other macrophages leading to a subsequent excessive ROS generation [120].

The level of ROS production determines the cellular reaction. Small amount of ROS are required for processes such as intracellular signaling and antioxidants control their presence. However, when a larger amount of ROS is generated, an oxidative stress can occur [124]. “Oxidative stress” is defined as the adverse condition resulting from an imbalance in cellular oxidants and antioxidants [120, 124]. Depending on the amount of oxidants, cell responses can evolve from an initial upregulation of cellular antioxidants such as heme oxygenase-1 (HO-1) via the activation of the nuclear factor erythroid-2-related factor 2 (Nrf2), catalase, superoxide dismutase and peroxidase to pro-inflammatory responses via the activation of NF-κB and AP-1, and finally to cytotoxicity and cell death [124, 125].

There is evidence that ROS produced by particles participate to their pathogenicity by initiating a sequence of pathological events, including inflammation, fibrosis, genotoxicity, and carcinogenesis [120, 121]. Oxidants are substances that readily transfer oxygen atoms or accept electrons and, thus, are able to induce adverse effects such as lipid peroxidation, protein oxidation and DNA damage [124]. Unsaturated fatty acids of cell membrane phospholipids are major targets of $HO^{\bullet}$. This radical can extract a hydrogen from the phospholipid and produce a lipid radical which can, in turn, react with molecular oxygen to produce lipid peroxyl radicals. This phenomenon can propagate and lead to cell membrane destruction. It is postulated that lipid peroxidation plays a major role in lung diseases [120]. ROS can also induce DNA damage by attacking deoxyribose, purine and pyrimidine bases of the DNA. These attacks result in DNA strand breaks which can lead to mutations (see the next chapter) and cancer [126]. Hydroxylation of guanine residues (dG) to produce 8-hydroxy-2'-deoxyguanosine (8-OHdG) is the most commonly

investigated damage of ROS produced by particles [127]. Base modification can lead to mispairing leading to mutations and oncogene activation [120]. ROS can also activate transcriptional factors such as NF-κB, AP-1 and Nrf2 [125, 126]. Through the activation of NF-κB and AP-1, particles producing ROS can trigger the increased expression of pro-inflammatory and fibrotic cytokines and the activation of inflammatory cells, which can, in turn, influence and increase the generation of ROS [120, 121]. ROS production, oxidative stress and inflammation are thus interlinked in the process of particle-induced lung injuries.

Genotoxic and mutagenic activity of particles

Both occupational and environmental exposure to particles are associated with an increased risk of cancer [128]. The genotoxic potential of inhaled particles is defined by their ability to induce DNA damage. Cells can, however, induce cell cycle arrest to repair DNA damage or induce apoptosis. If genotoxic events persist in proliferating cells, irreversible genetic changes occur, which are named mutations, and can lead to carcinogenesis [127] (**Figure 8**).

Particles can induce DNA damage via a primary or secondary mechanism. Primary genotoxicity implies an induction of DNA damage by the particles in absence of inflammation [127]. Primary genotoxicity is due to the intrinsic characteristics of the particles, including composition, shape, size, crystallinity or their capacity to produce ROS [129]. Primary damage can be direct or indirect. Direct primary damage requires a direct interaction between particles and DNA or with cellular constituents that guide chromosome segregation during cell division [123]. This occurs via the direct physical interaction of the particle with the DNA, via the intrinsic ROS generation from particles (e.g. ROS present at the particle surface) or the reaction with organic compounds associated with the particles (e.g. polycyclic aromatic hydrocarbons (PAH)) [123].

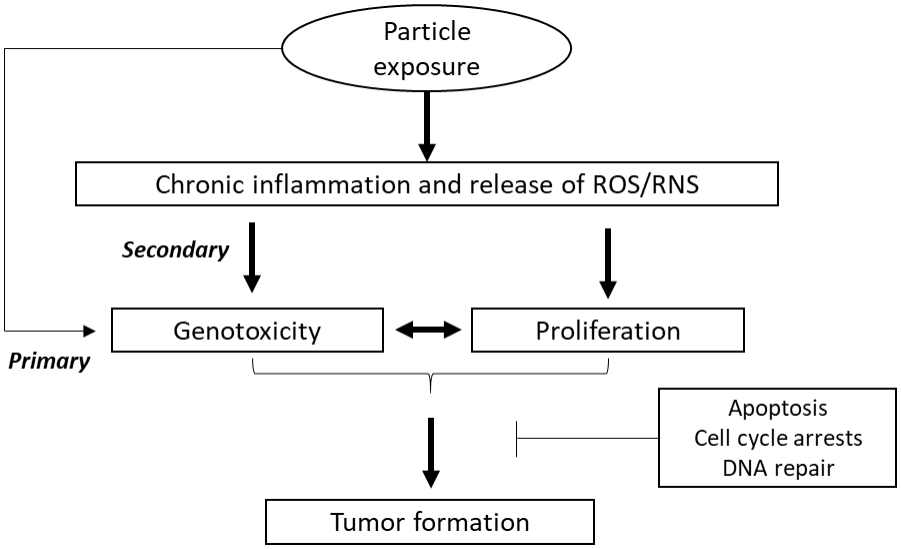

Figure 8: **Pathways of primary and secondary genotoxic events induced by particles and leading to tumor formation** (from Schins 2007 [127]).

Indirect DNA damage means that the first target is not the DNA. These DNA damage can be due to inactivation of DNA repair proteins, inhibition of DNA synthesis, etc. or to ROS generated by particles or to ROS generated by the interaction of particles with cells (e.g. enhanced production of ROS via mitochondria and membrane bound NADPH oxidase or the depletion of cell antioxidants) [123, 130]. Secondary genotoxicity is associated with the production of ROS/RNS by leukocytes recruited during lung inflammation induced by the inhalation of these particles [123].

The major types of DNA damage caused by particles are oxidative attacks and bulky DNA adducts [128, 130]. There are several different oxidative lesions and they can lead to base-pair mutations, deletions or insertions. $HO^{\bullet}$ is the most DNA-reactive radical species. The most investigated oxidative lesion caused by $HO^{\bullet}$ is 8-OHdG [126, 127, 131]. ROS/RNS can lead to exocyclic etheno-adducts, such as during lipid peroxidation, resulting in malondialdehyde and 4-hydroxynonenal formation which are mutagenic electrophiles [128, 130]. ROS can also induce DNA backbone damage, i.e. oxidation of deoxyribose sugar, which can lead to single DNA strand breaks. An accumulation of single strand breaks in the same area can lead to double-strand-breaks and chromosomal aberrations [128, 130]. Particles such as

PM, DEP or carbon black carry at their surface adsorbed components such as PAH which can induce DNA adducts via the endogenous production of highly reactive intermediates [128, 130, 132]. Finally, if the genotoxic events persist, they can lead to aneuploid or polyploid cells or to clastogenicity [133].

Thus, inhaled particles can induce an upregulation of cytokines, transcription factors, anti-oxidants and oxidants in the lungs, creating a milieu with inflammatory cells, synthesis of extracellular matrix and cell proliferation. The presence of particles can cause DNA damage (via primary or secondary mechanism) and proliferative effects to type II epithelial and Club cells via the production of radicals. All of these events create a promutagenic microenvironment adapted for proliferation of mutated cells that can lead to malignant lung diseases [127, 128].

HIF-1α as a potential mediator of lung toxicity induced by inhaled particles

The hypoxia-inducible factor (HIF)-1 is a heterodimeric transcriptional factor of two subunits, HIF-1α and HIF-1β, constitutively expressed in all cells [134, 135]. Under normoxia, HIF-1α, the oxygen sensitive-subunit regulating the levels of active HIF-1, is directly degraded through the ubiquitin-proteasome pathway by prolyl hydroxylase domain (PHD) proteins (**Figure 9**). PHD proteins use O_2, α-ketoglutarate and Fe(II) to convert a prolyl residue to hydroxy-prolyl, producing succinate and CO_2. Once hydroxylated, HIF-1α is recognized by the von Hippel-Lindau tumor suppressor protein (pVHL), an E3 ubiquitin ligase, and is degraded by the proteasome. HIF-1α ubiquination/degradation is promoted by binding of spermidine/spermine N-acetyltransferase-2 (SSAT2), which stabilizes the interaction of pVHL and elongin C [134, 135]. HIF-1α is also a substrate for the factor inhibiting HIF-1 (FIH-1), which is an asparaginyl hydroxylase [135]. This enzyme is also O_2 dependent. By hydroxylating HIF-1α, FIH-1 disrupts the interaction between HIF-1α and its co-activators p300 and CBP, inhibiting the transactivation of HIF target genes [135].

On the contrary, HIF-1α is stabilized under hypoxic conditions and accumulates in cells [134]. In addition to hypoxia, Co and Ni ions are also able to stabilize HIF-1α. Co ions stabilize HIF-1α by blocking the iron-binding site of PHD proteins and by

direct binding to HIF-1α, preventing its degradation [136, 137]. Ni ions inhibit PHD activity by inducing iron depletion due to its competition with divalent metal transporter 1 (DMT-1) or by blocking the iron-binding site of PHD [138]. It is also suggested that ROS produced during hypoxia can affect the oxidation status of PHD bound iron, leading to PHD inactivation and stabilization of HIF-1α [139]. O_2-sensing via hydroxylases is the major pathway to regulate the levels of HIF-1α, however, there are multiple other regulators of HIF-1α [135, 140]. When stabilized, HIF-1α heterodimerizes with HIF-1β, recruits co-activators P300 and CBP, binds to hypoxia responsive elements (HRE) of target genes and initiates their transcription [134, 135, 140].

HIF-1α plays many roles by activating the transcription of numerous genes. HIF-1α helps to restore oxygen homeostasis by inducing glycolysis, erythropoiesis and angiogenesis. HIF-1α also regulates genes involved in the control of cell cycle such as p53, p21 and Bcl-2 [141]. Therefore, HIF plays key roles in various aspects of cancer development: proliferation, angiogenesis, apoptosis, metabolism, extracellular matrix remodelling, cell migration, invasion, etc [135].

HIF-1α is also implicated in inflammation. HIF-1α activates myeloid cell function. Indeed, in the conditional knockout mice for HIF-1α, the cytokine response to lipopolysaccharide (LPS)-induced sepsis (TNF-α, IL-1β, IL-6, IL-12) is reduced [135, 142]. It has also been shown that HIF-1α boosts LPS-induced IL-1β mRNA. IL-1β is thus a direct target of HIF-α [143]. HIF activity has also been described as a key factor for the phagocytosis of bacteria by macrophages under hypoxic conditions and for the production of TNF and NO through the inducible NO synthetase (iNOS) [142]. Since NO can also stabilize HIF-1α proteins, an autocrine feedback occurs and amplifies the inflammatory activation of macrophages. HRE are also found in the genes of Toll-like receptors (TLRs) [142]. There is also an important synergic interlink between HIF and NF-κB [142]. HIF has been shown to mediate NF-κB activation in anoxic neutrophils and to regulate the expression of NF-κB in macrophages stimulated with LPS [135, 142, 144]. Hypoxia itself, by inhibiting PHD, also inhibits IκB kinases (IKK) hydroxylation leading to IKK activation and IKβ phosphorylation, inducing the liberation of NF-κB in the cytoplasm [135, 142, 144]. In turn, NF-κB signalling activated in macrophages regulates HIF-1α transcription

[135, 142, 144]. However, NF-κB alone is insufficient for HIF-1α stabilization, indicating that both transcriptional regulation by NF-κB and post-transcriptional regulation by hypoxia (or other) are necessary [142].

Figure 9: Regulation of HIF-α under normoxic or hypoxic conditions. CBP = cAMP-response element-binding protein; Cul2 = cullin 2; E2 = E2 ubiquitin-conjugating enzyme; p300 = histone acetyltransferase p300; Rbx1 = ring box protein 1; SDH

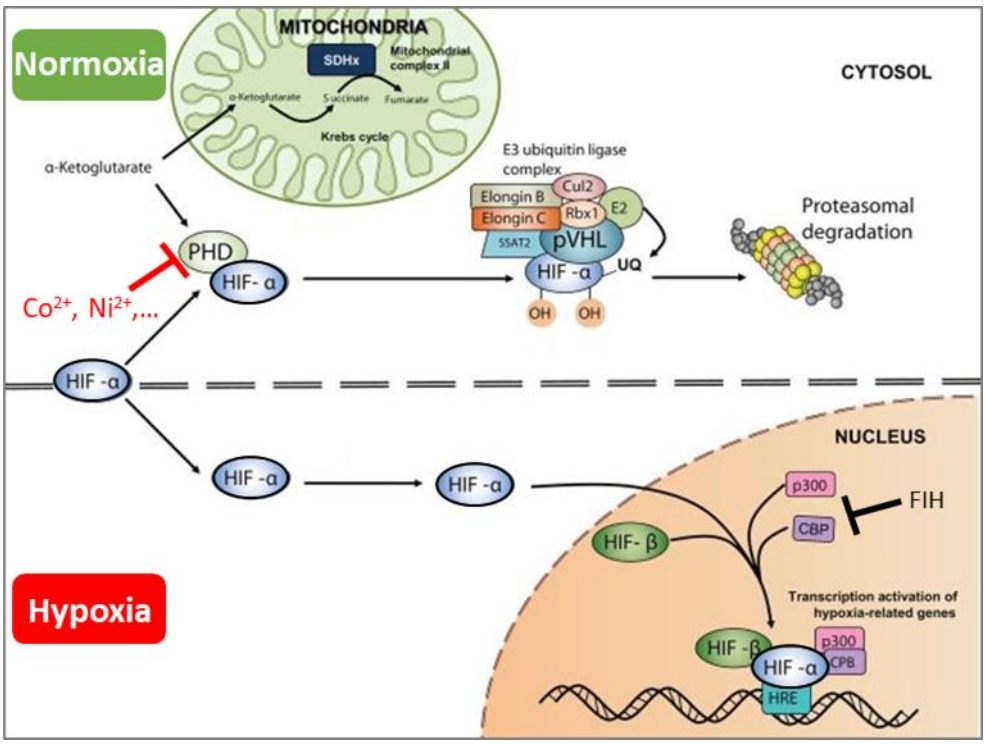

= succinate dehydrogenase; UQ = ubiquitin. FIH = factor inhibiting HIF-1. Adapted from Jochmanova et al 2013 [140].

Activation of HIF-1 has been associated with fibrotic responses such as renal fibrosis in chronic renal diseases [145], adipose tissue fibrosis [146], lung fibrosis induced by paraquat poisoning [147] or idiopathic pulmonary fibrosis [148]. It has recently been shown that HIF-1α can upregulate the levels of α-ketoglutarate, increasing the levels of lysine and proline hydroxylation on collagen, rendering the collagen more resistant to protease degradation [149]. Moreover, HIF-1 has been shown to

induce transcription of the pro-fibrotic factors tissue-inhibitor of metalloproteinases (TIMP)-1, plasminogen activator inhibitor (PAI)-1, and connective tissue growth factor (CTGF) [134]. HIF-1α might also be implicated in fibrosis by promoting myofibroblast differentiation and epithelial-mesenchymal transition (EMT) via the TGF-β pathway [140, 142, 147, 150, 151].

Since numerous particles used in LIB contain Co and/or Ni, we investigated the implication of HIF-1α in their lung toxicity.

1.4 TOXICITY OF METALS USED IN LIB PARTICLES

As mentioned above, LIB particles contain lithium and other elements. In this section we will outline the current knowledge about toxicologically relevant elements used in these particles.

1.4.1 Lithium

Lithium (Li) is an univalent cation present in the Earth's crust at an average of 0.006 % in mass [152].

Sources of exposure

Li is mined from petalite, triphylite, lepidolite, spodumene and amblygonite ores [153] and is also present in natural brines and lakes [152]. The main sources of human Li exposure is by ingestion. Indeed, Li is found in water and plants and its oral daily intake is on average 0.65-7 mg [152, 154]. Li is also orally administered for treating patients with bipolar disorders (500 to 1300 mg of Li carbonate/day).

Occupational skin, eye and inhalation exposure occurs in Li-based battery industries [154].

Metabolism and cellular transport

Li is not absorbed across the skin and inhalation exposure only occurs in specific occupational settings. Therefore, for the general population, the most common exposure route is by ingestion. Ingestion of soluble Li salts leads to a complete absorption by the gastrointestinal tract, with a peak plasma concentration after 2-5 h. Li passes across all biological barriers and is thus distributed uniformly in body fluids [154]. Li has a plasma half-life comprised between 12 and 58 h and is mainly excreted by the kidneys [154, 155]. Due to its small radius and high polarizing strength, Li has a large propensity to replace cations (Na^+, K^+, Mg^{2+} and Ca^{2+}) in cells [153]. Several Na or K transport proteins can also transport Li and provide a pathway for Li entry into cells. The major Li transport occurs via the Na channel and the Na/H exchanger [153, 155]. Other transporters such as the Na-K ATPase or the Na-K-2Cl cotransporters can also move Li across cell membranes [155]. Pathways

to transport Li out of the cells are more limited, generally resulting in the accumulation of Li in the cells. The best candidate is the Na-Na exchanger [155].

Beneficial effects

Li is a non-essential element for the human body but some studies showed that Li in minute quantity has positive effects on mental health by reducing the risk of suicide, violence and depression [154]. Schrauzer even proposes an intake of 1 mg Li/day for a 70 kg adult [156]. Li is the most efficient treatment of bipolar disorders, protecting against depression and mania [157]. It is generally administered orally in the form of lithium carbonate or citrate [154]. The exact role of Li in mood stabilization remains not well understood. A large body of evidence suggests that inflammation plays a role in the pathological processes of bipolar disorders and that lithium could be anti-inflammatory [158]. However, the activity of Li in inflammation is subject to debate and, although Li appears rather anti-inflammatory, many contradictory data exists [158, 159].

Lung toxicity

Existing knowledge on the lung toxicity of Li is sparse. Data about Li lung toxicity in humans do not exist and only some animal studies have been conducted. Inhalation of combustion aerosols of Li carbonate (weakly water soluble) caused moderate acute toxicity in the lungs of rats 14 days after exposure to 620, 1400 or 2300 mg/m^3 during 4 h [160]. Another study showed peribronchial and intraparenchymal lymphocyte and macrophage infiltration as well as alveolar destruction in rats exposed intraperitoneally to 25 mg/kg of Li_2CO_3 [161]. No significant effect was recorded in rabbits after inhalation of 0.6 and 1.9 mg/m^3 of Li from LiCl (water soluble) aerosols for 4-8 weeks, 5 days/week, 6 h/day [162].

Systemic toxicity

The toxicity of Li is largely described in the literature due to its use for the treatment of mood disorders. The therapeutic Li serum concentration range is narrow, comprised between 5.6 and 8.4 mg/l. Mild toxicity can be observed from 10.5 mg/l and at 20 mg/l there is a risk of death [152, 154].

Acute toxicity mainly affects the gastrointestinal tract (nausea, vomiting and diarrhea), the CNS (sedation, tremors, ataxia, agitation, convulsions and coma) and the kidney (polyuria, albuminuria and renal failure). In case of chronic toxicity, the most sensitive organ is the kidney. Nephrogenic diabetes insipidus is the most common renal effect, affecting 30-40 % of patients under Li medication [154]. Chronic kidney disease may also develop due to the dysregulation of aquaporin-2. The thyroid can also be affected with hypothyroidism, goiter, increased levels of serum thyroid-stimulating hormone, calcium and parathyroid hormones [157]. The chronic CNS toxicity is similar to acute toxicity but, in some rare cases, chronic Li intoxication can lead to irreversible neurotoxicity characterized by cerebellar dysfunction, extrapyramidal symptoms and cognitive decline [154].

1.4.2 Cobalt

The concentration of cobalt (Co) in the Earth's crust is on average 25 mg/kg [163]. The main oxidation states of Co are +2 and +3. However, 0, +1, +4 and +5 have also been reported [164].

Sources of exposure

Co is present in cobaltite, smaltite, erythrite, azurite and heterogenite ores. Co is also present in trace amounts in lakes, rivers, oceans, groundwater and soil [165].

For the general population, the diet is the main source of Co exposure [166]. The daily dietary intake of Co is about 0.13 to 0.48 µg/kg body weight (bw) for an adult [166]. Natural and anthropogenic sources such as wind-blown continental dust, volcanoes, forest fires, burning of fossil fuels and mining lead to Co emission into the atmosphere and constitute an exposure source for the general population. Surgical implants made of Co can represent a source of internal Co exposure [165].

Co is mainly used for the manufacture of Li-batteries, steel and alloys (e.g. made of Co and Cr) and is also used in diamond, paint and pigment industries. Hard metals are composed of Co and tungsten carbide (WC-Co). Workers can be exposed by inhalation, and to a certain extent via the skin, to Co particles emitted or produced in industries [165, 166].

Metabolism and cellular transports

The bioavailability of Co and its absorption depend on its bioaccessibility (% of available Co) [163]. Three groups of Co compounds can be distinguished based on their bioaccessibility: (i) the highly bioaccessible compounds (inorganic and organic salts, rather soluble in water), (ii) the compounds bioaccessible only at acidic pH, and (iii) low bioaccessible compounds (oxides and spinels) [167].

Highly bioaccessible Co is rapidly absorbed in the small intestine in case of oral exposure [168]. The gastrointestinal absorption of Co compounds varies from 5 to 45 %. Co absorption is influenced by the dose and by nutritional factors [165]. Co absorption is also influenced by iron levels. Indeed, iron deficiency induces an increase of Co absorption, probably because the transport mechanisms are similar [169].

Data about the pulmonary absorption of Co are limited. Animal and human studies indicate a substantial uptake of Co by inhalation. As in case of oral exposure, the pulmonary absorption of Co is dependent on its solubility in cellular medium [165]. If inhaled, soluble Co compounds can release Co ions. Low soluble Co particles can persist in the lung and low soluble ultrafine Co particles can disseminate through the lymph and vascular system and lead to a systemic dissemination [168]. Co particles can also be phagocytozed by cells and dissolve into the cells, releasing ions intracellularly [170].

If Co ions are extracellularly released, they can precipitate with phosphates or carbonates, or bind to albumin. The remaining bioavailable ions can pass through the cell membrane via filtration or cellular transporters. The mechanism of Co transport into cell membrane is not exactly known, but a role of natural resistance-associated macrophage protein 2 (NRAMP 2)/DMT-1 has been documented [165]. Pathways shared with calcium have also been described in red blood cells [171].

Co is mainly distributed in the liver, the kidney and excreted via the urine. The excretion rate is in 3 phases, a first rapid elimination of few hours, a slower elimination of few days, and a long-term retention with a half-time on the order of years [169].

Beneficial effects

Co is an essential element in the form of vitamin B_{12} [172].

Lung toxicity

Acute occupational inhalation of aerosols containing Co, metallic Co, Co oxides and Co salts can lead to dyspnea and pharyngeal irritation. The intensity of the effects is correlated with the exposure level. Chronic exposure to aerosols containing Co can lead to asthma and bronchitis [165, 173]. Chronic inhalation of Co particles in association with WC, can lead to "hard metal disease" [166]. The early phase is characterized by a reversible alveolitis and the chronic phase by a diffuse interstitial fibrosis [165, 173]. Co metal, Co sulfate and other soluble Co salts could lead to lung cancer and are classified as possibly carcinogenic for humans (group 2B) and WC-Co as probably carcinogenic for humans (group 2A) by the IARC [60].

Systemic and dermal toxicity

Non-occupational oral exposure to Co was observed in beer drinkers. This overexposure led to cardiac disorders. Chronic skin contact with Co can cause dermatitis characterized by erythematous papules [163, 165, 173]. It represents 4 % of the cases of contact dermatitis in occupational settings [166]. Systemic effects recorded in case of chronic inhalation overexposure include neurological, thyroidal and cardiovascular manifestations [163, 165, 173].

Toxicity mechanisms

The toxicity of Co depends on the interactions of Co ions with receptors, biomolecules or ions channels [174].

Co ions are able to produce ROS via the Fenton-like reaction: $Co^{2+} + H_2O_2 \rightarrow Co^{3+} + HO^{\bullet} + OH^-$ [175]. This production of radicals can lead to oxidative stress and protein or lipid oxidation and oxidative DNA damage [168, 174]. Co also has a high affinity for sulfhydryl groups which are co-factors for the mitochondrial respiration and the citric acid cycle. This disruption in mitochondrial function can lead to an increased production of ROS and cell death, with inflammatory responses [168, 174]. Co ions

are also able to interact with Ca, Fe and Zn homeostasis. Co ions can substitute Fe in proteins, are antagonists for Ca channels, modifying cell signalling and substitute Zn in the Zn domain of DNA repair enzymes, leading to persisting DNA damage [168, 174]. Co ions are also able to stabilize HIF-1α leading to metabolic, vascular and inflammatory responses [168, 174].

1.4.3 Nickel

Nickel (Ni) is present in the Earth's crust at about 0.01 % [176]. Ni appears as a silvery white metal and exists in different oxidation states; -1, +1, +2, +3 and +4, but the most common is +2 [138, 177].

Sources of exposure

Ni exists as sulfide or oxide ores [138]. All soils contain Ni [178]. Ni is also present in natural waters. Environmental oral exposure thus occurs via the ingestion of plants, animal products and water, representing a daily intake of 0.1-0.3 mg Ni [176]. The environmental exposure via inhalation is mainly due to the association of Ni with PM due to the combustion of fossil fuels and pollution from Ni industries [138, 179, 180]. Smoking increases the level of inhalation exposure to Ni particles. Dermal exposure is a major source of human exposure route because coins, jewelries, watches, dental tools etc. contain metal Ni [138].

Industrial uses of Ni are numerous, including steel and alloy products, electroplating, batteries, chemical catalysis, electronic vacuum, metal items etc. [138, 179]. Occupational exposure to Ni particles occurs in these industries and in mines, via inhalation or skin contact [138, 179].

Metabolism and cellular transports

Soluble Ni compounds are easily absorbed by the gut and the lungs [179]. The pulmonary persistence and absorption rate of Ni particles is also dependent of particle size [179]. Dermal absorption is not the major route of Ni uptake but Ni metal and Ni salts can solubilize during prolonged skin contact and penetrate dermally [178, 179].

The chemical form of Ni determines how it enters into cells [181]. Insoluble particles of Ni can be endocytosed by cells, Ni carbonyl is liposoluble and can pass through the cell membrane, Ni^{2+} is transported by diffusion or via Ca channels or DMT-1 [182].

Normally, Ni does not accumulate but in case of high Ni exposure level, the primary target organs for Ni retention are the lung, the brain and the pancreas [138]. The non-absorbed Ni (ingested) is excreted in feces. Ni absorbed by the intestine or the lungs is eliminated in urine [138, 178]. The half-life of ingested soluble Ni is about a couple of hours, while lung clearance of insoluble Ni can take months [138].

Beneficial effects

Ni is not essential for the human body [181, 182].

Lung toxicity

Short-term high-dose inhalation of Ni particles can lead to lung irritations, emphysema or lung fibrosis [138, 176, 177]. Deaths due to respiratory distress syndrome have been reported after acute occupational exposure to Ni particles [183]. Chronic toxicity of Ni particle inhalation leads to rhinitis, sinusitis and asthma [138]. Ni compounds are classified by the IARC as carcinogenic for humans (group 1). There is sufficient evidence in humans for the carcinogenicity of mixtures that include Ni compounds and Ni metal causing lung, nasal cavity and paranasal sinuses cancers [60].

Systemic and dermal toxicity

Inhalation of $Ni(CO)_4$, decomposing in Ni and CO, is extremely toxic, leading to systemic toxicity and death [138]. Acute poisoning by ingestion of Ni carbonyl or soluble Ni compounds can lead to headache, vertigo, nausea, vomiting and nephrotoxic effects [179]. Chronic dermal exposure to Ni can cause allergy and dermatitis [138, 179].

Toxicity mechanisms

Adverse effects of Ni are due to its capacity to generate ROS, leading to oxidative stress, to DNA damage, to stabilize HIF-1α and to activate NF-κB [138].

1.4.4 Iron

Iron (Fe) is the fourth most abundant element of the Earth's crust with an amount of approximately 5 % in mass [184]. Fe can have different oxidation states from -2 to +6, but the most common are ferrous (II) or ferric (III) Fe [184, 185].

Sources of exposure

Environmental exposure can occur by ingestion because Fe is present in water and soils. The forms of dietary Fe are heme iron, bound in a protoporphyrin ring, and non-heme iron bound to other molecules [185]. The average daily Fe intake in Western Europe is about 15 mg [186]. Environmental inhalation exposure to Fe can also occur via the inhalation of PM [180, 187].

Fe can be mined from numerous ores, such as magnetite, hematite or taconite [186]. Fe is used for numerous industrial applications such as structural element production for buildings, pigments, etc. [186]. Workers can thus be exposed by inhalation to Fe particles [186].

Metabolism and cellular transports

20-30 % of body Fe is stored in hepatocytes and macrophages and 70-80 % in hemoglobin in circulating erythrocytes [186, 188]. Complex Fe homeostasis mechanisms occur in cells. In blood, Fe binds to transferrin. The uptake of Fe by cells occurs mainly via the transferrin receptor 1 (TfR1) [184]. The complex undergoes endocytosis and Fe is freed from transferrin at acidic pH, and reduced by a ferrireductase [188]. TfR1 is then recycled back for further cycles [189]. Fe is transported across the endosomal membrane by the DMT-1. Other processes can transport Fe. In some cell types, DMT-1 and other transporters (ZIP8, ZIP14) bind Fe without transferrin [189]. Internalized Fe is then used for metabolic functions, stored (in ferritin) or exported out of the cell [185, 188]. Iron is mainly used by

mitochondria for the synthesis of heme and iron-sulfur clusters biogenesis. In case of Fe requirement, autophagy can occur and ferritin goes to the autolysosome to free Fe. Fe is then exported out of the cell by ferroportin [189].

Levels of Fe are controlled by hepcidin, a peptide derived from the liver. In case of hypoxia or anemia, hepcidin levels decrease and promote Fe absorption and Fe release from macrophages. In case of inflammation or Fe loading, hepcidin levels increase, inhibit Fe absorption and promote Fe accumulation in macrophages [185, 186, 188].

Beneficial functions

Fe is an essential element for growth and survival. Fe is involved in a broad spectrum of essential functions such as oxygen transport and storage, mitochondrial respiration, nucleic acid replication and repair, host defense and cell signaling [185, 186, 189].

Lung toxicity

Inhalation of Fe dusts or fumes (mainly Fe oxides), can lead to siderosis (iron pneumoconiosis), hematite pneumoconiosis or Fe pigmentation of the lung. These conditions are not considered to progress to fibrosis [186]. Occupational exposures during Fe and steel founding are classified as carcinogenic to humans (group 1) by the IARC, leading to lung cancer [60].

Systemic toxicity

Systemic Fe overload can be due to hereditary hemochromatosis, Fe loading anemias or transfusional Fe overload [189]. Accumulation of Fe due to chronic ingestion and genetic predisposition to absorb Fe are rare [186]. This overload can lead to cirrhosis, diabetes and heart dysfunction due to oxidative damage induced by Fe [186].

Toxicity mechanisms

The toxicity of Fe is largely based on its capacity to produce ROS. Free Fe can donate or accept an electron from another molecule and lead to the formation of ROS, mainly via the Fenton reaction, able to induce cellular and DNA damage [190]. The Fenton reaction can occur in presence of Fe ions as described here:

$Fe^{2+} + H_2O_2 \rightarrow Fe^{3+} + HO^{\bullet} + OH^{-}$ [191].

1.4.5 Titanium

Titanium (Ti) is the ninth most common element in the Earth's crust (0.6 %) [192]. The most common oxidation states of Ti are +3 and +4. The most common oxide is TiO_2 that can be in three crystalline forms: anatase, brookite and rutile. Amorphous forms of TiO_2 also exist [193].

Sources of exposure

TiO_2 is the main form of human exposure to Ti. Ti is poorly absorbed by plants and animals, and can be found in food where TiO_2 is an additive [194]. Food is the main source of exposure to TiO_2 for the general population, with an amount of 0.3 - 0.5 mg Ti/day [192].

Ti is mainly mined from ilmenite ores [193]. Ti metal is used in numerous industrial applications such as in aircraft and airspace alloys, biomaterials, pigments, food additives etc. Exposure to Ti in occupational settings mainly occurs via inhalation of Ti dusts [192]. TiO_2 nanoparticles are also intensively used as pigment in several applications in industry: coatings, plastics, papers, inks, medicines, pharmaceuticals, food products, cosmetics, and toothpaste, implying risk of inhalation exposure in workplaces [88].

Metabolism and cellular transports

Ti is poorly absorbed by the gastrointestinal tract (< 5 %). Transferrin acts as a specific carrier of Ti ions and thus plays a central role in its transport and absorption. Ti nanoparticles can be taken up via the respiratory route and after oral intake

[192]. TiO_2 nanoparticles can be absorbed through the gastrointestinal tract via the lymphoid tissues [88]. TiO_2 dusts can also be absorbed in the lungs. After ingestion or inhalation, TiO_2 nanoparticles can be distributed through all the body via the vascular system, lymphatic dissemination or phagocytosis of particles by macrophages [88, 192]. Ingested Ti is mostly eliminated in the feces [192].

Beneficial effects

No evidence exists that Ti is an essential element for human [192].

Lung toxicity

Ti is generally considered as a low toxicity element. Animal studies demonstrated inter-species variabilities after TiO_2 particle inhalation. Indeed, at similar doses of TiO_2, rat, mouse and hamster lungs are not equally affected. At low levels of exposure, clearance is efficient, and no toxicity is observed. However, at high doses, an overload occurs in rat and mice lungs, not in the hamster, leading to inflammation, fibrosis and cancer [195, 196]. In 2010, the IARC classified TiO_2 as possibly carcinogenic to human (group 2B) [60]. Inhalation of TiO_2 nanoparticles can also lead to lung inflammation and injury [88, 197].

Systemic toxicity

Ti can induce a systemic disease called “Yellow nail syndrome” which is characterized by a change in the nails, bronchial obstruction and lymphedema [194]. Ti is largely used in implants where corrosion occurs leading to inflammation in surrounding tissues [194]. TiO_2 nanoparticles can also pass through the blood brain barrier (BBB) and could be toxic for the CNS [194].

1.4.6 Manganese

Manganese (Mn) is ubiquitous in the environment, and represents 0.1 % of the Earth’s crust. Mn can be found in its native state as metal or in several ores including pyrolusite, rhodocrosite and rhodonate [198]. Mn commonly exists at positive oxidation states as +2, +3, +4, +6 and +7, but -3 can also be found [199].

Sources of exposure

Environmental exposure occurs via inhalation and ingestion. Mn exists as a component of environmental PM and can be inhaled by the general population [198]. Mn dusts can also be present in areas with major foundry facilities using Mn. Mn may also be released in water from industrial discharges. Soil naturally contains Mn but may be enriched by industries too. Mn is also naturally present in food which represents the major source of Mn intake. The highest concentrations are found in cereals and rice. The daily intake of Mn is estimated at 2 – 8.8 mg [198, 200].

Mn is used in metallurgical processes (steel manufacture, alloy constituent…), in fungicides, in dry cell batteries, etc. In occupational settings, workers can inhale airborne fumes and Mn particles. The most worrying places are the mines, dry-cell battery and welding industries [198, 199].

Metabolism and cellular transports

Upon oral exposure, Mn is rapidly absorbed in the intestine [199]. Adults absorb approximately 3-5 % of ingested Mn [200]. Inhaled Mn is absorbed in the lungs and directly enters the circulation [201].

Mn enters cells via passive diffusion or active transport. Systems responsible for Mn influx are the DMT-1, the transferrin receptor, the zinc transporter ZIP8 and ZIP14, the citrate transporter, the choline transporter, the dopamine transporter and calcium channels [202]. Therefore, the presence of other metals can influence the rate of Mn absorption [199].

After absorption, Mn is distributed via the blood in the liver, the pancreas, the bone, the kidney and the brain [199]. Mn can cross the BBB [200]. Most Mn is excreted in the bile and the feces [199, 200].

Beneficial effects

Mn is an essential element. It plays a role in bone mineralization, protein and energy metabolism, metabolic regulation, cellular protection from damaging free radical species, and the formation of glycosaminoglycans [198].

Lung toxicity

Upon acute exposure to Mn dusts (Mn dioxides or Mn tetroxides), lung inflammation (chemical pneumonitis) can be observed. At low concentration of exposure, insoluble Mn particles can induce alveolar inflammation with marked dyspnea and bronchitis [198, 203]. Long-term lung exposure to Mn particles associated to smoking habits could lead to chronic non-specific lung disorders (COPD, emphysema) [198].

Systemic toxicity

Overexposure to Mn can lead to diseases and mainly occurs in occupational settings where workers inhale fumes or dusts, or in the population living in industrial areas by ingestion and inhalation [200, 201, 203]. The CNS is the primary target of Mn toxicity where it can induce “manganism”. “Manganism” is characterized by psychiatric and neurological manifestations related to the extrapyramidal system: weakness, lethargy, slow and clumsy gait, speech disturbances, mask-like face and tremors [198]. Other organs or systems can also be targeted by Mn leading to reproductive, cardiovascular, hematological, endrocrine and immunological effects [198].

Toxicity mechanisms

The mechanism of Mn neurotoxicity is not clear [204]. Mn seems to perturb the cellular metabolism and the neurotransmitter content of neural cells, such as dopamine, gamma-aminobutyric acid and glutamate. There are contradictory data about the pro-oxidant potential of Mn. Mn could induce oxidation of dopamine and induce ROS production by interfering with mitochondria. Mn could also perturb Fe homeostasis [204] .

1.4.7 Aluminum

Aluminum (Al) is ubiquitous in the environment and represents 8 % of the Earth's crust. Bauxite is the major Al ore from which it is extracted [205].

Sources of exposure

Al is naturally present in water and food. The main environmental exposure source is the food where Al is often added as an additive (e.g. Al is used in cheese as an emulsifying agent, in salt as an anticaking agent etc.). The daily human intake of Al in Europe is 3.6 mg [205]. The general population is also exposed to Al via inhalation of PM [205, 206].

Al is used in a lot of industrial applications. Al and alloys are used in airplanes, trains, cars, construction materials and Al powders are used in paints, explosives, fireworks, etc. Al is also used as adjuvant in vaccines. Al silicate is added in cosmetics, and Al nanoparticles are added in food. Workers are mainly exposed to Al via inhalation during Al powder production and Al welding [205].

Metabolism and cellular transports

Al chemical form and solubility influence its absorption. Ingested Al is absorbed in the duodenum and the small intestine [207]. Only 0.3 % of orally ingested Al is absorbed [205]. In case of inhalation, 2 % of Al is absorbed [206]. Al is absorbed by cells via passive diffusion, pinocytosis, and transferrin/vitamin D-dependent active transport [207]. Al binds several plasma proteins, such as transferrin and albumin, and is distributed via the blood [208] in bone, lung, muscle, liver and brain [206]. Al is mainly eliminated in the urine and a small fraction in the feces [206].

Beneficial effects

Al is not an essential element for humans [209].

Lung toxicity

Adverse respiratory effects were reported upon occupational inhalation of Al. Potroom asthma characterized by wheezing, dyspnea and impaired lung functions

was observed and related to Al potroom exposure [210]. The cause of this asthma has not been fully elucidated and could be associated with other toxicants produced in the workplace [206, 210]. Exposure to Al-containing minerals such as bauxite is often accompanied by silica. This combined exposure can lead to lung fibrosis [205, 206]. Occupational health studies have also shown that high level of exposure to stamped Al powder in absence of silica can also induce lung fibrosis [205]. Long-term exposure to Al-welding fume has also been associated with chronic interstitial pneumonia and pulmonary fibrosis [205]. The carcinogenic risk of Al has not been evaluated by the IARC. However, IARC has classified certain exposures occurring during the production of Al as carcinogenic to human (group 1) leading to lung and bladder cancer [60].

Systemic toxicity

Several clinical reports document the adverse effects of non-occupational Al exposure in patients with renal diseases exposed to Al through the dialysate fluid. Anemia, bone disease, and dialysis encephalopathy are the most commonly reported toxic effects in these patients [206, 211]. Adverse neurological effects were also reported in Al workplaces [211].

1.5 PREDICTIVE TOXICOLOGY

To prevent disasters such as observed with Thalidomide (1950) or with asbestos (1938-1986), almost all regulatory authorities have adopted strategies for the safety testing of chemical compounds [212, 213], including micro and nanomaterials. Since 2007, the legal framework of REACH (Registration, Evaluation, Authorization and Restriction of Chemicals) in the European Union is imposed to manufacturers, importers and downstream users to provide physico-chemical properties, health and environmental risk assessment of their products [214]. Health hazards are principally assessed *in vivo*. However, cell cultures and molecular biology are now well developed and represent a way to reduce the use of animals, integrated in the 3Rs principle. The 3Rs principle (Replacement of *in vivo* studies, Reduction of the number of animals used and Refinement of the animal welfare) for research was first introduced by Russel and Burch in 1959, and is now a key concept in the European Union [215], Brazil and Japan. These principles are also integrated into international guidelines for toxicity testing, such as those developed by the Organization for Economic Cooperation and Development (OECD) [216]. Thus, the 3Rs principles are now fundamental for performing ethical experimental research [217].

One way to replace and reduce the use of animals is to categorize new materials. Considering the high number of different particles and nanomaterials with different physico-chemical properties (composition, size, structure, surface, solubility/bioaccessibility, etc.) on the market and under development, information requirements for the hazard assessment of each single material would lead to a myriad of testing. Therefore, many efforts are made to categorize the materials according to knowledge on the toxicity-determining characteristics of the materials [218-222]. The nature of the criteria used for grouping varies depending upon the type and purpose of the grouping [223]. Generally, the grouping concept implies that information on physico-chemical characteristics is available. It also implies that information on the hazard of a material for one specific adverse/toxic effect (adverse outcome, AO), can be derived from the respective material, from molecule or ions of its constituents, or from similar materials with the aim to obtain sufficient and relevant data and avoid unnecessary new testing and making hazard

assessment more efficient [218]. Thus, entities of similar profiles should be tested only once [221]. Grouping of materials is useful during the early stage of the hazard assessment of new materials to identify materials of concern which could be then targeted for more details [223]. Grouping strategies allow to better predict the hazard of the materials while limiting the number of assays [223]. The use of predictive assays, in combination with grouping or not, also allows to reduce the number of tests. Predictive toxicology plays an important role in the assessment of toxicity of chemicals and the drug development process [224]. Predictive toxicological approach for particles can be defined as the use of physico-chemical determinants or mechanism-based *in vitro* screening assays to make predictions about particles that may lead to the generation of pathology or disease outcomes *in vivo* [222]. A large variety of well-established and validated assays have been used in predictive toxicology testing such as the Ames test, the *in vitro* micronucleus assay and the *in vitro* chromosome aberration to predict the mutagenic potential of materials [224]. Thus, when possible, substances can be categorized/grouped on the basis of determinants or modes of action, identified via a predictive assay, potentially leading to an AO [220, 223]. Therefore, the use of adverse outcome pathways (AOPs) to select the determinants or modes of actions for testing is useful.

An AOP is defined as a sequence of events that links a molecular initiating event (MIE) to an AO at a biological level of organization relevant to risk assessment, progressing via a series of key events (KE) (**Figure 10**) [225]. KE relationships (KER) characterize the sequence of the KEs. KE can occur at different levels (organelle, cellular, tissue, organ responses). KE can be alterations of metabolic pathways, signaling events or modifications of cellular functions [226-228]. An AOP should have one MIE and one AO but the number of KEs is unlimited [226]. The pathway must be a plausible hypothesis of important events based on existing knowledge derived from *in vitro, in vivo*, or computational systems [227].

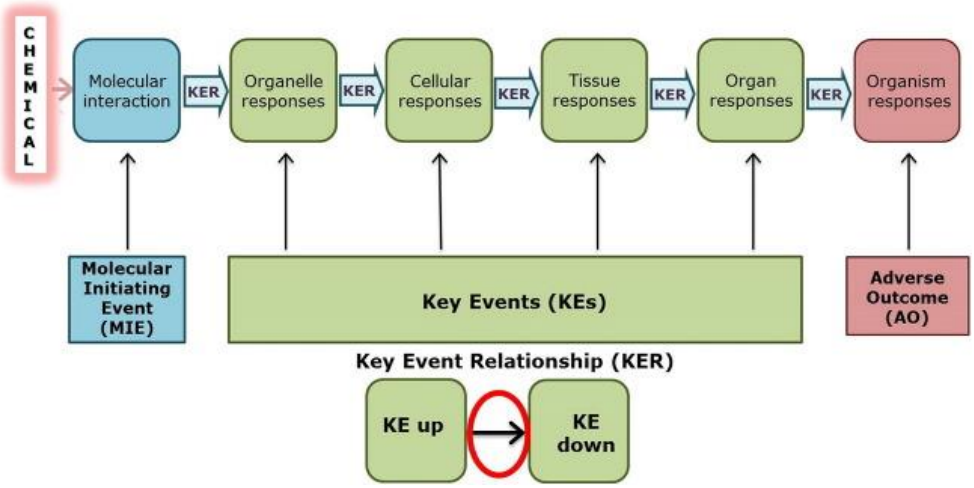

Figure 10: General diagram of the adverse outcome pathways. Figure from Bal-Brice and Meek, 2017 [228].

The AOP is based on the principle that understanding the mechanisms linking the initial event to the AO is a key aspect of predictive toxicology [226]. AOPs provide a useful structure within which existing knowledge can be organized, from which key uncertainties/knowledge gaps and research priorities can be identified, and through which we can improve predictive approaches needed to advance regulatory (eco)toxicology [227]. These AOPs can be useful for researchers by helping them in the investigation of new material toxicity by focusing on the key events of the AO studied. Incomplete AOPs can also be an incentive to identify new mechanisms of action. As KE are defined as measurable changes in a biological state [225], AOPs can also facilitate the development of simple and fast alternative methods and reduce the use of animals [229]. Regulatory toxicology currently moves towards AOPs.

In this project, the “predictive toxicology” concept appears relevant in view of the large diversity of particles used in LIB (different size, composition, solubility etc.) and their content in toxicologically relevant metals (see section 2.4). Based on an existing AOP that describes lung inflammatory and fibrotic events due to the exposure to exogenous substances (AOP 173 “Substance interaction with the lung

resident cell membrane components leading to lung fibrosis") and LIB particle physico-chemical properties, we assessed the induction of some markers (ROS, IL-1β and HIF-1α) potentially implicated in LIB particle lung responses. We investigated their implication in the inflammatory process. Based on mechanistic results, we investigated the link between lung inflammation, *in vivo* and *in vitro* HIF-1α stabilization and physico-chemical properties of the particles (Co and Ni content and bioaccessibility). We thus attempted to identify the determinants of the lung toxicity of LIB particles and to demonstrate their toxicological relevance via mechanistic data.

OBJECTIVES

In this thesis, we focused on the pulmonary toxicity of LIB particles, as inhalation appears the most relevant route of exposure to these particles.

The aim is to define the lung toxicity of particles used in LIB, by answering three specific research questions:

1. What is the respiratory toxicity (inflammatory, fibrotic and genotoxic responses) of LIB particles available on the market and in use in LIB?
2. What are the determinants and mechanisms of this toxicity?
3. Can we predict the lung toxicity of these particles with their physico-chemical properties and/or (an) *in vitro* assay(s)?

RESULTS

3.1 RESPIRATORY HAZARD OF Li-ION BATTERY PARTICLES AND RELATED MECHANISMS

As mentioned in section 2.3.2, physico-chemical properties of particles play crucial roles in lung toxicity. Therefore, before assessing LIB particle toxicity, their characterization was first needed. The size distribution, shape and density of these particles were thoroughly analyzed. We also analyzed their composition and evaluated elemental solubility at neutral and acidic pH to assess their capacity to release potentially toxic metals and to persist in the lungs.

After LIB particle characterization, we evaluated their lung toxicity. We firstly selected three commonly used LIB particles with different elemental compositions: lithium titanium oxide ($Li_4Ti_5O_{12}$, LTO), lithium cobalt oxide ($LiCoO_2$, LCO) and lithium iron phosphate ($LiFePO_4$, LFP). Lung toxicity (acute and sub-chronic inflammatory and fibrotic responses) was investigated in an *in vivo* murine model after a single oro-pharyngeal aspiration. Lung responses were compared to equimolar Li concentrations of lithium chloride (LiCl) to discriminate effects due to the Li content of LIB particles. Crystalline silica particles were used as positive control since these particles are known to induce chronic lung inflammatory responses and fibrosis in human and murine models [230-233]. Biopersistence was also evaluated in mouse lungs.

We observed different intensities of lung responses between the three particles, LTO inducing an acute lung inflammation, LFP an acute and chronic lung inflammation and LCO an acute and chronic lung inflammation and fibrosis. We also identified potential biomarkers of lung toxicity which were explored in the second publication (section 4.2). These results associated with bioaccessibility and bioavailability data of LCO particles suggested a predominant role of Co in its lung toxicity.

We showed here, for the first time, that LIB particles represent a respiratory hazard. Exposure to LIB particles should, therefore, be controlled in occupational settings and adequate monitoring of their life cycle and uses should be secured to avoid environmental pollution and indirect exposure of the general population.

Respiratory hazard of Li-ion battery components: elective toxicity of lithium cobalt oxide ($LiCoO_2$) particles in a mouse bioassay

Violaine Sironval[1,§], Laurence Reylandt[2], Perrine Chaurand[3], Saloua Ibouraadaten[1], Mihaly Palmai-Pallag[1], Yousof Yakoub[1], Bernard Ucakar[4], Jérôme Rose[3], Claude Poleunis[5], Rita Vanbever[4], Etienne Marbaix[6], Dominique Lison[1], Sybille van den Brule[1]

Archives of Toxicology (2018) 92:1673–1684
Received: 8 November 2017 / Accepted: 13 March 2018 / Published online: 17 March 2018

Online version of this article: https://doi.org/10.1007/s00204-018-2188-x

Author's affiliations:

[1]Louvain centre for Toxicology and Applied Pharmacology, Institut de Recherche Expérimentale et Clinique, Université catholique de Louvain, Avenue E. Mounier 52 - bte B1.52.12, 1200 Brussels, Belgium

[2]Institute of Mechanics, Materials and Civil Engineering, Université catholique de Louvain, Place Sainte Barbe, 2 - bte L5.02.02, B-1348 Louvain-la-Neuve, Belgium

[3]CEREGE, Aix Marseille Université, CNRS, IRD, Collège de France, Avenue Louis Philibert, 13090 Aix en Provence, France

[4]Louvain Drug Research Institute, Université catholique de Louvain, Avenue Mounier 73 - bte B1.73.12,

1200 Brussels, Belgium

[5]Institute of Condensed Matter and Nanosciences, Université catholique de Louvain, Place Louis Pasteur 1, bte L4.01.10, 1348 Louvain-la-Neuve, Belgium

[6]De Duve Institute, Université catholique de Louvain, Avenue Hippocrate 75 - bte B1.75.02, 1200 Brussels, Belgium

[§]Corresponding author

3.1.1 Abstract

Rechargeable Li-ion batteries (LIB) are increasingly produced and used worldwide. LIB electrodes are made of micrometric and low solubility particles, consisting of toxicologically relevant elements. The health hazard of these materials is not known. Here, we investigated the respiratory hazard of three leading LIB components ($LiFePO_4$ or LFP, $Li_4Ti_5O_{12}$ or LTO, and $LiCoO_2$ or LCO) and their mechanisms of action.

Particles were characterized physico-chemically and elemental bioaccessibility was documented. Lung inflammation and fibrotic responses, as well as particle persistence and ion bioavailability, were assessed in mice after aspiration of LIB particles (0.5 or 2 mg); crystalline silica (2 mg) was used as reference. Acute inflammatory lung responses were recorded with the 3 LIB particles and silica, LCO being the most potent. Inflammation persisted 2 months after LFP, LCO and silica, in association with fibrosis in LCO and silica lungs. LIB particles persisted in the lungs after 2 months. Endogenous iron co-localized with cobalt in LCO lungs, indicating the formation of ferruginous bodies. Fe and Co ions were detected in the broncho-alveolar lavage fluids of LFP and LCO lungs, respectively. Hypoxia-inducible factor (HIF) -1α, a marker of fibrosis and of the biological activity of Co ions, was upregulated in LCO and silica lungs.

This study identified, for the first time, the respiratory hazard of LIB particles. LCO was at least as potent as crystalline silica to induce lung inflammation and fibrosis. Iron and cobalt, but not lithium, ions appear to contribute to LFP and LCO toxicity, respectively.

3.1.2 Background

Li-ion batteries (LIB) are used in most portable electronics such as cellular phones and laptops, and are also present in power tools, electric vehicles, etc. [234]. The electrodes of conventional LIB are made of particulate materials such as lithium titanium oxide ($Li_4Ti_5O_{12}$/LTO) for the anode, and lithium cobalt oxide ($LiCoO_2$/LCO) or lithium iron phosphate ($LiFePO_4$/LFP) for the cathode [5, 28]. These materials are a source of concern because they contain (eco)toxicologically relevant elements

such as lithium, cobalt, iron and nickel [26, 28]. LIB particulate components are poorly water soluble and micrometric in size, suggesting that they might be respirable and biopersistent in the human respiratory tract. Currently, exposure to LIB components is potentially the most worrying for workers who produce and handle LIB particles, but future applications of LIB, such as multi-layer systems made for spray-paintable or printable batteries [15, 17, 18], could increase the potential for inhalation exposure, including for consumers. The high disposal rate of LIB and the current lack of strict regulatory policy may also lead to the dispersion of battery components in the environment and to a risk for the general population and the environment [28]. Thus, LIB particles might represent a possible inhalation risk for humans, similar to other insoluble micrometric particles or fibres inducing chronic lung inflammatory and fibrotic reactions [61, 235].

Existing knowledge on the toxicity of lithium compounds is sparse, and almost limited to systemic side effects recorded at high dose in bipolar patients treated orally with Li salts who can develop thyroid, neurological and heart toxicity [157]. LiCl inhalation induced no respiratory toxicity in rabbits [162] and Li combustion aerosols caused moderate lung inflammation in rats [160, 236]. *In vitro*, low cytotoxicity and the secretion of the pro-inflammatory cytokine, interleukin (IL) -8, were observed in epithelial cells in response to LCO microparticles [33]. In addition to Li, other LIB metallic constituents could cause toxicity. Fe and Co can cause chronic lung inflammation [165, 237]. Lung fibrosis was also observed after exposure to Co compounds [238]. Moreover, Fe and Co ions are potent inducers of oxidative stress [175], one of the major mechanisms incriminated in particle toxicity.

In view of the increasing production, use, disposal and almost absence of toxicological data on LIB particles, information is urgently needed to better control possible health risks. Here, we evaluated, for the first time, the lung toxicity of 3 leading LIB particles (LFP, LTO, and LCO). We investigated their respective mechanisms of action to identify critical particle characteristics and key events useful for a safer-by-design and sustainable development of LIB.

3.1.3 Methods

Particles

LIB particles ($LiFePO_4$ or LFP, $Li_4Ti_5O_{12}$ or LTO, and $LiCoO_2$ or LCO) were obtained from MTI Corporation (Richmond, USA), lithium chloride (LiCl 730 36) from Sigma-Aldrich (Missouri, USA) and micrometric crystalline silica particles (Min-U-Sil 5, d_{50} 1.6 µm) from US Silica (Berkley Springs, USA). Before all experiments, LIB and silica particles were heated 2 h at 200 °C to remove possible endotoxin contaminants.

Animals and treatments

Female C57BL/6 mice were purchased from Janvier Labs (St Bertevin, France) or obtained from the local breeding facility (Animalerie Centrale, Université catholique de Louvain, Brussels, Belgium). Eight-week-old animals were kept with sterile rodent feed and acidified water, and housed in positive-pressure air-conditioned units (25°C, 50 % relative humidity) on a 12h light/dark cycle. Particles and other compounds were suspended in sterile 0.9 % saline solution. After anaesthesia with a mix of Nimatek, 1 mg/mouse (Eurovet, Bladel, Nederland) and Rompun, 0.2 mg/mouse (Bayer, Kiel, Germany) given intraperitoneally, 50 µl suspensions of LIB particles, silica, LiCl or NaCl (control groups) were directly administered by oro-pharyngeal aspiration. Single dose administration of particles is validated as a convenient alternative to inhalation exposure for initial hazard identification (Sabaitis et al. 1999; Driscoll et al. 2000) and induces similar lung responses as inhalation exposure [239, 240]. Mice were sacrificed 18 hours, 3 days and 2 months after administration with an intraperitoneal injection of 12 mg sodium pentobarbital (Certa, Braine-l'Alleud, Belgium).

Broncho-alveolar lavage and lung sampling

Broncho-alveolar lavage (BAL) was performed by cannulating the trachea and infusing the lungs with 1 ml NaCl 0.9 %. Whole lungs were then perfused with NaCl 0.9 % and excised. Left lobes were placed in 3.65 % paraformaldehyde (Sigma-Aldrich, St Louis, Missouri, USA) in phosphate buffered saline (PBS) for later histological analysis, and remaining lobes in liquid nitrogen or lysis buffer for

homogenization. Lungs were homogenized on ice with an Ultra-Turrax T25 (Janke and Kunkel, Brussels, Belgium) and stored at -80°C. Particle biopersistence was assessed by inductively coupled plasma mass spectrometry (ICP-MS), time-of-flight secondary ion mass spectrometry (ToF-SIMS), scanning electron microscopy/energy dispersive X-ray spectrometry (SEM-EDX) and X-ray micro fluorescence (μ-XRF). BAL were centrifuged 10 min at 4°C (240 *g*). Cell-free supernatant (BALF) was used for biochemical measurements. After resuspension in PBS, total BAL cells were counted in Turch (crystal violet 1 %, acetic acid 3 %) and cytocentrifuged for differentiation by light microscopy after Diff-Quick staining (200 cells counted, Polysciences, Warrington, UK). Total proteins and lactate dehydrogenase (LDH) activity were assayed on BALF as described previously [231].

Quantification of cytokines, HIF-1α, HO-1 and lung collagen

IL-1β, IL-6, tumor necrosis factor (TNF) -α, IL-1α, transforming growth factor (TGF)-β1 and platelet-derived growth factor (PDGF)-bb were quantified by enzyme-linked immunosorbent assay (ELISA) (DuoSet ELISA, R&D Systems, Minneapolis, USA) in BALF following manufacturer's instructions. Hypoxia-inducible factor (HIF) -1α (DuoSet ELISA, R&D Systems) and heme oxygenase (HO)-1 (Immunoset, Enzo Life Sciences, Lausen, Switzerland) were assessed in supernatant (SN) of lung homogenates (centrifuged 10 min at 240 *g*, 4°C) following manufacturer's instructions. Collagen deposition was assessed by measuring the OH-proline content in lung homogenates by high-pressure liquid chromatography analysis on hydrolyzed lung homogenates as previously described [241].

Histology

Paraffin-embedded lung sections were stained with Masson's trichrome blue (total collagen staining), Sirius Red (type I collagen staining) or Perl's Prussian blue (Fe^{3+} staining). The stained sections were scanned (Leica SCN400, Brussels, Belgium) and examined with Tissue Image Analysis 2.0 (Leica Biosystems).

Particle solubilization

To assess the bioaccessibility of elements contained in LIB particles, 10 mg LIB particles and LiCl were incubated in 10 ml artificial fluids mimicking the extracellular (pH 7.3) and the phagolysosomal (pH 4.2) compartments as previously described [242]. Particles were incubated during 30 d (at 37°C) under gentle agitation. One ml aliquots were collected after 3 h, 24 h, 7 d and 30 d and centrifuged (20000 *g*, 10 min). Li, Fe, Ti and Co concentrations were determined in the SN by ICP-MS.

Particle characterization

The mass median geometric particle diameter (d_{50}) of the particles was measured by laser diffraction. The principle of laser diffraction of the Sympatec apparatus is Fraunhofer (Washington 2007). Measurements were made both in suspension in cyclohexane or in dry state. In the dry state mode, the powders were dispersed with compressed air at a pressure of 3 bars through a Venturi tube (RODOS, Sympatec GmbH, Clausthal-Zellerfelg, Germany) before sizing with a laser diffractometer (HELOS, Sympatec). In the wet state mode, the samples were suspended in cyclohexane in a 50 ml glass cuvette and stirred with a magnetic bar at 1000 rpm (CUVETTE, Sympatec). The particle size was measured immediately after suspension. For both methods, a R2 lens allowing measurements in the range of 0.25-87.5 µm was used. The particle size analysis was performed by the WINDOX 3.4 software (Sympatec) and the mass median particle diameter was taken into account [243].

The powder density (ρ) was determined by tap density measurements, i.e. following 1000 taps which allowed the density to plateau [244].

To assess the *in vitro* pulmonary deposition of the powders, hard gelatin capsules (capsugel, Bornem, Belgium), previously stored in a dessicator for at least two days, were filled to approximately 50 % of their volume with the powders. Capsules were placed in a Spinhaler dry powder inhaler (Fisons, Bedford, MA) and the released powder drawn through an Andersen cascade impactor (1 ACFM Eight Stage Non-Viable Cascade Impactor, Graseby Andersen, Atlanta, USA) operated at a flow rate of 28.3 L/min for 9 s [245]. The amount of powder deposited on each stage of the

impactor was determined by measuring the difference in weight of the filters (Graseby Andersen) placed on the different trays. Measurements were made under controlled laboratory relative humidity (30-40 %). The cumulative fraction of powder versus cut-off diameter of each stage of the Andersen impactor was plotted on a log probability scale. The experimental mass median aerodynamic diameter (MMADe) of the particles is defined from this graph as the particle size at which the line crosses the 50 % mark. The fine particle fraction (FPF) was calculated by interpolation from the same plot as the fraction of powder loaded in the inhaler device with an aerodynamic diameter ≤ 5 µm [245].

Particle composition and presence of contaminants were determined by ICP-MS. Particles were mineralized in acid (5 ml HNO_3 65 % and 3 ml HCl 30 %) during 24 h at 60°C. After total evaporation, residues were suspended in 5 ml HNO_3 0.05 N and analyzed by ICP-MS using a collision cell in helium mode and Rh as internal standard.

Biopersistence of LIB particles

Lung homogenates were mineralized as described above and the Li, Fe, Ti and Co contents were determined by ICP-MS. Localization of particle elements in the lung was studied by scanning electron microscopy/energy dispersive X-ray spectrometry (SEM-EDX), X-ray micro fluorescence (µ-XRF) and time-of-flight secondary ion mass spectrometry (ToF-SIMS). For SEM-EDX, 5 µm-thick lung sections embedded in paraffin and deposited on glass slides were coated with carbon by evaporation of graphite fibre with an evaporater (Balzers SCD 030, Liechtenstein). A high resolution field emission scanning electron microscope (Zeiss FEGSEM Ultra55, Carl Zeiss SMT, Marly le Roi, France) was used to observe the particles in the lung structure. Images were obtained using an acceleration voltage of 15 KV and recorded using a Secondary Electron (SE2) or Angle selective Backscattered Electron (AsB) detector. EDX spectrometry (Bruker Nano Quantax, Synergie^4, Evry, France), equipped with a Silicon Drift Detector, was used to identify the elemental composition of the particles. EDX spectra were obtained for individual particles and mapping of elemental spatial distributions were recorded for each sample on representative areas.

Chemical mapping of paraffin-embedded lungs was performed by µ-XRF. This technique allows a deeper analysis into the tissue with a high sensitivity. Measurements were carried out on a microscope (XGT7000, Horiba) equipped with a focused X-ray source (incident beam spot of 100 µm produced with a Rh-tube, accelerating voltage of 30 kV and current of 1 mA) and an EDX spectrometer. As the incident X-ray beam penetrates through the sample, the obtained element maps are 2D projections of the 3D analyzed sample. Chemical maps of 128 pixels with a pixel size of 76 µm and a total counting time of 8x1000 s were recorded to show the distribution of Fe, Co, Ti, P and S from Kα emission lines.

ToF-SIMS spectra and images were recorded by using an IONTOF V instrument (IONTOF GmbH, Münster, Germany). This technique allows to analyze sample surface with a high spatial resolution. Before analysing the samples, a pre-cleaning of the measured surfaces was done by an Ar gas cluster ion beam (Ar-GCIB) used as sputtering source. The Ar-GCIB ion source was operated at 10 keV with a direct current of 4 nA. The Ar-GCIB cluster distribution was centered on Ar_{3000}^{+}. For the pre-cleaning of the surface, the focused Ar-GCIB beam of primary ions was rastered over an area of 1000 x 1000 μm^2. The total pre-cleaning dose was 10^{15} $Ar_{3000}^{+}.cm^{-2}$. Then, a Bi_3^{++} liquid metal ion source was used to produce the analytical primary beam (energy 60 keV). An pulsed target current of 0.003 pA was used with the analytical burst mode (1 pulse selected with the sine blanker). Only positive secondary ion species were analyzed. A raster of 2048 x 2048 data points over an area of 500 x 500 μm^2 was used in the centre of the sputter crater. The total primary ion beam dose for each analyzed area was always kept below 10^{10} ions.cm^2, ensuring static conditions. Lateral resolution of 0.3 µm and mass resolution m/Δm >3000 at 29 m/z were maintained for acquisition of both images and corresponding spectra for positive ions. Charge compensation was done by electron flood gun (E_k = 20 eV). Data processing was carried out using the software supplied by the instrument manufacturer, SurfaceLab (version 6.5).

Statistics

Graphs and statistical analyses were performed with GraphPad Prism 5.0 and/or Microsoft excel 2013. All results are expressed as mean ± standard error on the

mean (SEM). Differences between control and treated groups were evaluated using one-way analysis of variance (ANOVA) followed by a Dunnett's multiple comparison or a Newman-Keuls multiple comparison test. Statistical significance was considered at $P < 0.05$.

3.1.4 Results

Particle characterization

Scanning electron microscopy (SEM) (**Table 1**) indicated that LIB particles are micrometric in size. LFP and LTO mainly consist of aggregates, contrary to LCO.

Mass median particle geometric diameter (d_{50}) measured by laser diffraction in cyclohexane were between 4 and 8 µm, with LFP=LTO<LCO. Measurements in dry state indicated strongly increased d_{50} for LFP and LTO, confirming that LFP and LTO particles form large aggregates in powder form, contrary to LCO. Particle size distributions are shown in Annexes (**Figure S1**).

LCO was approximately 3-fold denser than LFP and LTO. The Andersen cascade impactor showed that the experimental mass median aerodynamic diameter (MMADe) were similar among the 3 particles and that all samples presented a significant respirable or fine particle fraction (FPF, aerodynamic diameter ≤ 5µm) that can reach the deep lung when inhaled. LCO contained approximately 4 times more respirable particles than LFP or LTO. Low percentages of contaminants were detected by ICP-MS (Mn and Cu in LFP and LTO, respectively). Energy dispersive X-ray spectrometry (EDX) analysis confirmed the presence of Cu in LTO.

Table 1 LIB particle characterization.

	LFP	LTO	LCO
Morphology [a]	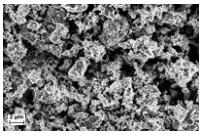	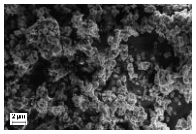	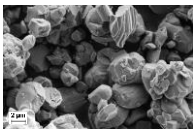
d_{50} (µm) [b]	4.66 ± 0.56*	4.75 ± 0.05#	8.04 ± 0.17
d_{50} (µm) [c]	28.02 ± 8.91*	25.23 ± 1.15#	6.73 ± 0.59
Density (g/cm^3) [d]	0.85	0.71	2.37
MMADe (µm) [e]	8.20 ± 0.57$	13.81 ± 2.91	9.93 ± 2.27
FPF (% of total weight) [f]	1.93 ± 1.48*$	1.23 ± 1.39#	7.21 ± 1.55
C (%) [g]	Mn 0.255 ± 0.013	Cu 1.551 ± 0.124	n.d.
Composition [h]	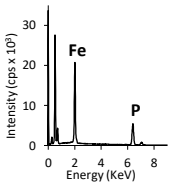	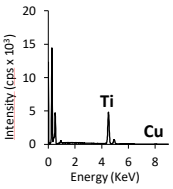	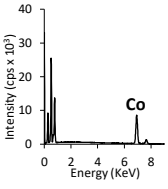

[a] Images of LIB particles obtained by SEM.

[b] Mass median particle geometric diameter (d_{50}) measured by laser diffraction in cyclohexane.

[c] d_{50} measured by laser diffraction in dry state.

[d] Density measured by powder tap density.

[e] Experimental mass median aerodynamic diameter (MMADe) determined with an Andersen cascade impactor.

[f] Fine particle fraction (FPF, ≤ 5 µm) determined with an Andersen cascade impactor.

[g] Contaminant concentration (C) in mass % of LIB particles, measured by ICP-MS.

[h] Particle composition obtained by EDX.

One-way ANOVA followed by a Newman-Keuls multiple comparison, $P < 0.05$, *LFP vs LCO, # LFP vs LTO, $ LTO vs LCO, n.d. not detected (n = 2 or 3, means ± SEM).

Bioaccessibility of metallic elements in LIB particles

To assess the release of ions from LIB particles, we analyzed their bioaccessibility in artificial fluids mimicking the extracellular (pH 7.3) and the phagolysosomal (pH 4.2) compartments over a period of 30 d.

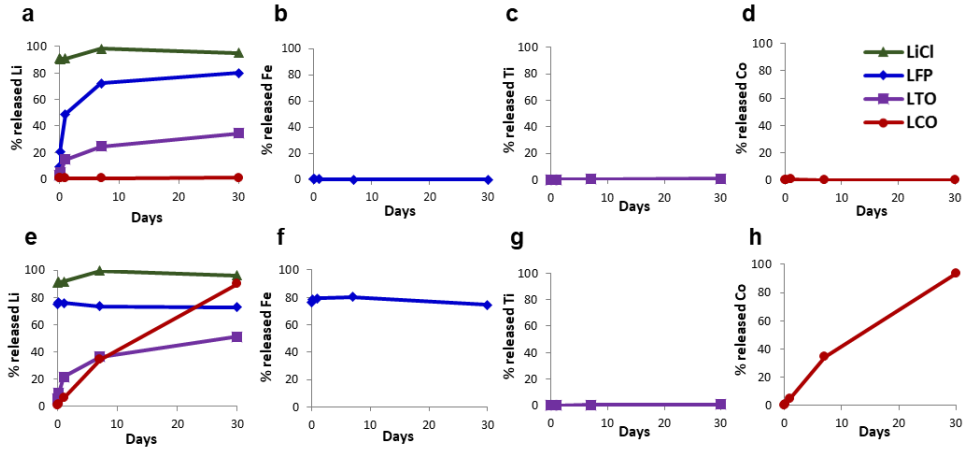

Figure 11: Bioaccessibility of constitutive elements from LIB particles. LIB particles and LiCl were incubated in artificial fluids mimicking the extracellular (pH 7.3) (**a-d**) and the phagolysosomal (pH 4.2) (**e-h**) compartments. Particles were incubated at 37°C under gentle agitation and released Li (**a, e**), Fe (**b, f**), Ti (**c, g**) and Co (**d, h**) concentrations were determined by ICP-MS in the SN after centrifugation of an aliquot of the suspensions after 3 h, 24 h, 7 d and 30 d.

Figure 11 illustrates the rate of ion release from particles, expressed as percent of initial content. As expected, LiCl was immediately and totally soluble in the tested media (**Figure 11 a, e**). The release of Li ions at pH 7.3 was time-dependent for LFP and LTO, whereas LCO released very low Li levels. The Fe release pattern for LFP was similar to Li at pH 4.2 (**Figure 11 e-f**) but not in neutral conditions, where very low Fe was released (**Figure 11 a-b**), suggesting that Fe ions are mainly released in the phagolysosomes. Ti was poorly bioaccessible from LTO in any condition (**Figure 11 c, g**), as expected from TiO_2-containing particles [246]. Finally, LCO was preferentially solubilized at acidic pH. The release of Li followed the Co release under neutral and acidic conditions (**Figure 11 a, d, e, h**).

LIB particles induce varying acute inflammatory responses in the lung

The lung response to LIB materials was assessed in a mouse bioassay with crystalline silica particles used as reference material. In this bioassay, inflammatory and fibrotic responses are recorded with a dose of 2 mg crystalline silica particles administered via oro-pharyngeal aspiration [230]. LIB particles were tested at doses of 0.5 and/or 2 mg to allow benchmarking of their respiratory toxicity relative to crystalline silica particles.

After 3 days, exposure to LFP, LCO and silica resulted in acute inflammatory responses (**Figure 12**). LCO induced the strongest increase in cytotoxicity (LDH activity), alveolo-capillary *permeability* (total proteins), inflammatory cell recruitment (macrophages and neutrophils) and secretion of pro-inflammatory mediators (IL-1β and IL-6), also compared to silica. TNF-α and IL-1α were at the control level or lower. LFP increased macrophages, TNF-α and IL-1α and LTO had no or weak effects. The expression of HO-1, a marker of oxidative stress [247], was upregulated by all LIB particles and silica (silica<LTO<LFP<LCO).

To assess the activity of Li ions present in all LIB particles, mice were exposed to LiCl (0.85 mg) at a Li dose equimolar to 2 mg LCO which has the highest relative Li content (4.4 %, 6 % and 7.1 % Li in LFP, LTO and LCO, respectively). No effect was noted 18 hours after LiCl (**Annexes, Figure S2**), suggesting that Li ions have no pro-inflammatory activity in and/or are rapidly eliminated from the lung. Differential inflammatory responses to LIB particles were also recorded after 18 hours. Thus, LFP, LTO and LCO can induce acute lung inflammatory reactions of varying intensities, associated with different patterns of pro-inflammatory cytokines and oxidative stress.

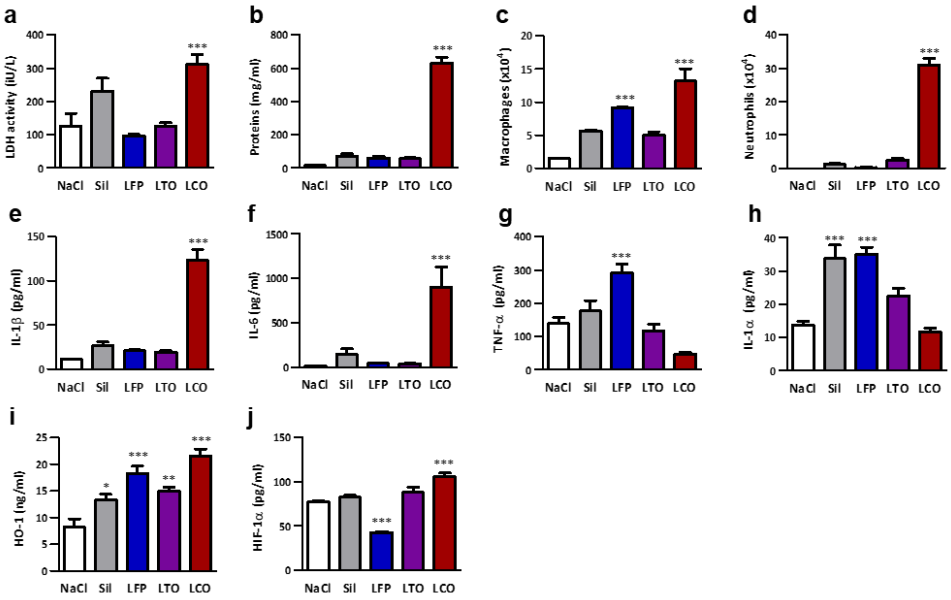

Figure 12: LIB particles induce varying inflammatory responses after 3 days. C57BL/6 mice were exposed by oro-pharyngeal aspiration to NaCl (control), 2 mg LIB particles or crystalline silica (Sil). Inflammation was assessed in the BAL after 3 days. LDH activity (a) and proteins (b) were measured in BALF; macrophages (c) and neutrophils (d) in BAL. Inflammatory cytokines IL-1β (e), IL-6 (f), TNF-α (g) and IL-1α (h) were quantified by ELISA in the BALF; HO-1 (i) and HIF-1α (j) in lung homogenates. *P < 0.05, **P < 0.01 and ***P < 0.001 relative to NaCl-treated mice (one-way ANOVA followed by a Dunnett's multiple comparison, n = 5, means ± SEM).

LCO induces sub-chronic inflammatory and fibrotic lung responses

Sub-chronic inflammatory and fibrotic lung responses were assessed 2 months after administration of 2 mg LIB particles, silica, or 0.85 mg LiCl (**Figure 13**).

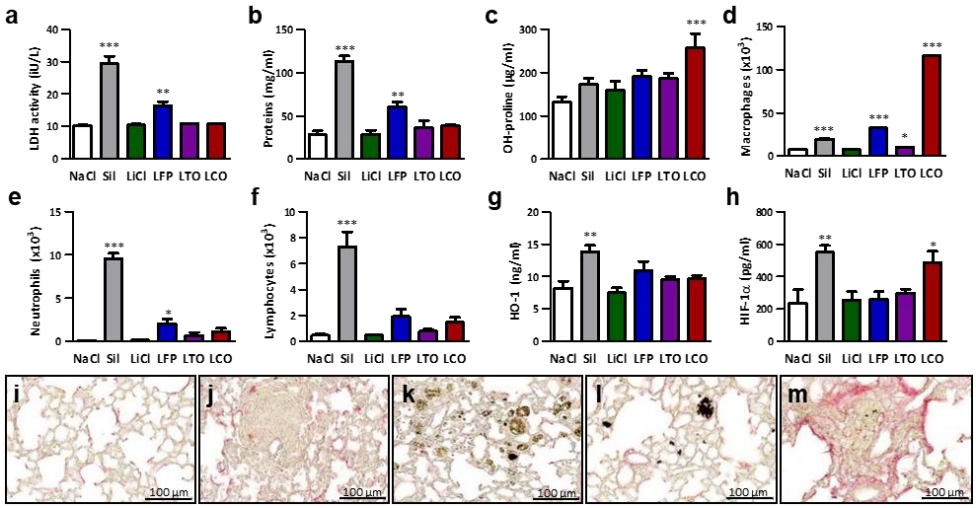

Figure 13: **Sub-chronic inflammatory and fibrotic responses to LIB particles**. C57BL/6 mice were exposed by oro-pharyngeal aspiration to NaCl (control), 2 mg LIB particles or crystalline silica (Sil), and 0.85 mg LiCl. Mice were sacrificed after 2 months. Inflammation was assessed in the BAL. LDH activity (**a**) and proteins (**b**) were measured in BALF; macrophages (**d**), neutrophils (**e**) and lymphocytes (**f**) in BAL; OH-proline (**c**), HO-1 (**g**) and HIF-1α (**h**) in lung homogenates. Lung sections from mice exposed to NaCl (**i**), silica (**j**), LFP (**k**), LTO (**l**), LCO (**m**) were stained with Sirius Red. *P < 0.05, **P < 0.01 and ***P < 0.001 relative to NaCl-treated mice (one-way ANOVA followed by a Dunnett's multiple comparison, n = 5, means ± SEM).

LDH activity and total proteins were still increased 2 months after silica and LFP. LCO induced a stronger macrophage recruitment in the alveoli compared to silica and other LIB particles while BAL neutrophils and lymphocytes were strongly increased by silica and weakly by LFP. Pro-inflammatory (IL-1β, IL-6 and IL-1α) and pro-fibrotic (TGF-β1 and PDGF-bb) cytokines in the BALF and/or lung homogenates were not increased after LIB particles (data not shown, TGF-β1 was increased by silica). LiCl and LTO had no or a weak effect on inflammatory markers. Only silica significantly increased HO-1. Accumulation of lung collagen was assessed by measuring total lung OH-proline content. OH-proline levels were only increased

significantly after LCO. Lung sections stained with Sirius Red showed accumulated collagen in lungs treated with silica and LCO (**Figure 13 j, m**). Focal collagen accumulation, lymphoid nodules and macrophage accumulation were observed in mouse lungs 2 months after silica (**Figure 13 j**). Similarly, numerous lymphoid nodules around the bronchioles with focal collagen and macrophage accumulation were observed in mouse lungs after LCO (**Figure 13 m**). In LFP lungs, many macrophages loaded with particles (**Figure 13 k**) and some lymphoid nodules were observed. Compared to controls (NaCl), no overt signs of inflammation or alteration of the lung structure was observed in LTO-treated lungs (**Figure 13 l**). Numerous black spots of particle aggregates/agglomerates were observed by light microscopy, while very few particles were visible in LCO lungs probably because these particles do not form aggregates (**Table 1**). Overall, LCO induced a stronger sub-chronic inflammation than LFP and LTO, together with a fibrotic response. The fact that no reaction was detected after LiCl, together with the observation that LIB particles induced varying patterns and intensities of lung responses, further indicated that Li content is not a determinant of the lung toxicity of LIB particles. It also suggested that different mechanisms of action are involved for each LIB particle.

LIB particles persist in mouse lungs 2m after administration

To further assess lung particle biopersistence, elements constitutive of LIB particles were first quantified by ICP-MS in lavaged lungs 18 hours and 2 months after administration. After 18 hours, the fraction of retained Li was higher after LCO compared to LFP and LTO (**Annexes, Figure S3, a**). Fe, Ti and Co were also detected in LFP, LTO and LCO lungs, respectively (**Annexes, Figure S3 b-d**). Retention of Li and Co was similar in LCO lungs, suggesting that intact LCO particles persisted. Ti levels were much lower than Li in LTO lungs probably because the preparation of the lung samples did not allow to completely mineralize Ti [246]. No Li was measured in LiCl lungs, indicating that this element is quickly eliminated from the lungs. In 2 months lungs, concentrations of Li were below the limit of detection for all particles and low levels of Fe (4.5 %), Ti (0.18 %) and Co (0.33 %) were still detected in LFP, LTO and LCO lungs, respectively (data not shown).

The persistence and localization of LIB particles, or at least their elements, were then analyzed qualitatively by different techniques. A ToF-SIMS cartography on lung sections 2 months after administration revealed Li and Fe in LFP-treated lungs, Li and Ti in LTO-treated lungs and Li in LCO-treated lungs (**Annexes, Figure S4**).

Fe, Ti and Co, but not Li, could be detected on lung sections by SEM-EDX. Scanning of lung sections 2 months after administration revealed brilliant zones attributed to the presence of LIB particles (**Annexes, Figure S5**). Fe and P were detected by EDX in these zones in the lungs of LFP-treated mice, Ti in LTO-treated lungs and Co in inflammatory lung areas of LCO-treated mice. A chemical mapping of these areas was then performed (**Figure 14**).

In LFP-treated lungs, Fe co-localized with P, showing that it was still associated with the phosphate groups. Ti was detected in LTO lungs, together with Cu (data not shown) present in particles alone (**Table 1**). Co was detected in inflammatory/fibrotic areas of LCO lungs. A broader cartography was performed on paraffin-embedded lungs by µ-XRF. The presence of LIB particle elements in extensive areas of the lung was confirmed with a heterogeneous distribution and high-spots (**Annexes, Figure S6**). The overall results indicated that LFP, LTO and LCO persisted in the lungs.

SEM-EDX and µ-XRF analyses also showed that some Fe co-localized with Co in LCO lungs 2 months after administration (**Figure 14 n and Annexes, Figure S6**). No Fe was, however, present in original particles alone (**Table 1**) or after 18 hours (**Figure 14 s**), thus suggesting a progressive deposition of endogenous Fe on the LCO particles. This was not observed with LTO and could not be assessed for LFP because of the constitutive Fe content. These observations suggested the formation of ferruginous bodies (FB) similar to those observed after asbestos exposure [248]. The distribution of Fe(III) (in blue) in lung sections exposed to LIB particles after 2 months was assessed by Perl's Prussian staining (**Figure 14 e, j, o, t**). Iron was detected in LFP lungs, probably due to the iron content of the particles, and in the inflammatory areas of LCO lungs. No iron staining was detected in silica (data not shown) and LTO (**Figure 14 n**) lungs.

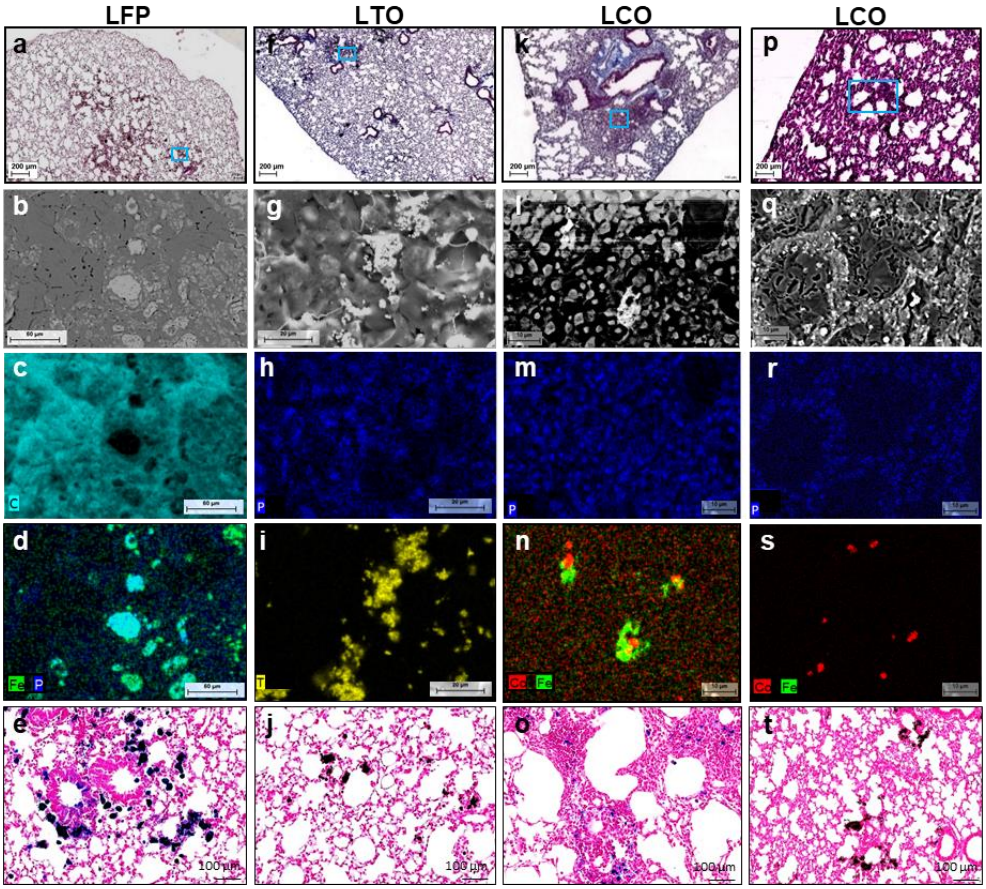

Figure 14: Localization of LIB particle elements in lung sections by SEM-EDX after 2 months. Lung sections from mice exposed to 2 mg LFP (**a-e**), LTO (**f-j**) or LCO (**k-o**) were analyzed after 2 months (**a-o**) and 18 hours (**p-t**). Lung sections were stained with Masson's Trichrome blue (**a, f, k, p**), scanned by SEM (**b-d, g-i, l-n, q-s**) and analyzed by EDX (**c, d, h, l, m, n, r, s**). Areas in blue squares (**a, f, k, p**) were zoomed and contain brilliant spots attributed to the presence of LIB particles. EDX maps show the distribution of Fe and P in LFP- (**d**), Ti in LTO- (**i**) and Fe and Co in LCO-treated lungs after 2 months (**n**) and the distribution of Co in LCO-treated lungs after 18 hours (**s**). C and P distributions represent the lung matrix (**c, h, m, r**). Lung sections were stained with Perls' Prussian blue. Fe^{3+} appears in blue in LFP (**e**) and LCO (**o**) lungs after 2 months. Black spots in LTO lungs (**j**) are attributed to particles alone. After 18 hours, no Fe^{3+} appears in LCO lungs (**t**).

In vivo bioavailability of LIB particle elements

The *in vivo* bioavailability of LIB metallic elements was investigated by measuring soluble elements in the BALF 18 hours, 3 days and 2 months after administration. LFP released more Li in the BALF after 18 hours and 3 days (**Figure 15 a, e**) than LTO and LCO, which was in agreement with the bioaccessibility data in artificial fluids (**Figure 11 a, e**). Fe, Ti and Co were also detected in the BALF after 18 hours and 3 days (**Figure 15 b-c, f-h**) and, like Li, the % of Fe was higher in LFP BALF than Ti and Co in LTO and LCO BALF, respectively. After 2 months, low but significant levels of Li and Fe were still detected after LFP, and Co after LCO (**Figure 15 i-l**). These *in vitro* and *in vivo* data indicate that, in the lungs, LFP and LCO continuously release Fe and Co, respectively.

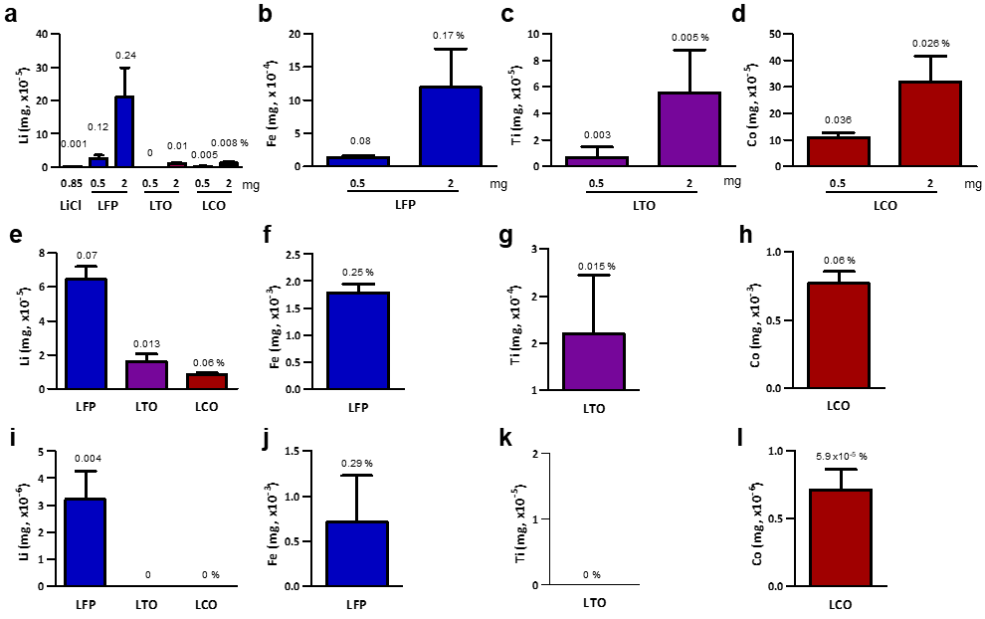

Figure 15: Bioavailibility of LIB particle elements. BALF of C57BL/6 mice exposed to NaCl, 0.85 mg LiCl, 0.5 and/or 2 mg LIB particles by oro-pharyngeal aspiration were analyzed after 18 hours (**a-d**), 3 days (**e-h**) or 2 months (**i-l**). Li (**a, e, i**), Fe from LFP **(b, f, j**), Ti from LTO (**c, g, k**) and Co from LCO (**d, h, l**) particles were measured by ICP-MS. Percentages were calculated on the basis of initial Li, Fe, Ti, Co particle content after subtraction of levels measured in NaCl-treated lungs (n = 5, means ± SEM).

Cobalt-like responses after exposure to LCO

Because of the known pulmonary toxicity of cobalt [168] and the release of Co from LCO, we investigated the implication of this element in LCO lung responses by measuring HIF-1α in mouse lungs after 3 days and 2 months. HIF-1α is stabilized and accumulates in cells in response to hypoxia or Co ions [168]. The quantification of its accumulation in lungs was used as a marker of the biological activity of Co ions. Contrary to LFP and LTO, LCO increased HIF-1α after 3 days and 2 months (**Figure 12 j and Figure 13 h**). Silica also increased HIF-1α after 2 months.

3.1.5 Discussion

We showed here, for the first time, that industrial LIB particles are respirable in size and can induce lung inflammatory responses with varying intensities. LTO induced a weak acute inflammation, LFP and LCO induced an acute and sub-chronic inflammation and only LCO led to fibrotic responses. The potency of LCO to induce inflammatory and fibrotic responses was at least of the same order as that of crystalline silica particles, suggesting that occupational exposure to this material should be kept below acceptable levels for crystalline silica, e.g. below 0.05 mg/m³ for the respirable fraction (SCOEL SUM/94 2003).

LIB particles induced an acute inflammatory response (including IL-1β, IL-6, TNF-α and IL-1α cytokines) and only LCO induced fibrosis and lymphoid nodules. Inflammatory responses play pivotal roles in pulmonary diseases induced by inhaled particles, including fibrosis [47, 249] and, therefore, might be involved in LIB toxicity. However, LCO did not exactly induce the same inflammatory pattern as silica.

Although *in vitro* solubilisation and ToF-SIMS data support the slow release and prolonged presence of Li in the lungs exposed to LIB particles, no evidence was recorded that Li ions could be involved in the lung toxicity of LIB particles. LiCl did not induce any inflammation *in vivo*, even as early as 18 hours after administration, as previously observed in rabbits [162]. No Li was detected in the lung at the same time point after administration of LiCl, suggesting that Li ions are rapidly washed out from the lung. Finally, the varying responses to the 3 Li-containing particles

(LFP, LTO and LCO) in the mouse bioassay does not argue in favour of a critical role of Li in LIB lung toxicity.

LTO particles induced an acute inflammation and persisted in mouse lungs 2 months after administration but no inflammation or fibrosis was detected at this time point. The low toxicity of LTO can be attributed to its TiO_2 content [250] which is considered a low toxicity material. Inhalation of TiO_2 appears to induce low acute inflammation and no fibrosis [88, 251], which is in agreement with our observations.

Inflammatory responses and persisting particles in the lung interstitium were observed 2 months after administration of LFP. Inhalation of iron compounds can lead to siderosis, a benign pneumoconiosis with little or no fibrosis [203]. However, free Fe in excess catalyses free radical formation, which induces cytotoxicity and oxidative stress, leading to cellular damages, carcinogenicity and mutagenicity [237] as also reported for particles such as asbestos [252]. Our data showed that LFP can release Fe ions *in vivo* and *in vitro* and increase the expression of HO-1. The transient pulmonary inflammation induced by LFP can thus be explained by its Fe content.

LCO particles appeared more potent than LFP and LTO. Administration of LCO induced acute and sub-chronic lung inflammation, and fibrosis in mice. In addition to pro-inflammatory mediators and structural modifications observed in the lungs exposed to LCO particles, these effects were accompanied by the persistence of their constitutive elements (Li and Co), the presence of FB, the increase of HO-1 and accumulation of HIF-1α. Pulmonary diseases (cancer, asthma and fibrosing alveolitis) have previously been reported in workers exposed to cobalt [175, 238]. A well-documented example of fibrosis caused by Co is due to the association of tungsten carbide with Co metal powder [253]. Cobalt compounds can also induce cytotoxicity, apoptosis, inflammatory responses and genotoxicity *in vitro* [168]. Some of the effects of cobalt are related to its high affinity for sulfhydryl groups leading to enzyme inactivation, to its antagonism for Ca^{2+} channel modifying cell signalling, to its production of reactive oxygen species leading to an oxidative stress, and finally to its ability to stabilize HIF-1α [168]. The two latter mechanisms were

identified with LCO, suggesting that Co plays an important role in LCO lung toxicity. HO-1, a robust oxidative stress marker, was increased 3 days after LCO, suggesting that LCO can induce an oxidative stress in mouse lungs. The fact that only LCO induced the accumulation of HIF-1α contrary to LFP and LTO highlights the importance of cobalt in LIB particle toxicity.

Iron co-localized with Co in mouse lungs 2 months after administration of LCO, suggesting the formation of FB. FB are particles or fibres coated with proteins and iron from the endogenous milieu [254] and were detected in lungs exposed to asbestos fibres [255]. LCO-induced lung inflammation could cause the disruption of iron lung homeostasis as observed during infection and inflammation [256, 257] and lead to the local increase of particle-associated iron. FB are thought to participate to lung toxicity, including fibrosis, by catalysing Fenton reactions and free radical generation [248, 254, 258]. This phenomenon could thus contribute, together with Co ions, to the elective lung toxicity of LCO. The oxidative potential of LCO particles, as well as the contribution of FB in this process, must be the subject of additional investigations.

As previously mentioned, only LCO induced HIF-1α accumulation reflecting the intensity of its pulmonary toxicity as compared to other LIB particles. HIF-1α is a pro-inflammatory and carcinogenic transcriptional factor continuously expressed in all cells. Under normoxic conditions, HIF-1α is directly degraded by the ubiquitin-proteasome pathway, via a prolyl hydroxylase (PH). However, under hypoxic conditions, HIF-1α is stabilized and accumulates in the cell [140, 259]. Co(II) ions are also able to stabilize HIF-1α by blocking the iron-binding site of PH and by direct binding to HIF-1α preventing its degradation [136, 137]. HIF-1α plays many roles in inflammation and induces the secretion of inflammatory mediators [140]. Its expression is also increased in animal models of bleomycin- and paraquat- induced lung fibrosis and in idiopathic lung fibrosis patients [134, 147]. In addition, we have shown here that HIF-1α is accumulated during the fibrotic phase of the silica model, reinforcing the association between this mediator and fibrosis. HIF-1α plays a role in fibrosis by promoting myofibroblast differentiation and epithelial-mesenchymal transition via the TGF-β pathway [147, 150, 151]. HIF-1α thus appears as a very useful biomarker of LCO particle toxicity as it not only allows tracing the

bioavailability of Co ions, but could also contribute mechanistically to the inflammatory and fibrotic responses induced by LCO. Interestingly, although some studies showed that the HO-1 response can increase HIF-1α expression [140, 247], LFP upregulated HO-1 but did not increase HIF-1α.

In addition to the potential mechanisms identified above for LCO lung toxicity, it should be noted that LCO contains the highest FPF and forms less aggregates than LFP and LTO, as indicated by the SEM images and the laser diffraction analysis in dry state (**Table 1**). Furthermore, many aggregates were observed in LFP and LTO lung sections 2 months after exposure contrary to LCO (**Figure 13 k-m**). Given that particle size and formation of aggregates can modulate their reactivity toward cells and tissues [258], it is very likely that these parameters also contribute to the elective toxicity of LCO by a more efficient dispersion and bioavailability of LCO particles/elements in the lung.

Thus, LCO was able to induce early oxidative stress responses, secretion of inflammatory mediators and HIF-1α accumulation. These responses are, at least partially, attributed to the Co content of LCO. Although it appears premature to conclude on the exact sequence of events, the formation of FB appears to be a consequence of the early inflammatory responses to LCO. Taken together, particle size distribution, Co ions/HIF-1α and ferruginous bodies/oxidative stress could represent the pathogenic cocktail responsible of the elective lung toxicity of LCO particles in the present study.

We conclude that LIB particles represent a respiratory hazard. Exposure to LIB particles should, therefore, be strictly controlled in occupational settings, and the life cycle of these components should be adequately monitored to avoid environmental pollution and indirect exposure of consumers and the general population.

3.1.6 Declarations

Ethics approval and consent to participate

All applicable international, national institutional guidelines for the care and use of animals were followed. All procedures performed in studies involving animals were in accordance with the ethical standards of the institution (Université catholique de Louvain, Comité d'Ethique pour l'Expérimentation Animale, Secteur des Sciences de la Santé, Brussels, Belgium (No LA1230312)) or practice at with the studies were conducted. This article does not contain any studies with human participants performed by any of the authors.

Consent for publication

Not applicable.

Conflict of interest

The authors declare that they have no conflict of interest.

3.2 *IN VITRO* PREDICTIVE ASSAY OF THE LUNG INFLAMMATION INDUCED BY LIB PARTICLES

In the first paper, LCO was at least as potent as crystalline silica to induce lung inflammation and fibrosis in a mouse model and stabilized HIF-1α in lung tissue. A large range of LIB particles are currently developed and tested in academic and industrial laboratories with different size, composition, metal content and synthesis processes. Identification of (physico-chemical) determinants of their toxicity and/or screening tools to predict lung toxicity are therefore needed for a safer-by-design approach allowing a sustainable development of LIB. This should ideally be achieved by integrating the 3Rs principles, i.e. by developing predictive *in vitro* assays based on mechanistic observations. Thus, we tested a panel of LIB particles with different cobalt and/or nickel contents and investigated (i) the role of cobalt and nickel content and their bioaccessibility in lung toxicity and (ii) the implication of pro-inflammatory mediators identified in our first study (IL-1β and HIF-1α, section 4.1). We found that HIF-1α is involved in lung inflammation induced by LIB particles and that, together with cobalt and nickel content and their bioaccessibility, it correlates with the intensity of the inflammation. Based on these results, we developed an *in vitro* assay to document HIF-1α stabilization induced by LIB particles in lung epithelial cells. With Co/Ni content or bioaccessibility data, this *in vitro* assay provides additional information about the toxicity mechanisms of the particles and can be used to refine the toxicological evaluation of LIB particles.

HIF-1α is a key mediator of the lung inflammatory potential of lithium-ion battery particles

Violaine Sironval[1,§], Mihaly Palmai-Pallag[1], Rita Vanbever[2], François Huaux[1], Jorge Mejia[3], Stéphane Lucas[3], Dominique Lison[1], Sybille van den Brule[1]

Particle and Fibre Toxicology (2019) 16:35

Received: 31 May 2019 / Accepted: 29 August 2019 / Published online: 18 September 2019

Online version of this article: https://doi.org/10.1186/s12989-019-0319-z

Author's affiliations:

[1] Louvain centre for Toxicology and Applied Pharmacology, Institut de Recherche Expérimentale et Clinique, UCLouvain, Avenue Hippocrate 57 - bte B1.57.06, 1200 Brussels, Belgium

[2] Louvain Drug Research Institute, Université catholique de Louvain, Avenue Mounier 73 - bte B1.73.12, 1200 Brussels, Belgium

[3] Research Centre for the Physics of Matter and Radiation (PMR-LARN), NARILIS, Université de Namur, rue de Bruxelles 61, 5000 Namur, Belgium

[§] Corresponding author

3.2.1 Abstract

Li-ion batteries (LIB) are increasingly used worldwide. They are made of low solubility micrometric particles, implying a potential for inhalation toxicity in occupational settings and possibly for consumers. $LiCoO_2$ (LCO), one of the most used cathode material, induces inflammatory and fibrotic lung responses in mice. LCO also stabilizes hypoxia-inducible factor (HIF) -1α, a factor implicated in inflammation, fibrosis and carcinogenicity. Here, we investigated the role of cobalt, nickel and HIF-1α as determinants of toxicity, and evaluated their predictive value for the lung toxicity of LIB particles in *in vitro* assays.

By testing a set of 5 selected LIB particles (LCO, $LiNiMnCoO_2$, $LiNiCoAlO_2$) with different cobalt and nickel contents, we found a positive correlation between their *in vivo* lung inflammatory activity, and (i) Co and Ni particle content and their bioaccessibility and (ii) the stabilization of HIF-1α in the lung. Inhibition of HIF-1α with chetomin or PX-478 blunted the lung inflammatory response to LCO in mice. In IL-1β deficient mice, HIF-1α was the upstream signal of the inflammatory lung response to LCO. *In vitro*, the level of HIF-1α stabilization induced by LIB particles in BEAS-2B cells correlated with the intensity of lung inflammation induced by the same particles *in vivo*.

We conclude that HIF-1α, stabilized in lung cells by released Co and Ni ions, is a mechanism-based biomarker of lung inflammatory responses induced by LIB particles containing Co/Ni. Documenting the Co/Ni content of LIB particles, their bioaccessibility and their capacity to stabilize HIF-1α *in vitro* can be used to predict the lung inflammatory potential of LIB particles.

3.2.2 Background

Li-ion batteries (LIB) represent one of the best solutions for various electric grid applications, to improve the quality of energy harvested from wind, solar, geo-thermal and other renewable sources [5]. LIB electrodes are made of poorly water-soluble particles, micrometric in size, that might thus be respirable and biopersistent in the human respiratory tract. Exposure to LIB components is the most worrying for workers producing and handling LIB particles but future

applications of LIB, such as multi-layer systems made for spray-paintable or printable DIY batteries [15, 17, 18], might extend the potential for inhalation exposure to consumers.

We previously assessed the lung toxicity of three commonly used LIB particles, lithium iron phosphate ($LiFePO_4$/LFP), lithium titanium oxide ($Li_4Ti_5O_{12}$/LTO) and lithium cobalt oxide ($LiCoO_2$/LCO), and concluded that they represent a respiratory hazard independently of their Li content [260]. Acute inflammatory responses were recorded with the three particles. Long-term inflammation was maintained after LFP and LCO, and only LCO induced fibrotic responses. Increased hypoxia-inducible factor (HIF)-1α was recorded in the lung of mice exposed to LCO. HIF-1 is a heterodimeric transcriptional factor consisting of two subunits, HIF-1α and HIF-1β, constitutively expressed in all cells [140]. HIF-1α is the oxygen-sensitive subunit regulating the level of active HIF-1 [261]. Under normoxia, HIF-1α is continuously degraded by ubiquitin- and proteasome-dependent pathways. HIF-1α degradation is mainly controlled by the hydroxylation of two specific prolyl residues by prolyl hydroxylase. During hypoxia, HIF-1α is stabilized, heterodimerizes with HIF-1β, recruits coactivators, and induces the transcription of target genes such as interleukin (IL)-6, vascular endothelial growth factor (VEGF)-A, erythropoietin (EPO) and transforming growth factor (TGF)-β [140]. Ions such as Co^{2+} or Ni^{2+} mimic hypoxia and stabilize HIF-1α by blocking the iron-binding site of prolyl hydroxylase or directly binding to HIF-1α, thus preventing its degradation [136, 137, 262].

A wide diversity of particles, containing metals such as cobalt and/or nickel, are used in LIB electrodes [5, 28] . In view of the large variety of existing and future LIB materials, their increasing production, use and disposal, it appears essential to better identify their health hazards and to generate information about mechanisms of toxicity. Here, we investigated the role of Co and Ni and their capacity to stabilize HIF-1α in the lung responses to LIB particles, and evaluated the value of *in vitro* assays to predict their potential for lung toxicity.

3.2.3 Methods

Particles

LCO ($LiCoO_2$) was obtained from MTI Corporation (Richmond, USA), NCA ($LiNiCoAlO_2$), NMC 1:1:1 ($LiNi_{0.33}Co_{0.33}Mn_{0.33}O_2$), NMC 6:2:2 ($LiNi_{0.6}Co_{0.2}Mn_{0.2}O_2$) and NMC 8:1:1 ($LiNi_{0.8}Co_{0.1}Mn_{0.1}O_2$) from Umicore, cobalt oxide (Co_3O_4, size < 10 µm, 221643) from Sigma-Aldrich (Missouri, USA) and micrometric crystalline silica particles (Min-U-Sil 5, d_{50} 1.6 µm) from US Silica (Berkley Springs, USA). Before all experiments, particles were heated 2 hours at 200 °C to inactivate any possible endotoxin or other microbial contaminants.

Particle solubilization

To assess the bioaccessibility of elements contained in LIB particles, 10 mg particles were incubated in 10 ml artificial fluids mimicking the extracellular (pH 7.3) or the phagolysosomal (pH 4.2) compartments as previously described [242]. Particles were incubated during 30 days at 37°C under gentle agitation. One ml aliquots were collected after 3, 24 h, 7, 14 and 30 days and centrifuged (20000 *g*, 10 min). Element concentrations were determined in the supernatants (SN) by inductively coupled plasma mass spectrometry (ICP-MS).

Particle characterization

The density of LIB particles was assessed by tap density measurement and their aerodynamic size distribution in an Andersen cascade impactor (1 ACFM Eight Stage Non-Viable Cascade Impactor, Graseby Andersen, Atlanta, USA) as previously described [260]. The particle size distribution, based on the hydrodynamic diameter was also assessed by centrifugal liquid sedimentation (CLS) on a DC24000 system (CPS instruments Inc., Stuart, Florida, USA), equipped with a 405-nm wavelength laser detector, with PVC standard (nominal particle size = 719 nm). Sizes are expressed in terms of hydrodynamic diameter assuming all particles are spherical. Each measurement was done by injecting 0.1 ml of a 1 mg particle/mL suspension in NaCl 0.9%.

Animals and treatments

Female C57BL/6JRj mice were purchased from Janvier Labs (St Bertevin, France). Interleukin (IL)-1β deficient (knock-out, $^{-/-}$) mice (C57BL/6J background) were obtained from the Transgenose Institute (Orleans, France). Eight-week-old animals were kept with sterile rodent feed and acidified water, and housed in positive-pressure air-conditioned units (25°C, 50 % relative humidity) on a 12h light/dark cycle. Particles were suspended in sterile 0.9 % saline. Mice were randomly allocated to experimental groups. After anaesthesia with a mix of Nimatek, 1 mg/mouse (Eurovet, Bladel, Nederland) and Rompun, 0.2 mg/mouse (Bayer, Kiel, Germany) given intraperitoneally, a 50 µl suspension of particles or NaCl (controls) was directly administered by oro-pharyngeal aspiration. Single dose administration of particles is a convenient alternative to inhalation exposure for initial hazard identification [263, 264] and induces qualitatively similar lung responses as inhalation exposure [239, 240]. Crystalline silica particles were used as reference material. Inflammatory and fibrotic responses are recorded in mice with a dose of 2 mg crystalline silica particles administered via oro-pharyngeal aspiration [230-233]. LIB particles were tested at doses of 0.1, 0.5 or 2 mg to allow benchmarking of their respiratory toxicity relative to crystalline silica particles.

Chetomin (Sigma-Aldrich) or vehicle (saline solution with 10 % dimethylsulfoxide (DMSO, Sigma-Aldrich)) was injected intraperitoneally at 0.5 mg/kg bw/d for the 3 days experiment, one day before administration of the particles and during the 2 following days, or 3 times per week for long term experiments. PX-478 (S-2-amino-3-[4'-N,N,-bis(2-chloroethyl)amino]phenyl propionic acid N-oxide dihydrochloride, Cayman Chemicals, Michigan, USA) or vehicle (saline solution with 10 % DMSO) was injected intraperitoneally at 20 mg/kg bw/d, one day before administration of the particles and during the 2 following days. Mice were euthanized 3 days or 2 months after particle administration with an intraperitoneal injection of 12 mg sodium pentobarbital (Certa, Braine-l'Alleud, Belgium).

Broncho-alveolar lavage and lung sampling

Broncho-alveolar lavage (BAL) was performed by cannulating the trachea and infusing the lungs with 1 ml NaCl 0.9 %. Whole lungs were then perfused with NaCl

0.9 % and excised. Left lobes were placed in 3.65 % paraformaldehyde (Sigma-Aldrich, St Louis, Missouri, USA) in phosphate buffered saline (PBS) for later histological analysis, and remaining lobes in liquid nitrogen or lysis buffer for homogenization. Lungs were homogenized on ice with an Ultra-Turrax T25 (Janke and Kunkel, Brussels, Belgium) and stored at -80°C. BAL were centrifuged 10 min at 4°C (240 *g*). Cell-free supernatant (BALF) was used for biochemical measurements. After resuspension of the pellet in PBS, total BAL cells were counted in Turch (crystal violet 1 %, acetic acid 3 %) and cytocentrifuged for differentiation by light microscopy after Diff-Quick staining (200 cells counted, Polysciences, Warrington, UK). Lactate dehydrogenase (LDH) activity was assayed on BALF as described previously [231].

Quantification of IL-1β, IL-6 and HIF-1α

IL-1β and IL-6 were quantified by enzyme-linked immunosorbent assay (ELISA) (Limit of detection (LOD): 7.8 pg/ml, DuoSet ELISA, R&D Systems, Minneapolis, USA) in BALF following manufacturer's instructions. HIF-1α (LOD: 31.25 pg/ml, DuoSet ELISA, R&D Systems) was assessed in SN of lung homogenates (centrifuged 10 min at 240 *g*, 4°C) or in the cell culture after lysis following manufacturer's instructions.

Histology and fibrosis scoring

Paraffin-embedded lung sections were stained with hematoxylin and eosin (HE) (lung structure staining) or Sirius Red (type I and III collagen staining). The sections were scanned (Leica SCN400, Brussels, Belgium) and examined with Tissue Image Analysis 2.0 (Leica Biosystems). Fibrotic responses was quantified using a modified Ashcroft scale (grade 0 to 8) standardized for fibrosis evaluation in small animals (clear fibrotic changes are observed from the grade 2) [265]. Analyses were performed under blind conditions by the same investigator.

Cell culture and in vitro exposure

BEAS-2B cells (human bronchial epithelial cell line, ATCC, Virginia, USA) were cultured at 37°C in complete medium, i.e. LHC-9 medium (Gibco, Paisley, UK) supplemented with 1 % antibiotic-antimycotic (Gibco) on coated surfaces. Culture

flasks and plates were precoated with a mixture (60 µl/cm²) of 0.01 mg/mL fibronectin (Fibronectin from human plasma 0.1 %, Sigma), 0.03 mg/mL bovine collagen type I (collagen coating solution 50 µg/ml, Sigma) and 0.01 mg/mL bovine serum albumin (7.5 % in PBS, Sigma) at least 2 hours at 37°C and then washed 1 x with PBS (Gibco, Paisley, UK) before cell seeding. Cells were subcultured and exposed before reaching confluence. Before exposure, BEAS-2B were plated in 96-well plates or 48-well plates (30 000 cells/cm² culture well surface area) in complete medium. After 24 h, cells were exposed to the particles during 24 hours in culture medium (150 µl/well for 48-well plates (0.95 cm^2/w) and 100µl/well for 96-well plates (0.32 cm^2/w)). Given the similar size and density of the tested particles (Table 1), differential sedimentation and cellular doses are unlikely to confound the results. All tested particles directly sedimented in the cell culture well.

SN of cell culture were collected and stored at -80°C for later analysis. Cells were then washed once with LHC basal medium and viability was evaluated by using the water soluble tetrazolium salts (WST-1) assay (Roche, Mannheim, Germany, 5 %) following manufacturer's instructions (96-well plates). Cells cultured in 48-well plates were washed and lysed for HIF-1α dosage following manufacturer's instructions.

Statistics

Graphs and statistical analyses were performed with GraphPad Prism 5.0 and/or Microsoft excel 2013. Bivariate analyses were performed with IBM SPSS statistics 25. All results are expressed as means ± standard errors on the mean (SEM). Differences between control and treated groups were evaluated by one-way analysis of variance (ANOVA), followed by a Dunnett's multiple comparison, or by a t test. Statistical significance was considered at $P < 0.05$.

3.2.4 Results

Contrasting lung toxicity of LIB particles

We first documented the dose-responses for lung inflammatory and fibrotic responses induced by LCO. Mice were exposed by oro-pharyngeal aspiration to LCO (0.1, 0.5 or 2 mg). Crystalline silica particles were selected as positive control. Two months after exposure, no mortality was recorded at any of the doses tested. A clear inflammatory cell accumulation was observed from 0.5 mg LCO and at 2 mg silica (**Figure 16 a**). LCO also induced a stronger fibrotic response than silica (**Figures 16 b, d**). LCO particles are thus more potent than crystalline silica particles, despite their larger size distribution (7.21 vs > 50 % fine particle fraction, respectively). HIF-1α was strongly stabilized in lung cells by LCO in a dose-dependent manner, only weakly by silica (**Figure 16 c**).

We next assessed the lung responses to other particles used in LIB, with different compositions (**Table 2**) and containing fine particles (**Table 2 and Annexes, Figure S7**). $LiNiMnCoO_2$ (NMC) and $LiNiCoAlO_2$ (NCA) also contain nickel. Co_3O_4 was used as a reference low solubility cobalt particle [170].

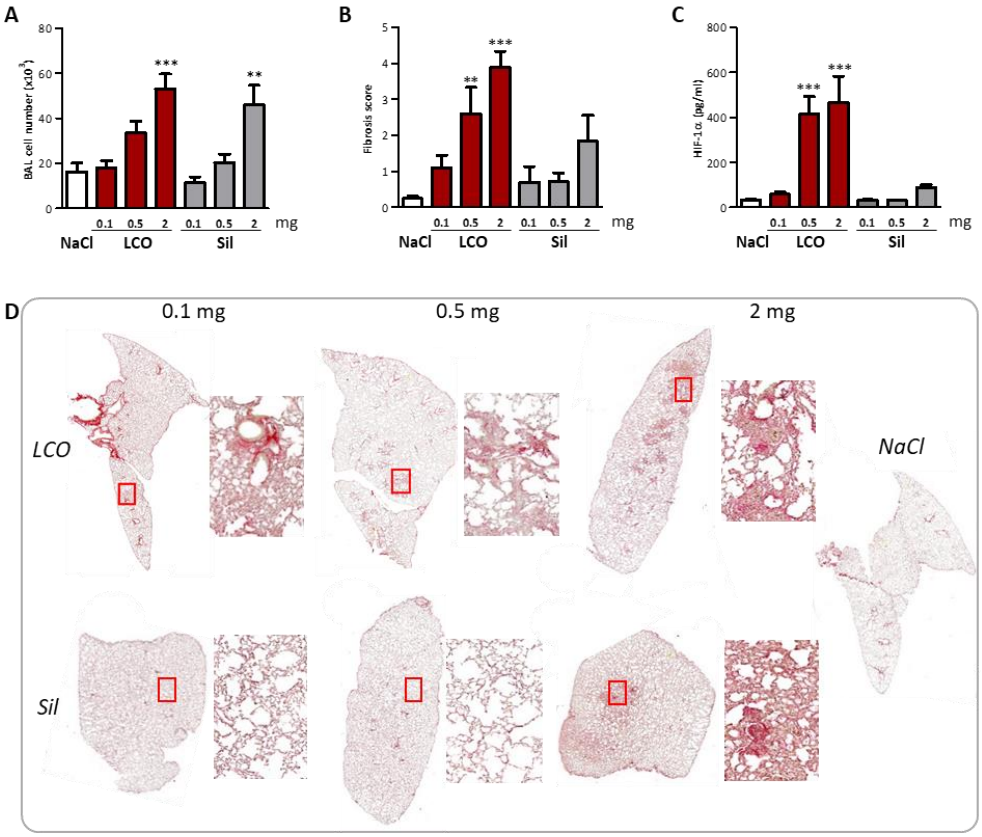

Figure 16: LCO induces stronger lung toxicity than silica particles. C57BL/6Jrj mice were treated with an oro-pharyngeal aspiration of NaCl (control), 0.1, 0.5 or 2 mg LCO or crystalline silica (Sil). Mice were euthanized after 2 months. Inflammatory cell infiltration (**a**) was measured in BAL; HIF-1α (**c**) in lung homogenates. Severity of fibrotic responses was scored according to Hübner et al. (2008) on lung sections stained with Sirius red (**b**). Lung sections stained with Sirius red (magnification 10x and 200x) (**d**). *P < 0.05, **P < 0.01 and ***P < 0.001 relative to NaCl-treated mice (one-way ANOVA followed by a Dunnett's multiple comparison, N = 1, n = 5, means ± SEM).

Mice were first exposed to 1 or 2 mg LIB particles by oro-pharyngeal aspiration. Surprisingly, some mice died shortly after exposure, except with Co_3O_4 (**Figure 17 a**). The dose was then reduced to 0.5 mg for the most active particles (NMC6:2:2, NMC8:1:1, NCA and LCO). After 2 months, all LIB particles induced inflammation (cell infiltration) at the dose of 2 mg (**Figure 17 b**). Co_3O_4 induced a slight inflammation.

Table 2 Particle characterization.

	LCO	NCA	NMC 1:1:1[a]	NMC 6:2:2	NMC 8:1:1
Density (g/cm^3) [b]	2.37	2.95	1.93	2.84	1.93
Diameter (µm) [c]	6.47	6.13	5.16	11.34	7.53
FPF (% of total weight) [d]	7.21	2.01	1.64	1.84	2.15
Li (%) [e]	7.1	3.28	7.24	7.16	7.14
Co (%) [e]	60.2	27.86	20.22	12.12	6.03
Ni (%) [e]	/	27.75	20.22	36.35	48.28
Mn (%) [e]	/	/	18.92	11.34	5.65
Al (%)[e]	/	25.98	/	/	/
O (%) [e]	32.7	15.13	33.40	33.03	32.9

[a] The three digits reflect the Ni:Mn:Co mass ratio in the particles.
[b] Measured by powder tap density.
[c] Median hydrodynamic diameter determined by centrifugal liquid sedimentation (CLS) (weight-based distribution).
[d] Fine particle fraction (FPF, ≤ 5 µm) determined by Andersen cascade impaction.
[e] as reported by the producers.

Lung fibrotic manifestations (score ≥ 2) were induced by LCO and NCA particles at 0.5 mg whereas, at 1 and 2 mg, LCO, NMC1:1:1 and NCA induced clear fibrotic changes with fibrotic masses (**Figure 17 c**). NMC 6:2:2, 8:1:1 and Co_3O_4 induced some isolated fibrotic changes (**Annexes, Figure S8**). All particles induced different (dose-dependent) levels of HIF-1α stabilization (**Figure 17 d**). As these LIB particles induced acute toxicity (mortality) and severe lung responses, it appeared crucial to identify the mechanisms of this toxicity.

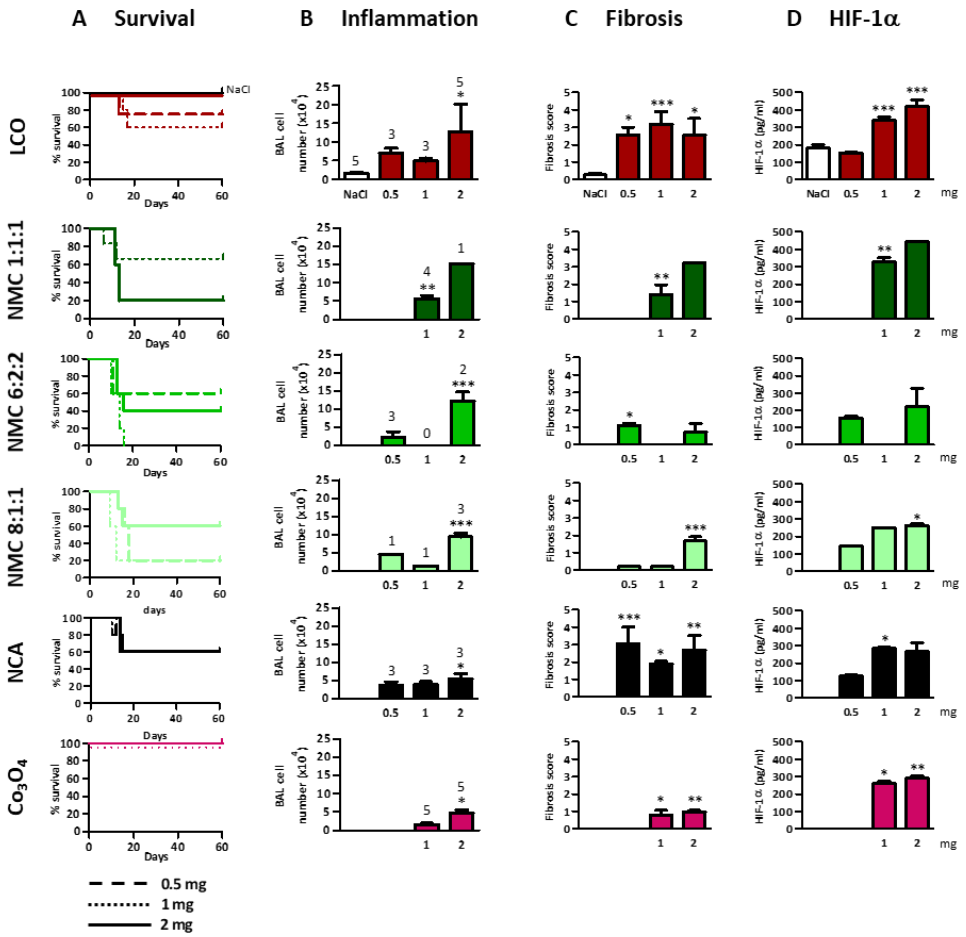

Figure 17: Lung inflammatory and fibrotic responses induced by LIB particles. C57BL/6Jrj mice were treated with an oro-pharyngeal aspiration of NaCl (control), 0.5, 1 or 2 mg LCO, NMC 1:1:1, NMC 6:2:2, NMC 8:1:1, NCA or Co_3O_4. Mortality is shown in survival curves (**a**). Surviving mice were euthanized after 2 months. Inflammatory cell infiltration (**b**) was measured in BALF. Fibrotic response (**c**) severity was scored according to Hübner et al. (2008). HIF-1α (**d**) was measured in lung homogenates. Number of surviving mice is indicated for each condition above the columns (**b**). *P < 0.05, **P < 0.01 and ***P < 0.001 relative to NaCl-treated mice (one-way ANOVA followed by a Dunnett's multiple comparison or t test, N = 1, n = 4-6 (treated mice), means ± SEM).

We first focused on the determinants of acute toxicity. Because tested LIB particles contained Co and/or Ni, 2 elements able to induce pulmonary toxicity [175, 181, 238], we assessed the bioaccessibility of these metals in artificial fluids mimicking

the extracellular (pH 7.3) and the phagolysosomal (pH 4.2) cellular compartments over a period of 30 days (**Figure 18**). The amount of Co released at pH 7.3 was very low for all particles (**Figure 18 a**) in comparison to pH 4.2 (**Figure 18 b**), suggesting that Co ions can be released in the phagolysosomes.

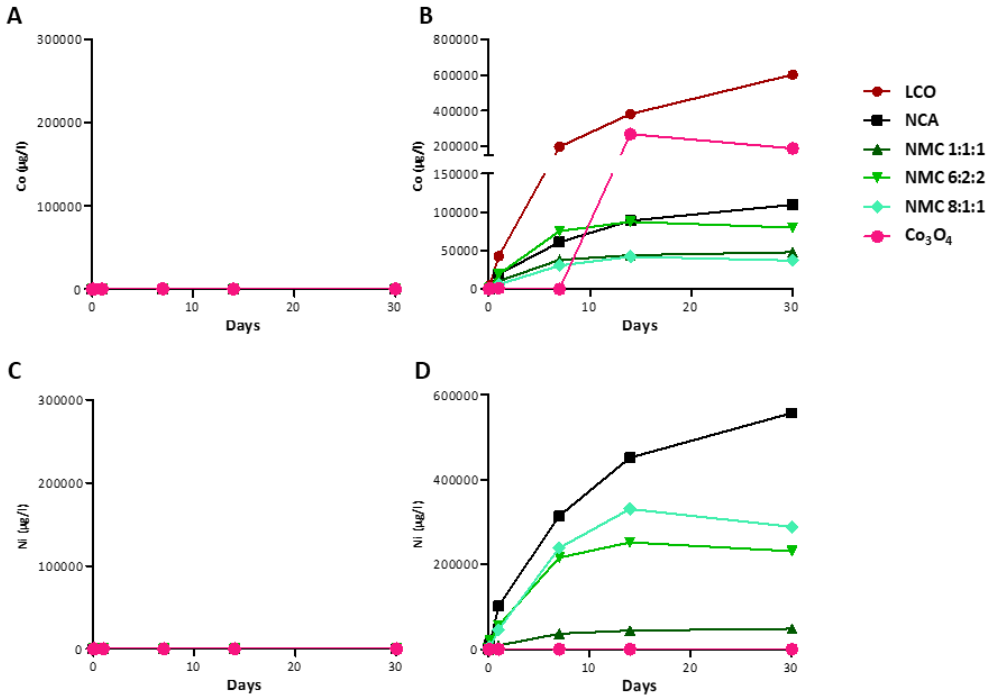

Figure 18: Bioaccessibility of Co and Ni from LIB particles. LIB particles and Co_3O_4 were incubated in artificial fluids mimicking the extracellular (pH 7.3) (**a, c**) or the phagolysosomal (pH 4.2) (**b, d**) compartment. Particles were incubated at 37°C under gentle agitation and released Co (**a, b**) and Ni concentrations (**c, d**) were determined by ICP-MS in the SN after centrifugation of an aliquot of the suspensions after 3, 24 h, 7, 14 and 30 days.

The pattern of Co release at pH 4.2 was different for all LIB particles, LCO releasing the largest amount of Co. Co_3O_4 particles released more Co than the other LIB particles. NCA and NMC6:2:2 released a higher amount of Co than NNC1:1:1 and NMC8:1:1. At pH 7.3, Ni bioaccessibility was also very low (**Figure 18 c**). At pH 4.2, the Ni bioaccessibility pattern was different for all LIB particles, NCA and NMC8:1:1 releasing the highest amount of Ni (**Figure 18 d**). Thus, the patterns of Co and Ni released from LIB particles did not follow their Co or Ni % content. We next

performed a bivariate analysis to identify the determinants of acute toxicity (mortality) after exposure to LIB particles. We analyzed the implication of the Co and Ni amount contained in the administered doses (0.5, 1 or 2 mg LIB particles) and their bioaccessibility (calculated from ion % released at pH 4.2) either separately or together (**Table 3**). The acute toxic potential (mortality) of these LIB particles was related to the Ni content and its release from the particles.

Table 3 Correlation between mortality recorded at day 18 and Ni/Co content or Ni/Co released by the particles

	Correlation coefficient	p-value
Co content	-0.064	0.801
Ni content	**0.760**	**0.0002**
Bioaccessible Co	-0.079	0.755
Bioaccessible Ni	**0.719**	**0.001**
Ni + Co content	0.163	0.517
Bioaccessible Ni + Co	0.176	0.484

Mice were treated with 0.5, 1 or 2 mg LIB particles (see Figure 17). Bivariate analysis (Spearman Rho) between the mortality % at day 18, and the particle Ni and/or Co content (µg) or the amount of Ni and/or Co ions (µg) released. Co and/or Ni contents were calculated from the administered doses and from the Co and/or Ni % of the particles. Bioaccessible Co and/or Ni represent the amount of bioaccessible ions, calculated from the Co/Ni contained in the administered doses and the % released at pH 4.2 at day 14 (mortality was recorded between day 6 and 18). Significant relationships are identified in bold.

HIF-1α is a determinant of the lung inflammation induced by LIB particles

We next performed similar analyses to identify the determinants of the late inflammatory response (inflammatory cell infiltration in the BAL 2 months after administration) (**Table 4**), including lung HIF-1α content, BAL fuid (BALF) lactate deshydrogenase (LDH) activity as a marker of cytotoxicity, Ni and/or Co contents of LIB particles and their bioaccessibility (calculated from the % released at pH 4.2).

Table 4 Tracing the determinants of lung inflammation induced by LIB particles after 2 months.

	Correlation coefficient	p-value
LDH	0.183	0.195
HIF-1α	**0.311**	**0.025**
Co content	0.245	0.080
Ni content	0.065	0.270
Bioaccessible Co	-0.020	0.886
Bioaccessible Ni	0.035	0.806
Ni + Co content	**0.480**	**0.0003**
Bioaccessible Ni + Co	**0.445**	**0.0004**

Bivariate analysis (Pearson correlation) between the inflammatory cell recruitment, selected as marker of lung inflammation and HIF-1α, LDH activity, the particle Ni and/or Co content (μg) or the amount of Ni and/or Co ions (μg) released. Inflammatory cell recruitment was assessed in the BAL, HIF-1α (μg/ml) was measured in lung homogenates, LDH activity (iU/l) in BALF. Co and/or Ni contents were calculated from the administered doses and from the Co and/or Ni % of the particles. Bioaccessible Co and/or Ni represent the amount of bioaccessible ions, calculated from the Co/Ni contained in the administered doses and the % released at pH 4.2 at day 30. Significant relationships are identified in bold.

HIF-1α stabilization in lung tissue, the sum of Co and Ni content in particles and their summed bioaccessibility significantly correlated with lung inflammation (**Table 4**). The sum of Ni and Co content and their bioaccessibility also positively correlated with the stabilization of HIF-1α (r = 0.539, p-value = 0.0001 and r = 0.500, p-value = 0.0001 respectively). The same analysis did not show any significant association of the same variables with fibrotic responses (data not shown). These results thus supported the hypothesis that HIF-1α stabilization induced by Co and Ni ions drives the lung inflammatory responses of these LIB particles.

HIF-1α mediates lung inflammation induced by LCO

We next evaluated the implication of HIF-1α in the toxic activity of LIB particles by inhibiting its activity with chetomin, a disrupter of HIF binding to its transcriptional co-activator P300 [266]. This was assessed with LCO, the LIB particle inducing the strongest lung inflammation and fibrotic responses, and crystalline silica particles as control. We previously observed that LCO early stabilized HIF-1α in the lung 3 days after exposure and later after 2 months. Crystalline silica weakly stabilized HIF-1α only 2 months after exposure (**Figure 16**), suggesting that late inflammatory of fibrotic responses might also contribute to HIF-1α stabilization [260]. Therefore, we first focused on the implication of HIF-1α in early lung responses to isolate the specific effect of LCO. Three days after administration of 0.5 or 2 mg LCO, inflammatory cell recruitment including neutrophils and the pro-inflammatory cytokines IL-1β and IL-6 in BALF were largely reduced by the inhibition of HIF-1α (**Figures 19 a, b, c, d**). This reduction was not observed in silica-exposed mice. To further assess inflammation, lung sections of mice exposed to 2 mg particles were stained with HE. Aggregates of lymphocytes and macrophages, and accumulation of cellular debris were observed in LCO lungs to a larger extent than in silica lungs (**Figure 19 e**). In LCO lungs from mice treated with the inhibitor, inflammation was drastically reduced. In silica lungs, the formation of inflammatory foci was not prevented by chetomin (**Figure 19 e**).

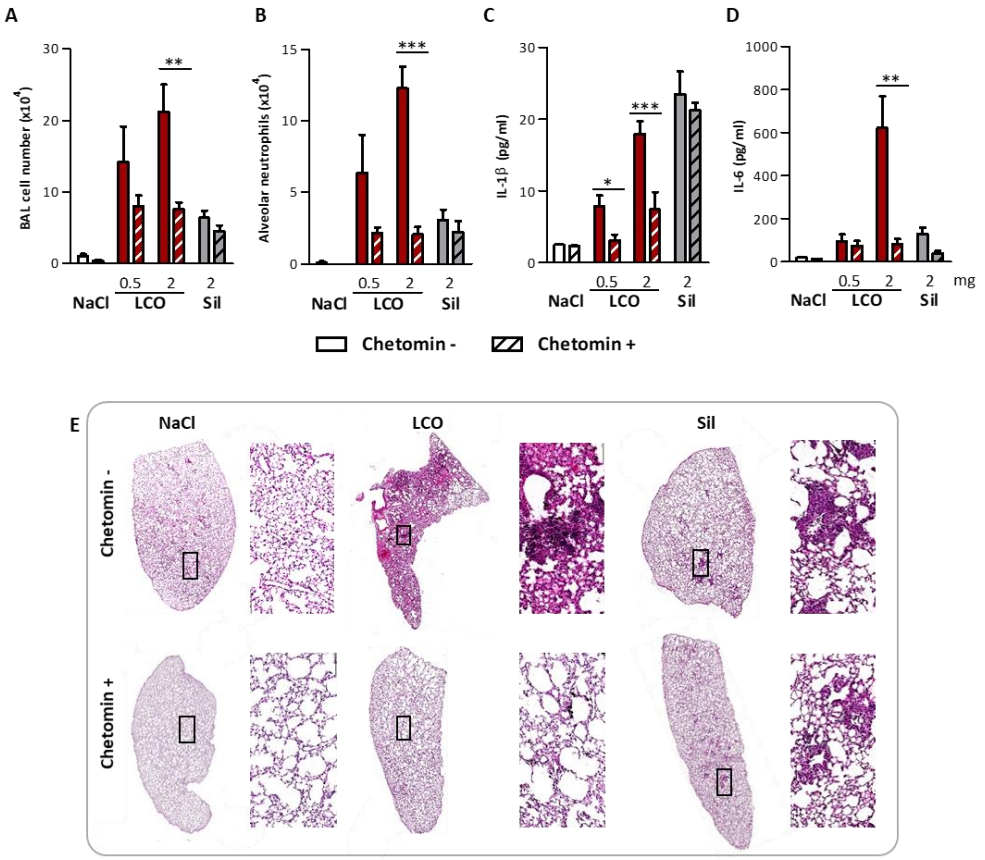

Figure 19: HIF-1α drives lung inflammation induced by LCO. C57BL/6Jrj mice were treated with an oro-pharyngeal aspiration of NaCl (control), 0.5 or 2 mg LCO or crystalline silica (Sil). Mice received i.p. injections of 0.5 mg/kg bw/d chetomin or vehicle (saline solution with 10 % DMSO) at day -1, 1 and 2 and were euthanized at day 3. Alveolar inflammatory cell infiltration and neutrophils were assessed in the BAL (**a, b**). IL-1β (**c**) and IL-6 (**d**) were measured in BALF; Lung sections of mice exposed to 2 mg particles were stained with HE (magnification 10x and 200x) (**e**). *P < 0.05, **P < 0.01 and ***P < 0.001 (t-test between chetomin - and + mice for each condition, N = 1, n = 5, means ± SEM).

These results suggested that HIF-1α is specifically implicated in early lung inflammation induced by LCO. To confirm this observation, we used PX-478, another inhibitor of HIF-1α responses targeting a different pathway. PX-478 inhibits HIF-1α by decreasing its translation and transcription, as well as de-ubiquitination [267-269]. Similar results were observed with this inhibitor (**Annexes, Figure S9**), confirming the implication of HIF-1α in early lung inflammation induced by LCO.

Similar experiments were conducted over a period of 1 and 2 months to assess the potential implication of HIF-1α in later lung responses to LCO, but mice did not tolerate a longer treatment with chetomin or PX-478 (not shown).

HIF-1α stabilization acts upstream of lung inflammation

We next investigated the possible influence of lung inflammation on HIF-1α stabilization. To minimize the number of animals used, IL-1β knock-out (KO) mice were treated only with 2 mg of LCO or crystalline silica particles and compared to their wild-type (WT) counterparts (C57BL/6JRj) after 3 days. Inflammatory cells, including neutrophils, were recruited after LCO and crystalline silica particles in WT mice. Only LCO induced HIF-1α stabilization in WT mice. All inflammatory parameters induced in WT mice were strongly reduced in IL-1β KO mice after LCO and (although not significantly) after silica **(Figures 20 a, b, c**). HIF-1α stabilization induced by LCO was, however, not modified in IL-1β KO mice (**Figure 20 d**), indicating that HIF-1α stabilization induced by LCO particles is not a consequence of inflammation.

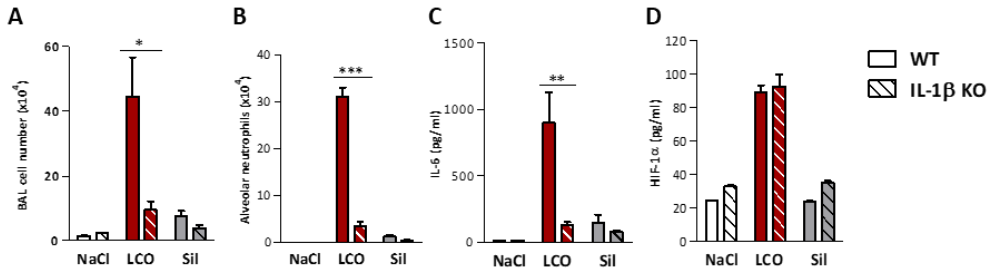

Figure 20: HIF-1α stabilization after LCO acts upstream of inflammation. C57BL/6Jrj or IL-1β KO mice were treated with an oro-pharyngeal aspiration of NaCl (control), 2 mg LCO or crystalline silica (Sil). Mice were euthanized after 3 days. Alveolar inflammatory cell infiltration (**a**) and neutrophils (**b**) were assessed in the BAL, and IL-6 (**c**) was measured in BALF; HIF-1α in lung homogenates (**d**). *P < 0.05, **P < 0.01 and ***P < 0.001 (t-test between WT and IL-1β KO mice for each condition, N = 1, n = 5, means ± SEM).

In vitro HIF-1α stabilization predicts the lung inflammatory potential of LIB particles

To further substantiate the mechanistic association between HIF-1α stabilized by Co/Ni ions and lung inflammation (**Table 4**), we next assessed *in vitro* the HIF-1α

response to LIB particles in BEAS-2B cells. This simplified model allows isolating the HIF-1α response from the multiple inflammatory components present in the lung. BEAS-2B cells were exposed to increasing doses of LIB particles (30 to 1000 µg/ml), the lowest concentration matching *in vivo* doses (**Annexes, Figure S10**). Higher concentrations were also tested because, *in vivo,* lung cells were exposed to Co ions released during 2 months while, *in vitro*, cells were exposed only during 24 hours. NMC8:1:1 and 6:2:2 were cytotoxic at 30 µg/ml and LCO at 1000 µg/ml. A very slight cytotoxicity appeared at 1000 µg/ml for the other particles (**Figure 21 a**). At 30 and 100 µg/ml, HIF-1α stabilization was stronger for LCO and NMC1:1:1. At 1000 µg/ml, all LIB particles induced a strong HIF-1α stabilization (**Figure 21 b**). Co_3O_4, which did not induce high lung inflammation *in vivo* compared to the LIB particles (**Figure 17**), induced a weaker HIF-1α stabilization than LIB particles *in vitro*. Using the results of *in vivo* experiments (**Figure 17**), bivariate analyses revealed a positive correlation between the *in vivo* inflammatory response (BAL inflammatory cell infiltration) and *in vitro* HIF-1α stabilization in BEAS-2B cells. Analyses were performed on HIF-1α stabilization at all doses tested *in vitro* (30, 100, 300 or 1000 µg particles/ml). All correlations were significant, the relation at 30 µg particles/ml which best matches the *in vivo* doses is illustrated here (**Figure 22**). These results confirm that the simple presence and release of Co/Ni from LIB particles and their ability to stabilize HIF-1α determine the *in vivo* inflammation, independently of all other possible components.

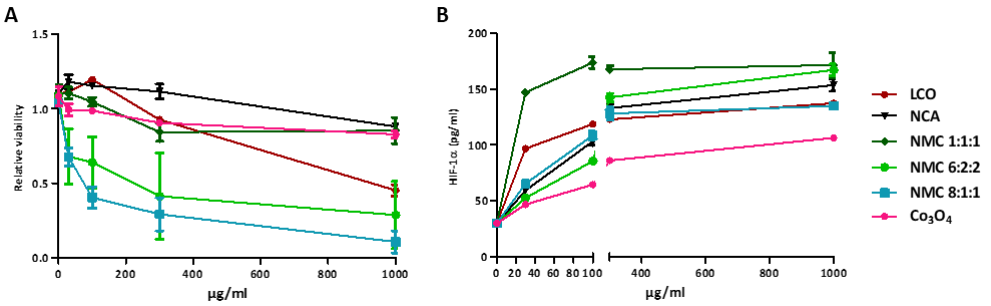

Figure 21: Cytotoxicity and HIF-1α stabilization induced by LIB particles in BEAS-2B cells. BEAS-2B cells were exposed to NaCl (control), 30, 100, 300 or 1000 µg/ml of LCO, NCA, NMC 1:1:1, NMC 6:2:2, NMC 8:1:1 or Co_3O_4. Cytotoxicity was assessed after 24h (**a**) by the WST-1 assay. HIF-1α (**b**) protein contents were measured in cell lysates. (N = 2, n = 4, means ± SEM).

Compared to % Co + Ni content or bioaccessibility, HIF-1α stabilization *in vitro* integrates a number of factors such as intracellular distribution of Co/Ni ions, and measures the bioactivity of these elements, offering an additional option to predict the toxic potential of (new) LIB particles, hence reducing *in vivo* testing.

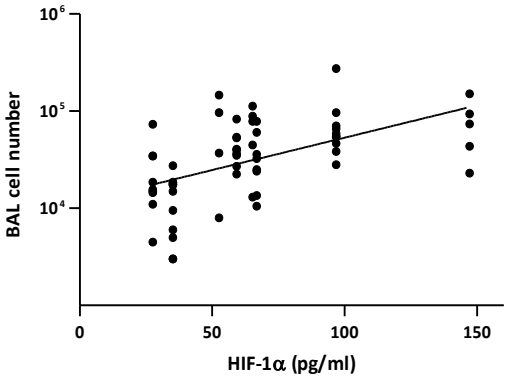

Figure 22: Correlation between inflammation induced by LIB particles *in vivo* and HIF-1α stabilization *in vitro*. Scatter graph and bivariate analysis demonstrate a positive correlation between the inflammatory cell recruitment level induced by LIB particles after 2 months in mice (see Figure 17) and the stabilization of HIF-1α (pg/ml) in BEAS-2B at the concentration of 30 µg LIB particle/ml (see Figure 21). ($y = 0.006671 x + 4.06$; $p < 0.0001$; $r = 0.532$).

The measurement of HIF-1α stabilization *in vitro* in BEAS-2B cells, the Co/Ni content of LIB particles and their bioaccessibility are, therefore, useful predictors of the lung inflammatory potential of LIB particles.

3.2.5 Discussion

We observed here that LIB particles containing Co and/or Ni induce lung inflammation and even fibrotic responses in mice. We show that Co and/or Ni contents and bioaccessibility, as well their capacity to stabilize HIF-1α, are determinants of lung inflammation. We also demonstrated that HIF-1α in lung cells mediates LCO-induced inflammation and is an upstream signal of the responses. In addition to the well-known implication of HIF in the development of cancer, invasion and metastasis, HIF-1α also plays many roles in inflammation, induces the secretion of inflammatory mediators and promotes myofibroblast

differentiation as well as epithelial-mesenchymal transition via the TGF-β pathway [140, 147, 150, 151].

Pulmonary diseases including cancer, asthma and fibrosing alveolitis have previously been reported in workers exposed to cobalt [175, 238]. Cobalt compounds can induce cytotoxicity, apoptosis, inflammatory responses and genotoxicity *in vitro* [168]. Some of the effects of cobalt are related to its high affinity for sulfhydryl groups leading to enzyme inactivation, antagonism for Ca^{2+} channel cell signalling, production of reactive oxygen species leading to oxidative stress, and finally to its ability to stabilize HIF-1α [168, 270]. LCO containing the highest % of Co among the range of particles tested, and Co being suspected to be the element responsible for the high toxicity of LCO, we hypothesized that other particles (with lower Co content) would induce lower lung effects than LCO. However, acute toxicity was observed early after exposure. In addition to cobalt, some LIB particles contain nickel, which appears as the element responsible for the observed mortality. Previous studies have shown that acute inhalation exposure to Ni induced lethal injury characterized by inflammatory cell infiltration, haemorrhage and destruction of alveolar epithelial cells [271, 272]. Chronic exposure to Ni can lead to asthma, inflammation, pulmonary fibrosis, kidney diseases and cancer [181, 262]. Like Co, Ni is able to stabilize HIF-1α by blocking the iron-binding group of the prolyl hydroxylase [262]. As inhibition of prolyl hydroxylase activates nuclear factor (NF)-κB [273], Co and Ni ions can thus both participate to the activation of NF-κB, leading to inflammation, as previously suggested [274]. The Co and Ni contents of LIB particles and their bioaccessibility are, indeed, correlated to the *in vivo* lung inflammation in the present study.

HIF-1α was also correlated to the *in vivo* lung inflammation induced by LIB particles. Moreover, inhibition of HIF-1α led to a reduction of lung inflammation induced by LCO particles, indicating the key pathogenic role of this transcription factor. HIF-1α can promote NF-κB activity in macrophages, neutrophils and non-immune cells, resulting in the transcription of target genes of inflammation such as pro-inflammatory cytokines (tumor necrosis factor (TNF)-α, IL-6, IL-1, IL-12) [135, 142]. To test the implication of HIF-1α in LCO lung inflammation, we first used chetomin which binds to the Zn^{2+}-binding cysteine/histidine rich 1 (CH1) domain of p300,

leading to a reduction of the interaction between HIF-1α and P300 [266] and reduces the expression of HIF-1α target genes [266, 275]. Chetomin drastically reduced LCO lung inflammation. These observations were confirmed by the use of PX-478 which inhibits HIF-1α transcription and translation by another mechanism than chetomin [16,18]. Thus, we showed here, for the first time, the implication of HIF-1α in lung inflammation induced by particles containing Co and/or Ni. We conclude that inflammation induced by LCO is dependent on HIF-1α.

In addition, the HIF-1α response to LCO was maintained in the absence of inflammation in IL-1β KO mice. We can thus conclude that HIF-1α is an upstream signal of the lung inflammatory responses to LIB particles containing Co. These results are consistent with Rius et al. [144] who showed that if NF-κB can regulate HIF-1α transcription in activated macrophages, NF-κB activation alone is, however, not sufficient to stabilize HIF-1α, indicating that both transcriptional and post-transcriptional (like Co and Ni ions) regulators are implicated in HIF-1α production/stabilization.

The Co and Ni content of LIB particles and their bioaccessibility at pH 4.2 represent thus good indicators of the toxic potential of LIB particles. To refine the predictive information, we can also measure HIF-1α protein stabilization in BEAS-2B cells exposed to LIB particles. A study comparing 10 commonly used cell lines concluded that BEAS-2B cells are useful for toxicological studies because they exhibit the highest homology in gene expression pattern with human primary cells and the lowest number of dysregulated genes compared with non tumoral lung tissues [276]. Moreover, BEAS-2B have been previously used to study the toxicity of cobalt compounds [170, 277]. The BEAS-2B cell line is an appropriate model to evaluate the lung inflammatory potential of LIB particles by measuring the stabilization of the key mediator HIF-1α.

A large variety of materials are in use in or under consideration for the development of LIB materials. While micro-sized particles, as tested in the present study, are currently used in most commercialized batteries, nano-sized materials are in intense development to improve technical performances [1]. The nanosize is a plausible source of additional concern as it can result in more hazardous properties

and increased particle exposure via inhalation. Thus, toxicological evaluation of existing and newly developed LIB particles appears as a priority. We identified the Ni and Co content of LIB particles and their bioaccessibility, as well as HIF-1α as key determinants of the lung inflammatory responses to LIB particles. Evaluating HIF-1α levels in BEAS-2B cells exposed to LIB particles is a predictor of their inflammatory potential.

3.2.6 Conclusions

We report the implication of HIF-1α induced by Ni and Co ions in lung inflammatory responses induced by LIB particles. HIF-1α is the upstream signal of the inflammatory responses induced by these LIB particles, participating to the secretion of IL-1β. Documenting the amount of Co and Ni in LIB particles, their bioaccessibility as well as HIF-1α stabilization in BEAS-2B cells, predict the lung toxicity of LIB particles.

3.2.7 Declarations

Ethics approval and consent to participate

All animal experiments were approved by the local committee for animal research at the Université catholique de Louvain, Comité d'Ethique pour l'Expérimentation Animale, Secteur des Sciences de la Santé, Brussels, Belgium (No LA1230312).

Consent for publication

Not applicable.

Availability of data and material

The datasets used and/or analyzed during the current study are available from the corresponding author on reasonable request.

Competing financial interest statements

The authors declare that they have no competing interests.

Funding

"Programme d'excellence BATWAL 1318146 from the SPW DG06 (Belgium)" supported the research project and financed SV. VS is financed by a grant from the "Fonds pour la Formation à la Recherche dans l'Industrie et dans l'Agriculture (FRIA)".

Authors' contributions

VS, SV and DL designed the experiments, co-wrote the paper and contributed to data analysis and interpretation. VS performed most experimental work. MP and FH contributed to *in vivo* experiments. RV performed density and FPF analysis of the particles. JM and SL performed CLS measurements. All authors read and approved the final manuscript.

Acknowledgements

Not applicable.

3.3 GENOTOXIC AND MUTAGENIC POTENTIAL OF $LiCoO_2$ PARTICLES

As reported in the previous sections, LCO particles induced chronic lung inflammation, and oxidative stress. Moreover, LCO contain bioaccessible Co ions which are classified as possibly carcinogenic for humans (group 2B) by the IARC [60]. Given that inflammatory responses, induction of oxidative stress and the presence of genotoxic Co ions represent key characteristics of carcinogens [278], evaluating the genotoxic potential of LCO appears very relevant in the process of assessing its health hazard. The mutagenic and carcinogenic potential of LCO particles have not been examined before. In the present study, we therefore assessed the genotoxic and mutagenic potential of LCO particles in comparison to LTO particles, selected as "low activity" particles which did not induce chronic lung inflammation, long-term oxidative stress, and do not contain possible carcinogenic bioaccessible ions.

It is known that Co ions have a genotoxic activity due to their ability (i) to produce hydroxyl radicals ($HO^{\bullet}$) via a Fenton-like reaction and (ii) to interact with and inhibit proteins, including those implicated in DNA repair [167]. We thus suspected that LCO particles could be able to induce primary indirect genotoxic events. We showed the mutagenic potential of LCO particles in an *in vitro* micronucleus assay and confirmed the effect *in vivo* at non-inflammatory doses. The production of ROS was assessed and their implication evaluated via several approaches. We identified LCO as a mutagenic particle via oxidative DNA damage induced by the production of ROS. Thus, we highlighted in this study the primary genotoxic potential of LCO. Given that other LIB particles containing Co and/or Ni can cause strong lung inflammation and strongly stabilize HIF-1α [279], a transcription factor involved in tumor growth, angiogenesis and metastasis [135], and that Ni compounds can also exert a mutagenic activity [280], our data highlight the need for also documenting their genotoxic potential.

$LiCoO_2$ particles used in Li-ion batteries induce primary mutagenicity in lung cells via their capacity to generate hydroxyl radicals

Violaine Sironval[1,§], Vittoria Scagliarini[1], Sivakumar Murugadoss[2], Maura Tomatis[3], Yousof Yakoub[1], Francesco Turci[3], Peter Hoet[2], Dominique Lison[1], Sybille van den Brule[1]

Particle and Fibre Toxicology (2020) 17:6

Received: 06 August 2019 / Accepted: 14 January 2020 / Published online: 29 January 2020

Online version of this article: https://doi.org/10.1186/s12989-020-0338-9

Author's affiliations:

[1] Louvain centre for Toxicology and Applied Pharmacology, Institut de Recherche Expérimentale et Clinique, Université catholique de Louvain, Avenue Hippocrate 57 - box B1.57.06, 1200 Brussels, Belgium

[2] Laboratory of Toxicology, Unit of Environment and Health, Department of Public Health and Primary Care, Katholieke Universiteit Leuven, Herestraat 49 - O&N1 - Room: 07.702, box 706, 3000 Leuven, Belgium

[3] Department of Chemistry and "G. Scansetti" Interdepartmental Center for Studies on Asbestos and Other Toxic Particulates, University of Torino, Via P. Giuria 7, 10125 Torino, Italy

[§] Corresponding author

3.3.1 Abstract

Li-ion batteries (LIB) are used in most portable electronics. Among a wide variety of materials, $LiCoO_2$ (LCO) is one of the most used for the cathode of LIB. LCO particles induce oxidative stress in mouse lungs due to their Co content, and have a strong inflammatory potential. In this study, we assessed the mutagenic potential of LCO particles in lung cells in comparison to another particulate material used in LIB, LTO ($Li_4Ti_5O_{12}$), which has a low inflammatory potential compared to LCO particles.

We assessed the mutagenic potential of LCO and LTO particles *in vitro* by performing a cytokinesis-block micronucleus (MN) assay with rat lung epithelial cells (RLE), as well as *in vivo* in alveolar type II epithelial (AT-II) cells. LCO particles induced MN *in vitro* at non-cytotoxic concentrations and *in vivo* at non-inflammatory doses, indicating a primary genotoxic mechanism. LTO particles did not induce MN. Electron paramagnetic resonance and terephthalate assays showed that LCO particles produce hydroxyl radicals ($HO^{\bullet}$). Catalase inhibits this $HO^{\bullet}$ production. In an alkaline comet assay with the oxidative DNA damage repair enzyme human 8-oxoguanine DNA glycosylase 1, LCO particles induced DNA strand breaks and oxidative lesions. The addition of catalase reduced the frequency of MN induced by LCO particles *in vitro*.

We report the mutagenic activity of LCO particles used in LIB *in vitro* and *in vivo*. Our data support the role of Co(II) ions released from these particles in their primary genotoxic activity which includes the formation of $HO^{\bullet}$ by a Fenton-like reaction, oxidative DNA lesions and strand breaks, thus leading to chromosomal breaks and the formation of MN. Documenting the genotoxic potential of the other LIB particles, especially those containing Co and/or Ni, is therefore needed to guarantee a safe and sustainable development of LIB.

3.3.2 Background

Li-ion batteries (LIB) are used in most portable electronics. This technology has replaced nickel-cadmium and nickel metal hydride batteries because of its higher energy density, higher efficiency and longer life. Low weight, design flexibility and size are other advantages of LIB [6, 281]. The LIB anode usually consists of porous

carbon, and the cathode is made of Li metal oxide particles. As these particles are respirable in size, poorly soluble and persist in the lung, the health risks associated with human exposure should be carefully evaluated, especially in occupational settings. Moreover, future applications of LIB, such as multi-layer systems made for spray-paintable or printable DIY batteries [15, 17, 18], might extend the potential for inhalation exposure to consumers. $LiCoO_2$ (LCO) particles are one of the most used cathode material for LIB [19]. We showed in recent experimental studies that LCO particles induce lung oxidative stress, inflammation, and fibrosis in mice [260, 279]. The mutagenic and carcinogenic potential of LCO particles has not been examined yet.

The genotoxic potential of inhaled particles is defined by their ability to induce DNA damage via a primary and/or a secondary mechanism. Primary genotoxicity is due to the intrinsic characteristics of the particles, including composition, shape, size, crystallinity or their capacity to produce reactive oxygen species (ROS). Secondary genotoxicity is associated with the production of ROS by leukocytes recruited during lung inflammation induced by the inhalation of these particles [129]. Mutations occur when DNA damage is not (well) repaired and persists after cell division. Several inhaled particles or fibres have a mutagenic activity, including crystalline silica via a secondary mechanism [282] or asbestos via primary and secondary mechanisms [283]. Assessing the genotoxicity and mutagenic activity of LCO particles appears, therefore, relevant as these particles have a strong inflammatory potential, even stronger than crystalline silica particles, and induce oxidative stress in mouse lungs [260]. Moreover, LCO particles contain bioaccessible cobalt [260, 279]. Co(II) ions have a genotoxic activity due to their ability (i) to produce hydroxyl radicals ($HO^{\bullet}$) via a Fenton-like reaction and (ii) to interact with and inhibit proteins, including those implicated in DNA repair [167]. In 2006, the International Agency for Research on Cancer (IARC) classified cobalt sulfate, other soluble cobalt(II) salts and cobalt metal as possibly carcinogenic to humans (Group 2B) and cobalt metal with tungsten carbide (WC-Co) as probably carcinogenic to humans (Group 2A) [284]. In this paper, we assess the mutagenic potential of LCO particles, and related mechanisms, in comparison with another

particulate material used in LIB, LTO ($Li_4Ti_5O_{12}$) which does not contain genotoxic metals and has a low inflammatory potential compared to LCO [260].

3.3.3 Methods

Particles

LTO ($Li_4Ti_5O_{12}$) and LCO ($LiCoO_2$) particles were obtained from MTI Corporation (Richmond, USA), WC-Co from Metron (USA). Before all experiments (including characterization), particles were heated during 2h at 200°C to inactivate any possible endotoxin or other microbial contaminants. The physico-chemical characterization of heat-treated LTO and LCO particles was reported previously [7]. Particles were suspended in complete culture medium (*in vitro* assays) or 0.9 % saline solution (*in vivo* experiments) without any further treatment.

Epithelial cell culture

RLE cells (rat alveolar epithelial type II cells, RLE-6TN, doubling time > 30 h [285], ATCC, Virginia, USA) were cultured at 37°C in complete medium, i.e. Ham's F12 Nutrient Mix (Gibco, Paisley, UK) supplemented with 1 % antibiotic-antimycotic (Gibco), 10 % fetal bovine serum and 1% Glutamine (Gibco). Before exposure, RLE were plated in 96-well plates for assessing cell viability (55556 or 15600 cells/cm^2), 24-well plates for comet assays (15600 cells/cm^2), or Lab-Teck plates (55556 cells/cm^2) for micronucleus (MN) assays. After 24 h incubation in complete medium at 37°C, cells were exposed to particles during 24 h in complete culture medium. For experiments inhibiting the formation of hydroxyl radicals, catalase (3000 U/ml, Sigma-Aldrich) was added to the cells with the particles.

Cell viability assays

Cell viability was evaluated by using the water soluble tetrazolium salts (WST-1) assay (Roche, Mannheim, Germany, 5 %) or the CellTiter-Glo Luminescent viability assay (Promega, USA) following manufacturer's instructions.

In vitro cytokinesis-block micronucleus assay

Four h after the addition of particles to the cells, cytochalasin B was added (3 µg/ml, Sigma-Aldrich, Missouri, USA). After 24 h exposure, cells were washed twice with phosphate buffered saline (PBS), fixed 20 min in methanol and stained with acridine orange (0.012 % in PBS). Five hundreds cells per well were counted with a Zeiss AxioImager fluorescence microscope (magnification x400) for assessing the cytokinesis-block proliferation index (CBPI) [286, 287]:

$$\text{CBPI} = \frac{\text{number of mononucleated cells} + 2 \times \text{number of binucleated cells} + 3 \times \text{number of multinucleated cells}}{\text{Total number of cells}}$$

One thousand binucleated cells per well were examined for the presence of 1, 2 or more MN following the criteria described previously [288].

Particle endocytosis

We performed the *in vitro* cytokinesis-block micronucleus assay and examined the presence of particles in the cytoplasm of one hundred binucleated cells with a Zeiss AxioImager flurorescence microscope (magnification x400).

Animals and treatments

Female Wistar rats were purchased from Janvier Labs (St Bertevin, France). Eight-week-old animals were kept with sterile rodent feed and acidified water, and housed in positive-pressure air-conditioned units (25°C, 50 % relative humidity) on a 12h light/dark cycle. LTO and LCO particles were suspended in sterile 0.9 % saline solution and WC-Co in sterile H_2O. Rats were randomly allocated to experimental groups. After anaesthesia with a mix of Nimatek, 7.5 mg/rat (Eurovet, Bladel, Nederland) and Rompun, 1.5 mg/rat (Bayer, Kiel, Germany) given intraperitoneally, 300 µl particle suspensions or NaCl (control groups) were directly administered by oro-pharyngeal aspiration. Rats were exposed to 5 or 1 mg of LCO or LTO, corresponding to an inflammatory and a low inflammatory dose of LCO in mice (see Figure 16), and to 0.3 and 0.1 mg in order to identify non-inflammatory doses in rats. Rats were also exposed to 2 mg of WC-Co. Rats were sacrificed 3 days after particle administration with an intraperitoneal injection of 30 mg sodium pentobarbital (Certa, Braine-l'Alleud, Belgium). Rats were sacrificed randomly.

Assessment of the in vivo inflammatory responses

Broncho-alveolar lavage was performed by cannulating the trachea and infusing the lungs with 5 ml NaCl 0.9 %. Broncho-alveolar lavage (BAL) was centrifuged 10 min at 4°C (240 *g*). Cell-free supernatant (BALF) was used for biochemical measurements. After resuspension in NaCl, total BAL cells were counted in Turch (crystal violet 1 %, acetic acid 3 %). Lactate dehydrogenase (LDH) activity and total proteins were assayed on BALF (Cobas 8000, Roche Diagnostics).

Ex vivo micronucleus assay on type II pneumocytes

The *in vivo* mutagenic potential of particles was evaluated on type II pneumocytes (AT-II cells) isolated 3 days after rat exposure as described previously [289]. Isolated cells (an average of $12x10^6$ ATII cells/rat) were cultured during 2 d at 37°C and then fixed 20 min in methanol 100 % and stained with acridine orange. Cells were then analyzed with a Zeiss AxioImager fluorescence microscope. 1000 AT-II cells per rat were evaluated for the presence of MN.

Electron paramagnetic resonance/spin trapping

Twenty-five mg particles were incubated in 0.5 ml PBS (0.5 M, pH 7.4, Sigma-Aldrich), 0.25 ml 5,5-dimethyl-l-pyrroline-N-oxide (DMPO, 0.15 M, Alexis, Lausen, Switzerland) used as spin-trapping agent and 0.25 ml H_2O_2 (0.2 M, Sigma-Aldrich) in order to analyse the $HO^{\bullet}$ radical production. Particle suspensions were incubated under gentle agitation. Aliquots of 50 µl were withdrawn after 10, 30 and 60 min of incubation, filtered to remove particles and the generation of free radicals was monitored by electron paramagnetic resonance (EPR) spectroscopy with a Miniscope MS 100 (Magnettech, Berlin, Germany) EPR spectrometer. The instrument settings were as follows: microwave power 10 mW, modulation 1000 mG, scan range 120 G, center of field approximately 3345 G.

Sodium terephthalate (TA) assay

Particles (5 mg/ml) were suspended in TA solution (10 mM in PBS, pH 7.4) supplemented with H_2O_2 (0.2 M) and incubated 30 min (for LTO and LCO) or 15 min (for WC-Co) under gentle agitation at 25°C [290]. To inhibit hydroxyl radical

formation, catalase was added (3000 U/ml). After incubation, solutions were filtered (Millex-GS sterile filter Unit with MF-Millipore MCE membrane, 0.22 µm, Merck, Darmstadt, Germany). Fluorescence was measured with SpectraMax (excitation light= 324 nm, emission light = 425 nm).

Comet assay (single-cell gel electrophoresis)

The DNA strand breaks induced by particles after 24 h were assessed in RLE cells by using an alkaline comet assay (Trevigen, Kampenhout, Belgium) [291] following manufacturer's instructions. The analyses of oxidative DNA damage were performed by using comet assay in conjunction with *E. coli* formanidopyrimidine-DNA glycolase (FPG) and human 8-oxoguanine DNA glycosylase 1 (hOGG1) (Trevigen). Results were analyzed with a Zeiss AxioImager fluorescence microscope (magnification x100) as described in the OECD test guidelines 489. Fifty cells from 2 replicates were measured for DNA damage by means of the % DNA tail metric using the CaspLab program (casplab 1.2.3b2) according to the following formula:

$$\text{DNA tail (\%)} = \frac{\text{Tail}}{\text{Head + Tail}} \text{ x } 100$$

The means of the two medians for each condition were represented (OECD test guidelines 489).

Statistics

Graphs and statistical analyses were performed with GraphPad Prism 5.0. All results are expressed as means ± standard error on the mean (SEM of N independent experiments, each conducted with n replicates). Differences between control and treated groups were evaluated by one-way analysis of variance (ANOVA) followed by a Dunnett's multiple comparison or a t-test as appropriate. Statistical significance was considered at $P < 0.05$.

3.3.4 Results

LCO particles induce micronuclei in lung epithelial cells in vitro

Within the framework of the 3R's (Replacement, Reduction and Refinement) strategy proposed by the European legislation [215], we first assessed the mutagenic activity of LCO particles *in vitro* by using the cytokinesis-block MN assay on rat lung epithelial cells (RLE) [288]. WC-Co particles were used as positive control. We first determined non-cytotoxic concentrations. After 24 h, WC-Co was non-cytotoxic up to 50 µg/ml, LCO was non-cytotoxic up to 30 µg/ml and very weakly cytotoxic at 50 µg/ml, and LTO was non-cytotoxic up to 100 µg/ml (**Figure 23 a**). Fifty µg/ml WC-Co, 5-50 µg/ml LCO and 30-100 µg/ml LTO were selected to perform the cytokinesis-block MN assay.

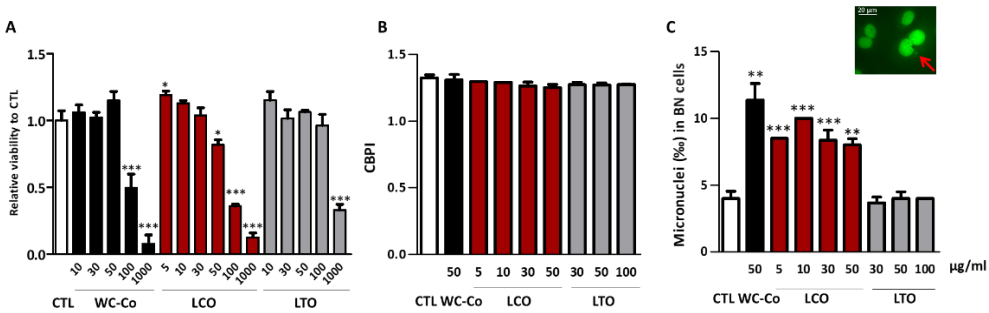

Figure 23: LCO particles induce MN in lung epithelial cells *in vitro*. Rat lung epithelial cells (RLE, 55556 cells/cm^2) were exposed to culture medium (control, CTL), WC-Co, LCO or LTO, and cytotoxicity was assessed after 24 h by the WST-1 assay **(a)**. The CBPI **(b)** was assessed in 500 cells exposed to non-cytotoxic particle concentrations, and the frequency of MN determined in 1000 binucleated cells **(c)**. Image of a binucleated cell containing a micronucleus designated by the red arrow **(c)**. *P < 0.05, **P < 0.01 and ***P < 0.001 relative to CTL cells (t-test or one-way ANOVA followed by a Dunnett's multiple comparison). Bars represent means ± SEM (N = 2 for results obtained with 5 µg/ml LCO; N = 4 for all other results with n = 2 for CTL and n = 4 for all other conditions).

We next performed the cytokinesis-block MN assay. The proliferation of RLE (assessed by the cytokinesis-block proliferation index, CBPI) was not significantly altered by the particles at these concentrations (**Figure 23 b**, LCO: ANOVA p = 0.63, trend test p = 0.23, LTO: ANOVA p = 0.97, trend test p = 0.87). Like WC-Co, LCO particles increased MN frequency at all concentrations tested, indicating a primary

mutagenic activity (**Figure 23 c**). LTO particles did not increase MN frequency. To assess the influence of endocytosis on our results (cytochalasin B used to block cytokinesis can inhibit endocytosis), we counted binucleated cells containing particles in their cytoplasm and the number of particles per binucleated cells. Particles were visible in approximately 80 % of the binucleated cells 24 h after treatment and this proportion, as well as the number of particles per binucleated cells, were similar for both LCO or LTO particles (**Annexes, Figure S11**).

LCO particles induce micronuclei in lung epithelial cells in vivo

We next confirmed the mutagenic activity of LCO particles *in vivo,* as proposed by the REACH regulation [292], using a MN assay in isolated rat alveolar type II epithelial (AT-II) cells.

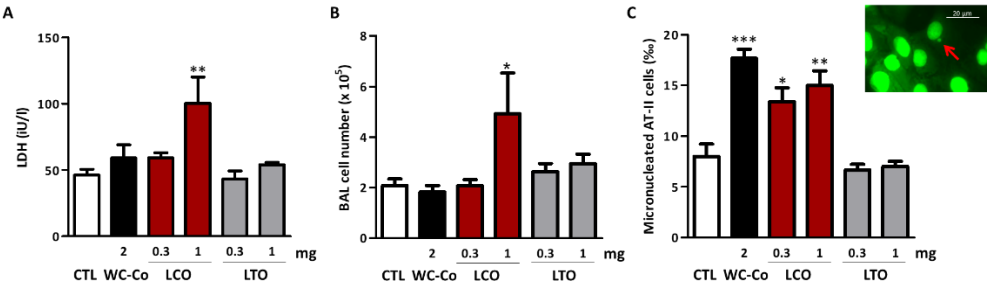

Figure 24: LCO particles induce MN in lung epithelial cells *in vivo*. Wistar rats were treated with an oro-pharyngeal aspiration of NaCl (control, CTL), WC-Co, LCO or LTO particles. Inflammation and MN were assessed after 3 days. LDH activity **(a)** was measured in the BALF, recruited inflammatory cells **(b)** in the BAL and the frequency of micronuclei **(c)** in AT-II cells isolated from rat lungs. Image of an AT-II cell containing a micronucleus designated by the red arrow **(c)**. *P < 0.05, **P < 0.01 and ***P < 0.001 relative to CTL mice (t-test or one-way ANOVA followed by a Dunnett's multiple comparison). Bars represent means ± SEM (N = 2, n = 4 for the first experiment and n = 2 for the second experiment).

To determine non-inflammatory and inflammatory doses, rats were first treated with an oro-pharyngeal aspiration of 0.1, 0.3, 1 or 5 mg of LCO or LTO particles. LDH activity (a marker of cytotoxicity), protein concentrations (a marker of alveolar permeability) and inflammatory alveolar cell infiltration were measured in BAL 3 days after administration (**Annexes, Figure S12**). Based on these results, doses of 0.3 and 1 mg LCO were selected for the MN assay as non-inflammatory and inflammatory doses, respectively, to help to discriminate mutations due to primary

and secondary genotoxic mechanisms (**Figures 24 a, b**). WC-Co was used as positive control at the dose of 2 mg [293]. The frequency of MN was assessed in rat lung AT-II cells isolated 3 days after administration of the particles (**Figure 24**). This time point captures the impact of acute inflammation [260, 294], and allows AT-II cells to undergo *in vivo* division and to reveal MN [293]. As expected, increased MN frequencies were detected after WC-Co (**Figure 24 c**). LCO particles also increased MN frequencies at the doses of 0.3 and 1 mg, confirming that they act, at least, via a mechanism of primary genotoxicity. LTO particles did not increase MN frequency *in vivo*.

LCO particles have an intrinsic capacity to generate hydroxyl radicals

Because of their cobalt content, we investigated the capacity of LCO particles to produce $HO^{\bullet}$ by using an EPR assay (**Figure 25 a**). LCO particles constantly produced $HO^{\bullet}$ over 60 min. No $HO^{\bullet}$ production was observed with LTO particles (**Figure 25 a**). As $HO^{\bullet}$ are the most potent DNA interacting ROS and can induce DNA breaks [128], they could account for the primary genotoxic activity of LCO particles.

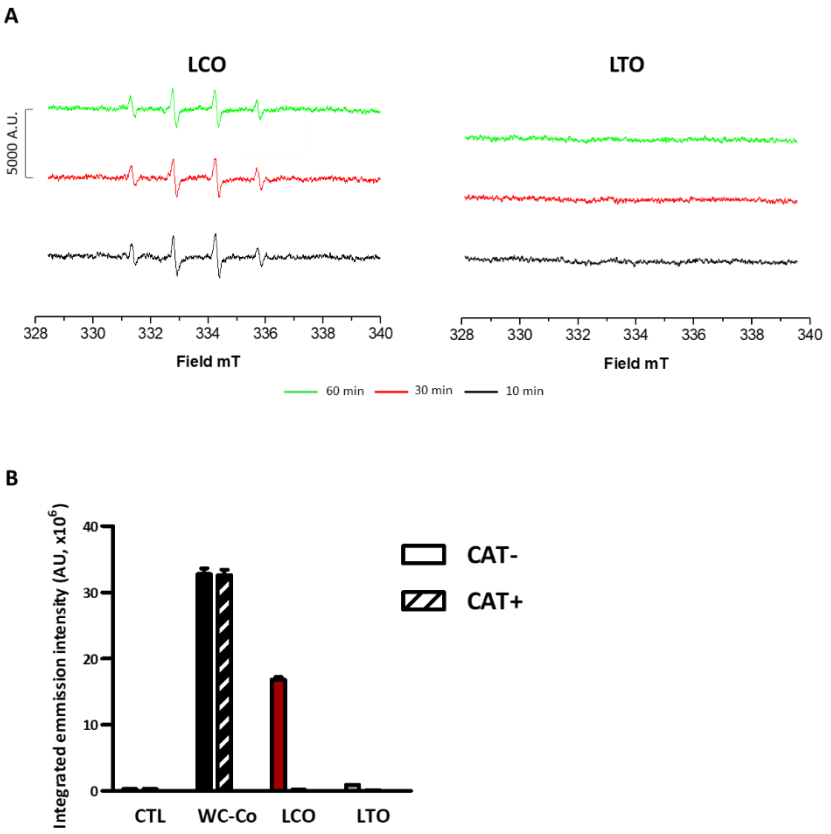

Figure 25: Generation of hydroxyl radicals by LCO particles. EPR spectra **(a)** of [DMPO-HO]• adducts after incubation with 25 mg/ml LCO or LTO particles in the presence of H_2O_2 (0.2 M) under gentle agitation. Spectra were collected after 10, 30 and 60 min. Fluorescence intensity **(b)** recorded on the supernatant from 5 mg/ml WC-Co, LTO or LCO particles incubated 15 min (for WC-Co) or 30 min (for LCO and LTO) in a PBS solution of disodium TA (10 mM) with H_2O_2 (0.2 M) under gentle agitation, in absence (CAT-) or in presence of 3000 U/ml catalase (CAT+). Control (CTL) did not contain particles (N = 2, n = 4 for the control condition and n = 6 for all other conditions).

LCO particles induce oxidative DNA damage in RLE in vitro

To further investigate whether $HO^{\bullet}$ produced by LCO particles contribute to their genotoxic activity, we applied the comet assay in the presence of the oxidative DNA damage repair enzyme hOGG1.

hOGG1 specifically recognizes and cleaves oxidative lesions leading to additional DNA fragments. We first assessed the cytotoxicity of particles on RLE (**Figure 26 a**) in the culture conditions used for the comet assay. RLE were exposed to 10-1000 µg/ml WC-Co, 10-1000 µg/ml LCO or LTO particles during 24 h. After 24 h, WC-Co was non-cytotoxic up to 50 µg/ml and LCO and LTO up to 100 µg/ml (**Figure 26 a**). Fifty µg/ml WC-Co, 10-100 µg/ml LCO and 100 µg/ml LTO were used to perform the comet assay. As expected, WC-Co induced DNA strand breaks and oxidative lesions as the % tail DNA increased when cells were treated with hOGG1 (**Figure 26 b**) [295].

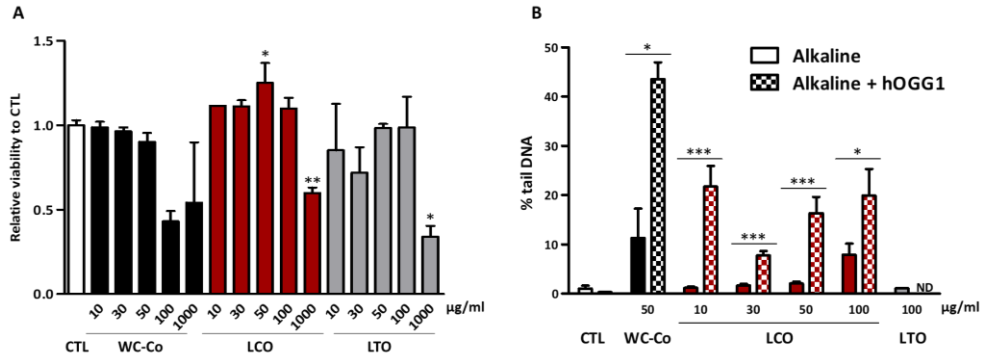

Figure 26: LCO particles induce DNA strand breaks and DNA oxidative lesions in lung epithelial cells *in vitro*. Rat lung epithelial cells (RLE, 15600 cells/cm^2) were exposed to culture medium (control, CTL), WC-Co, LCO or LTO and cytotoxicity was assessed after 24h by the WST-1 assay **(a)**. Alkaline comet assay, with or without oxidative DNA lesion repair enzyme (hOGG1), was performed 24 h after exposure to particles **(b)**. *P < 0.05, **P < 0.01 and ***P < 0.001 (t-test between alkaline and alkaline + hOGG1 conditions). Bars represent means ± SEM (N = 4 with n = 4 for the WST-1 assay, N = 4 for the alkaline comet assay performed without hOGG1 and N = 2 for the alkaline comet assay performed with hOGG1, n = 2). ND = not determined.

DNA strand breaks were induced in a dose-dependent manner by LCO particles. The addition of hOGG1 revealed additional DNA breaks, reflecting the presence of oxidative lesions. LTO particles did not induce DNA breaks (**Figure 26 b**). The same results were obtained with another oxidative damage repair enzyme, the *E. Coli* formamidopyrimidine-DNA glycosylase (FPG, data not shown).

Catalase prevents the formation of MN by LCO particles

To assess the implication of oxidative DNA lesions in the induction of MN by LCO particles, we used catalase to block the formation of $HO^{\bullet}$ in the Fenton-like reaction. We first performed a terephthalate (TA) assay with catalase to verify its capacity to inhibit $HO^{\bullet}$ formation in our system. LCO, LTO or WC-Co particles were incubated in TA with or without catalase during 15 or 30 min. Addition of catalase prevented $HO^{\bullet}$ production by LCO particles (**Figure 25 b**). LTO particles did not generate $HO^{\bullet}$ in this test. As expected, $HO^{\bullet}$ produced by WC-Co were not affected by catalase as $HO^{\bullet}$ produced by WC-Co are independent of the presence of H_2O_2 [296].

We next performed the cytokinesis-block MN assay in RLE with catalase (**Figure 27**).

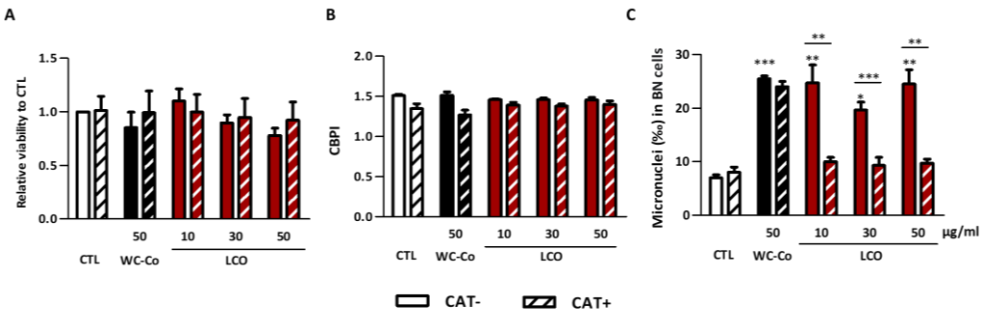

Figure 27: LCO particles induces MN via $HO^{\bullet}$ generation. Rat lung epithelial cells (RLE, 55556 cells/cm^2) were exposed to culture medium (control, CTL), WC-Co, LCO particles in absence (CAT-) or in presence of 3000 U/ml catalase (CAT+). Cytotoxicity was assessed after 24 h by the CellTiter-Glo Luminescence viability test **(a)**. The CBPI **(b)** was assessed in 500 cells, and the number of MN in 1000 binucleated cells **(c)**. *P < 0.05, **P < 0.01 and ***P < 0.001 (t-test or one-way ANOVA followed by a Dunnett's multiple comparison relative to the control condition, and t-test between CAT- et CAT+ conditions). Bars represent means ± SEM (N = 2 for cytotoxicity assessment and N = 3 for CPBI and MN assessment, n = 4 for cytotoxicity assessment and n = 2 for CBPI and MN assessment).

RLE were exposed to 50 µg/ml WC-Co, or 10-50 µg/ml LCO particles with or without catalase. This assay was not conducted with LTO particles as they did not induce MN (**Figure 23**). Twenty-four h after particle exposure without catalase, cell viability and proliferation was not affected by the particles (**Figures 27 a, b**). For this experiment, we performed the CellTiter-Glo Luminescent viability assay to avoid

possible interference between the yellow color of catalase and the colorimetric WST-1 assay used in previous experiment (**Figure 23 a**). Addition of catalase did not affect cell viability or proliferation. Catalase did not modify the mutagenic potential of WC-Co particles (**Figure 27 c**) as expected (**Figure 25**). In contrast, MN induced by LCO particles were less frequent in presence of catalase, indicating that $HO^{\bullet}$ produced by LCO particles contribute to the formation of MN.

3.3.5 Discussion

We demonstrate here the primary mutagenic activity of LCO particles used in LIB. These particles are able to induce mutations *in vitro* and *in vivo*, while LTO particles do not appear genotoxic.

We selected the MN assay to assess the genotoxic potential of these particles because this test detects mutations relevant for the carcinogenic process [288]. Advantages of the MN assay compared to other genotoxicity tests are its capacity to detect both clastogenic and aneugenic events, and the epidemiological evidence of its predictive value in terms of cancer risk [283, 297].

LCO particles induced MN in AT-II cells isolated from rat lungs at a non-inflammatory dose indicating that they can act in the lung via a primary genotoxic mechanism. LCO particles also induced a slightly higher MN frequency at the inflammatory dose reflecting either a secondary mechanism of genotoxicity or a dose-dependent primary effect. The primary genotoxic activity of LCO particles was also observed *in vitro* where the use of cytochalasin B allowed controlling any confounding of altered cell division or cytotoxicity induced by the particles [288]. In the *in vitro* assay, the formation of MN was not dose-dependent, suggesting a maximum of MN induction at the lowest concentration, or a slight cytotoxicity not detected by the CBPI.

LCO particles contain bioaccessible Co [260]. We suspected cobalt ions and their capacity to produce $HO^{\bullet}$ [167] to be involved in the mutagenic activity of LCO particles. ROS are implicated in the genotoxic activity of several inhaled particles. They can attack DNA and lead to base pair mutations, deletions or insertions, and induce DNA strand breaks. Two types of ROS may be generated, (i) ROS intrinsically

generated by particles and (ii) ROS produced by inflammatory and/or target cells in response to particles [128]. We assessed the capacity of LCO particles to intrinsically produce ROS by the EPR and TA assays. H_2O_2 was included to mimic the reaction that might occur in the lysosomes of macrophages or polymorphonucleated cells, or in lung epithelial cells interacting with inhaled particles [298, 299]. Both assays showed that, unlike LTO, LCO particles produced $HO^{\bullet}$ probably via a Fenton-like reaction which occurs between transition metal ions and H_2O_2 [175, 300]. LCO particles formally contain Co(III), but it has been previously shown that both Co(II) and Co(III) ions can be present at the particle surface [301]. In acidic conditions, Co(II) is the most stable oxidation state and Co(III) is rapidly reduced to Co(II) [164]. Both Co species can participate in their ionic form to a Fenton-like reaction by reacting with OOH^- deriving from H_2O_2 or directly with H_2O_2 [302]. $HO^{\bullet}$ is the most potent ROS to interact with DNA and is a crucial factor in the clastogenic activity of inhaled particles [128]. In the *in vitro* alkaline comet assay with addition of the oxidative DNA damage repair enzymes, LCO particles induced oxidative DNA lesions, suggesting that $HO^{\bullet}$ contribute to their primary genotoxic activity. The blocking effect of catalase supports this hypothesis. For particles, direct DNA damage requires their localization in the nucleus to interact with DNA [303]. Here, DNA damage seemed to be mainly mediated by the production of $HO^{\bullet}$, thus via an indirect mechanism, indicating that particle localization is not determinant in their genotoxic activity. On the other hand, Ortega et al. [170] showed that Co ions released from low soluble Co nanoparticles (Co_3O_4) can be found in the cytoplasm and the nucleus of epithelial cells, suggesting that the Fenton-like reaction induced by LCO Co(II/III) ions could occur in both cellular compartments.

Thus, these results indicate that LCO particles should be considered as presenting a carcinogenic hazard in case of inhalation since they exhibit 3 key characteristics of human carcinogens identified by Smith et al. [278]: the capacity to induce lung oxidative stress, and chronic inflammation [260], and a mutagenic activity. The capacity of LCO particles to release Co(II) ions appears responsible for their mutagenic activity.

In our previous study on a panel of LIB particles (LCO, LTO, $LiNiCoAlO_2$, $LiNiCoMnO_2$ and $LiFePO_4$), we showed that particles containing Co and/or Ni can cause lung

inflammation and fibrosis in mice [260, 279]. Since Ni compounds can also exert a mutagenic activity [280], other LIB particles containing Co and/or Ni could also be mutagenic. In addition, LCO and other LIB particles containing Co and/or Ni, strongly stabilize hypoxia-inducible factor (HIF) -1α in lung tissue [279], a transcription factor involved in tumor growth, angiogenesis and metastasis [140], further suggesting a potential carcinogenic activity of these particles.

3.3.6 Conclusions

We established the primary mutagenic activity of LCO particles used in LIB *in vitro* and *in vivo*. Our data support the role of Co(II) ions released from these particles in their mechanism of mutagenicity, which includes the formation of $HO^{\cdot}$ by a Fenton-like reaction and oxidative DNA lesions, thus leading to chromosomal breaks and the formation of MN. Documenting the genotoxic potential of the other particles containing Co/Ni used in LIB is needed to guarantee a safe and sustainable development of LIB.

3.3.7 Declarations

Ethics approval and consent to participate

All animal experiments were approved by the local committee for animal research at the Université catholique de Louvain, Comité d'Ethique pour l'Expérimentation Animale, Secteur des Sciences de la Santé, Brussels, Belgium (No LA1230312).

Consent for publication

Not applicable.

Availability of data and material

The datasets used and/or analyzed during the current study are available from the corresponding author on reasonable request.

Competing financial interest statements

The authors declare that they have no competing interests.

Funding

"Programme d'excellence BATWAL 1318146 from the SPW DG06 (Belgium)" supported the research project and financed SV. VS is financed by a grant from the "Fonds pour la Formation à la Recherche dans l'Industrie et dans l'Agriculture (FRIA)".

Authors' contributions

VS, SV and DL designed the experiments, contributed to data analysis and interpretation, and co-wrote the manuscript. VS performed most experimental work. VSC contributed to micronuclei experiments. SM and PH contributed to comet assays. MT and FT contributed to EPR analyses. YY participated to *in vivo* experiments. All authors read and approved the manuscript.

Acknowledgements

Not applicable.

CONCLUSIONS AND PERSPECTIVES

Overall, this work contributes to the identification and evaluation of the respiratory hazard of particles used in LIB. We focused on the respiratory toxicity of inhaled LIB particles, in terms of inflammation, fibrosis and genotoxicity and related mechanisms were investigated. We showed that some LIB particles can induce lung inflammation and fibrosis in mice, and mutations in rats. LIB particles can thus represent a respiratory hazard and exposure to LIB particles should, therefore, be strictly controlled in occupational settings. This work also provides mechanistic knowledge and tools to rapidly screen the toxic potential of existing and new LIB particles and highlights the role of Co and Ni in their toxicity. Thus, our study prepares the way for a sustainable development of LIB components.

Given that some LIB particles contain dermal and respiratory sensitizers such as Ni and Co (see sections 2.4.2 and 2.4.3), their effects on the development of asthmatic reactions and dermal allergies should also be evaluated in the future.

Mechanistic overview of the lung toxicity of Co/Ni LIB particles

We found that LIB particles containing Co and/or Ni can induce strong and chronic inflammatory responses in the lung, more severe than for other LIB particles. Although Li ions can substitute Ca^{2+} and K^{+} in physiological processes [153], and could participate to the activation of the NRLP3 inflammasome [304, 305], our data suggest that Li does not play an essential role in the inflammatory activity of LIB particles. Instead their Co/Ni content and bioaccessibility are major determinants of toxicity.

Based on the literature and mechanistic data obtained during this study (mainly with LCO), we identified pathways and determinants of lung injury induced by Co/Ni LIB particles. This network of events is illustrated in **Figure 28**. Inhaled particles can activate NF-κB, controlling the transcription of pro-IL-1β, via various pathways described in the introduction (chapter "inflammation" in section 2.3.3). Co and Ni ions can directly stabilize NF-κB [273, 274], and also HIF-1α [138, 168] promoting NF-κB activity in macrophages, neutrophils and non-immune cells [135, 142]. Based on our experimental data, we conclude that HIF-1α is an upstream signal for IL-1β (transcription and/or secretion), and that both IL-1β and HIF-1α are implicated in lung inflammation induced by LCO particles [279]. In view of the particle properties, we also suggest that IL-1β can be activated either by lysosomal disruption (after particle endocytosis) or by ROS produced by particles via a Fenton-like reaction. We did not observe reduced fibrosis in IL-1β KO mice 2 months after LIB particle exposure (data not shown), supporting the fact that other events are necessary for the development of lung fibrosis. Some evidence support the role of an immunosuppressive phase (activation of Th2 lymphocytes and M2 macrophages and secretion of immunosuppressive cytokines and growth factors), activated by inflammation, that in turn deregulates the wound healing process [107, 117]. We also propose that Fe contained in ferruginous bodies (FB) present after 2 months in mouse lungs exposed to LCO [260], that can produce ROS via the Fenton reaction [124, 258], may further contribute to the oxidative stress and inflammation. In addition to inflammation, LCO particles also induce genotoxicity via the production of $HO^{\bullet}$, leading to mutations [306]. Given that LCO particles are able to induce chronic inflammation, oxidative stress and mutations, as well as to stabilize HIF-1α

which is involved in tumor growth, angiogenesis and metastasis [135], they might also be considered as able to induce lung cancer [278].

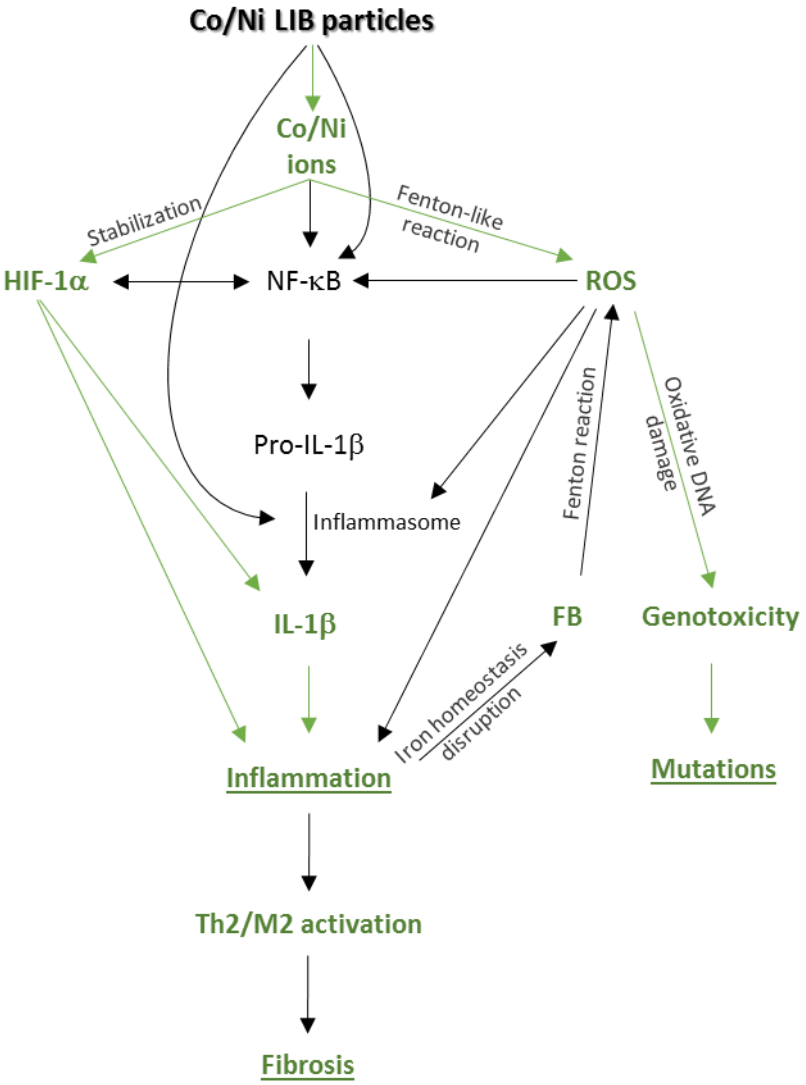

Figure 28: Potential pathways induced by Co/Ni LIB particles leading to lung inflammation, fibrosis and mutations. **Green** = pathways or events observed in the present study, **black** = hypothetical pathways or events based on the literature.

Overall, LIB particles induce a range of events leading to different intensities of lung responses. We identified the Co/Ni content and their bioaccessibility as indicators of the toxic potential of LIB particles. A ranking in this subgroup of LIB particles can thus be established based on these characteristics.

Mechanisms of LIB particle toxicity in a broader context

We showed that some LIB particles can induce sub-chronic inflammation and fibrotic responses in mice. The mechanisms involved in the development of lung fibrosis (related to chronic inflammation induced by exogenous substances) are still incompletely understood but several efforts recently contributed to build a putative AOP organizing the events leading to lung fibrosis [229, 307, 308]. The AOP 173 for lung fibrosis ("substance interaction with the lung resident cell membrane components leading to lung fibrosis") places inflammation as an important mechanistic step [309] (**Figure 29**).

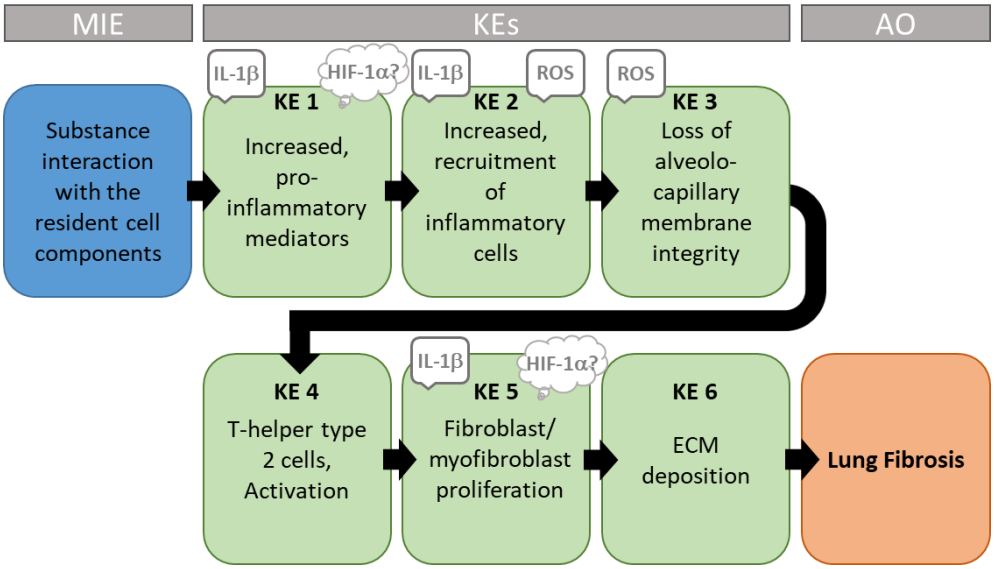

Figure 29: AOP 173 "Substance interaction with the lung resident cell membrane components leading to lung fibrosis". IL-1β and ROS (bubbles) are inflammatory mediators described in AOP 173. HIF-1α (clouds) was identified in this study and could participate in KE1 and 5. Adapted from [309].

In this AOP, the MIE is the interaction between the substance and the components of the cellular membrane, which leads to the release of alarmins. The first KE is the secretion of pro-inflammatory and fibrotic mediators (KE 1), leading to inflammatory cell recruitment (KE 2). This results in the loss of alveolo-capillary membrane integrity (KE 3) and the activation of Th2 type cell signaling (KE 4), followed by fibroblast proliferation and differentiation (KE 5), as well as excessive extracellular matrix (ECM) and collagen deposition (KE 6). IL-1β has an important place as a pro-inflammatory cytokine implicated in the recruitment of inflammatory cells (KEs 1 and 2) and in fibroblast proliferation (KE 5). Several studies have investigated the implication of IL-1β in lung fibrosis by using KO mice or inhibitors, and showed a decrease of the fibrotic response [111, 112, 115, 310] or no change [114, 311]. In the present study, we confirmed the role of IL-1β in the development of inflammation. Thus, our data contribute to strengthen the essentiality of IL-1β in the lung responses to particles.

ROS are also present in this AOP as actors of chronic inflammation and loss of alveolar membrane integrity (KEs 2 and 3). There is strong evidence that ROS, produced by particles or by cells in response to particles, or both, participate to their toxicity by initiating a sequence of pathological events, including inflammation, fibrosis, genotoxicity, and carcinogenesis [120, 121]. In this study, we showed that LCO [306] and LFP particles (data not shown) intrinsically produce ROS. However, we do not know if cells exposed to LIB particles produce ROS. We observed oxidative stress 3 days after particle exposure but not after 2 months [260]. This might indicate that only ROS directly produced by particles participate to the lung responses. In AOP 173, only secondary ROS (ROS produced by cells) are mentioned but not primary ROS (produced by the particles), probably because an AOP is not substance-specific, and not all particles produce ROS. We identified HIF-1α as a key mediator of inflammation induced by LIB particles. The early HIF-1α stabilization was probably due to the presence of Co/Ni ions. Stabilization of HIF-1α two months after particle exposure was also observed with crystalline silica particles [260, 279], indicating that HIF-1α is also stabilized by other mechanisms than Co/Ni ions such as phenomena related to chronic inflammation and/or the establishment of fibrosis. Since hypoxia is the main inducer of HIF-1α stabilization,

this could be due to hypoxia resulting from the developing fibrotic tissue. HIF-1α stabilization in fibrotic tissues was reported earlier in kidney and lung [145, 312, 313], and HIF-1α deficiency in mouse attenuated bleomycin-induced pulmonary fibrosis [313]. The implication of HIF-1α in fibrosis is also supported by its role in myofibroblast differentiation as well as epithelial-mesenchymal transition via the TGF-β pathway [140, 142, 147, 150, 151]. Unfortunately, we were not able to assess the implication of HIF-1α at long-term with inhibitors because mice did not tolerate the treatment.

Overall, this suggests that HIF-1α could be included in AOP 173 as a central mediator in KEs 1 (pro-inflammatory mediators) and 5 (fibroblast proliferation and differentiation) (**Figure 29**). Further investigations on the role of HIF-1α in the early and later stages of lung inflammation and fibrosis could be useful to refine the existing AOP.

Perspectives

Exposure to LIB particles

Our research focused on the hazard identification of particles used in LIB. To document the risk of lung toxicity associated to LIB particles for workers, or even for the general population in case of spray-paintable LIB, it is necessary to evaluate exposure levels. Currently, no data are available. Therefore, exposure monitoring of LIB particle air concentrations should be performed in industries. In this study, the no adverse effect level (NOAEL) for sub-chronic lung toxicity was 0.1 mg LCO/mouse and LCO was at least as toxic as crystalline silica. An appropriate inhalation study should be performed to derive tolerable exposure values, such as TLV-TWA, allowing the implementation of control and safety measures. Meanwhile, occupational exposure levels for crystalline silica (e.g. ACGIH TLV-TWA of 0.05 mg/m³, respirable fraction) may serve as upper limit values to control the risk of respiratory toxicity in LCO industries.

Categorization/grouping of LIB particles

Because grouping strategies should allow predicting the hazard of the materials while limiting the number of testings, a ranking of LIB particles in terms of lung toxicity could be useful for industries. In this study, a distinction appeared between LIB particles containing Co/Ni and the others in terms of lung inflammation/fibrosis and associated mechanisms. Particles containing Co and/or Ni appear the most inflammatory. We thus suggest categorizing LIB particles in two groups: LIB particles containing Co and/or Ni (stronger lung inflammation via the capacity to stabilize HIF-1α) and those without Co and/or Ni. To confirm the relevance of this grouping and refine the ranking, we need to perform additional studies, especially with LIB particles that do not contain Co or Ni, to strengthen the key role of Co and Ni. This approach might also be valid for lung fibrosis and should be further investigated, although we could not demonstrate so far any correlation between fibrotic responses and Co/Ni in [279]. However, this might not be appropriate for genotoxicity. Indeed, LFP particles are able to release Fe ions and to produce ROS as observed with EPR analysis (data not shown). LFP particles could thus also induce genotoxicity/mutagenicity but might have a lower cancer potency in the absence of HIF-1α stabilization.

Other determinants of lung toxicity of LIB particles?

During this study, we mainly focused on the implication of the chemical composition of LIB particles on their lung toxicity. However, size distribution, shape and presence of contaminants on or in the particles are other parameters that could strongly influence their toxicity. These parameters may in particular vary with the production process. The evaluation of the lung toxicity of particles with the same composition but from different origins could be useful to determine the possible impact of these parameters. In an exploratory experiment, we evaluated the *in vitro* stabilization of HIF-1α by LCO, LFP and LTO particles from three different producers (data not shown). None of the LFP and LTO particles induced HIF-1α stabilization. The three LCO induced HIF-1α stabilization. However, LCO from MTi (used in [260, 279, 306]) induced a stronger HIF-1α stabilization at low particle concentrations than LCO from the two other producers. Further particle

characterization showed that LCO from MTi has the highest Co ion bioaccessibility at acidic pH and the smallest size distribution. This suggests that other parameters than those explored in this work, such as the particle size, should additionally be considered as determinants of the hazard of LIB particles. According to one of the main paradigms in particle toxicology stating that the smaller the size the greater the toxicity [103], it appears especially important to explore these aspects in the development of nanoparticles for LIB.

Role of HIF-1α in lung fibrosis induced by particles

Additional investigations on the role of HIF-1α in lung inflammation and fibrosis should be performed to refine mechanistic knowledge on the fibrotic process. Since mice did not survive to long-term treatment with HIF-1α transcriptional inhibitors, other models should be used, such as the cell-specific HIF-1α deficient mice [313]. Short-term administration of inhibitors at different stages of the fibrotic process could also help to identify the specific events involving HIF-1α.

ANNEXES

Supplementary data: publication 1 RESPIRATORY HAZARD OF LI-ION BATTERY COMPONENTS: ELECTIVE TOXICITY OF LITHIUM COBALT OXIDE ($LiCoO_2$) PARTICLES IN A MOUSE BIOASSAY, ARCHIVES OF TOXICOLOGY (2018)

Figure S1: Particle size distributions
Figure S2: LIB particles induce different acute inflammatory responses after 18h
Figure S3: Elementary analysis of lung tissue 18 hours after exposure to LIB particles
Figure S4: Localization of LIB particle elements in lung sections by ToF-SIMS after 2 months
Figure S5: Detection of elements by SEM-EDX in lung sections after 2 months
Figure S6: Detection of elements in lungs by x-ray micro fluorescence (µ-XRF)

Supplementary data: publication 2 HIF-1α IS A KEY MEDIATOR OF THE LUNG INFLAMMATORY POTENTIAL OF LITHIUM-ION BATTERY PARTICLES, PARTICLE AND FIBRE TOXICOLOGY (2019)

Figure S7: Particle size distributions
Figure S8: Lung sections of mice 2 months after treatment with LIB particles
Figure S9: HIF-1α drives lung inflammation induced by LCO
Figure S10: Comparison of *in vivo* and *in vitro* dose

Supplementary data: publication 3 $LiCoO_2$ PARTICLES USED IN LI-ION BATTERIES INDUCE PRIMARY MUTAGENICITY IN LUNG CELLS VIA THEIR CAPACITY TO GENERATE HYDROXYL RADICALS, PARTICLE AND FIBRE TOXICOLOGY (2020)

Figure S11: LCO and LTO particle endocytosis by RLE cells
Figure S12: Inflammatory dose-response to LCO and LTO particles

Supplementary data: publication 1

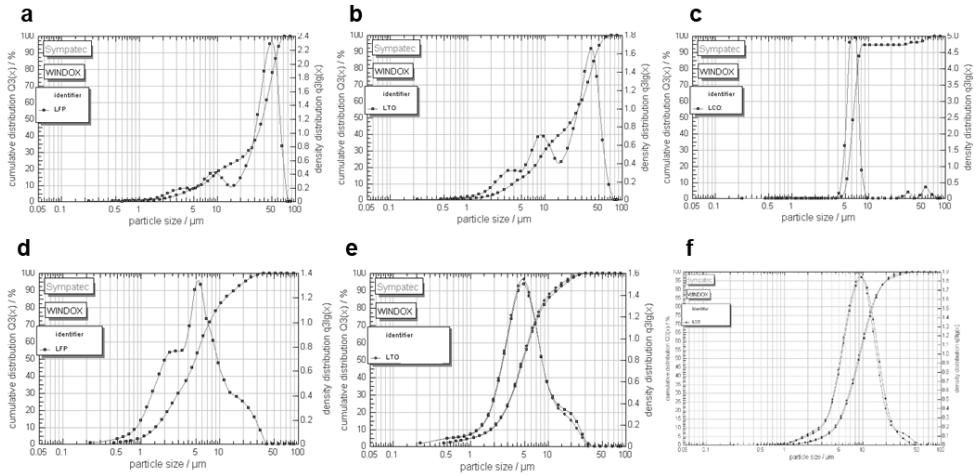

Figure S1: Particle size distributions. LFP **(a, d)**, LTO **(b, e)** and LCO **(c, f)** particle size distribution was assessed by laser diffraction in dry state **(a-c)** or in cyclohexane **(d-f)**.

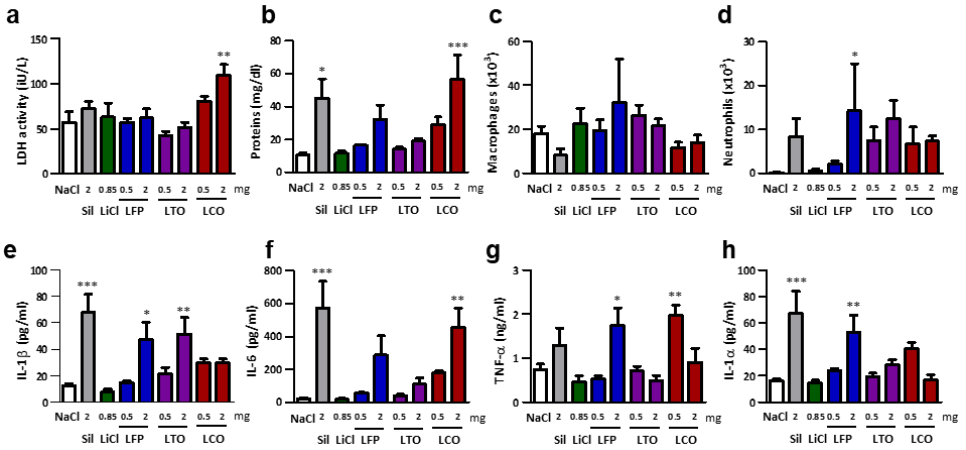

Figure S2: LIB particles induce different acute inflammatory responses after 18h. C57BL/6 mice were exposed by oro-pharyngeal aspiration to NaCl (control), 0.5 or 2 mg LIB particles, 2 mg crystalline silica (Sil) or 0.85 mg LiCl. Inflammation was assessed in the BAL after 18 hours. LDH activity **(a)** and proteins **(b)** were measured in BALF; macrophages **(c)** and neutrophils **(d)** in BAL. Inflammatory cytokines IL-1β **(e)**, IL-6 **(f)**, TNF-α **(g)** and IL-1α **(h)** were quantified by ELISA in the BALF. Only the highest dose of LCO increased LDH activity. Total proteins, IL-1β, IL-6 and IL-1α were increased by all particles and slight increases in neutrophils were observed. LFP and LCO also upregulated TNF-α levels. LCO had the strongest effect on all cytokines at the lowest dose. At the dose of 2 mg LCO, cytokine levels, except for IL-6, did not increase further, consistent with the slight decrease in BAL macrophages and increased LDH activity in BALF at the same dose, which could collectively reflect LCO damage to macrophages and/or epithelial cells. *P < 0.05, **P < 0.01 and ***P < 0.001 relative to NaCl-treated mice (one-way ANOVA followed by a Dunnett's multiple comparison, n = 5, means ± SEM).

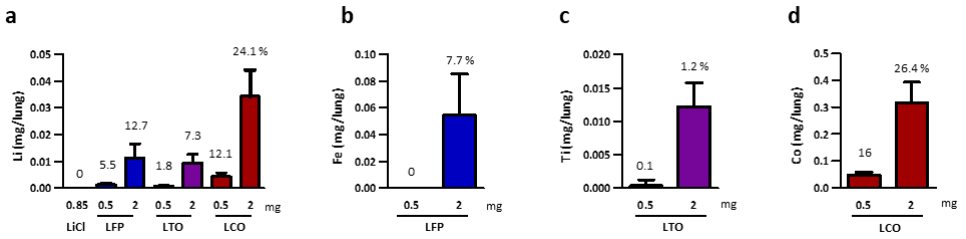

Figure S3: Elementary analysis of lung tissue 18 hours after exposure to LIB particles. Lungs of C57BL/6 mice exposed to NaCl, 0.85 mg LiCl, 0.5 and 2 mg LIB particles by oro-pharyngeal aspiration were analyzed after 18 hours by ICP-MS. Li **(a)**, Fe **(b)**, Ti **(c)** and Co **(d)** contents were measured in mineralized lavaged lung homogenates. Graphs show concentrations calculated by subtracting levels measured in control lungs from values in treated lungs. Percentages were calculated as a ratio to the exposure dose (n = 5, means ± SEM).

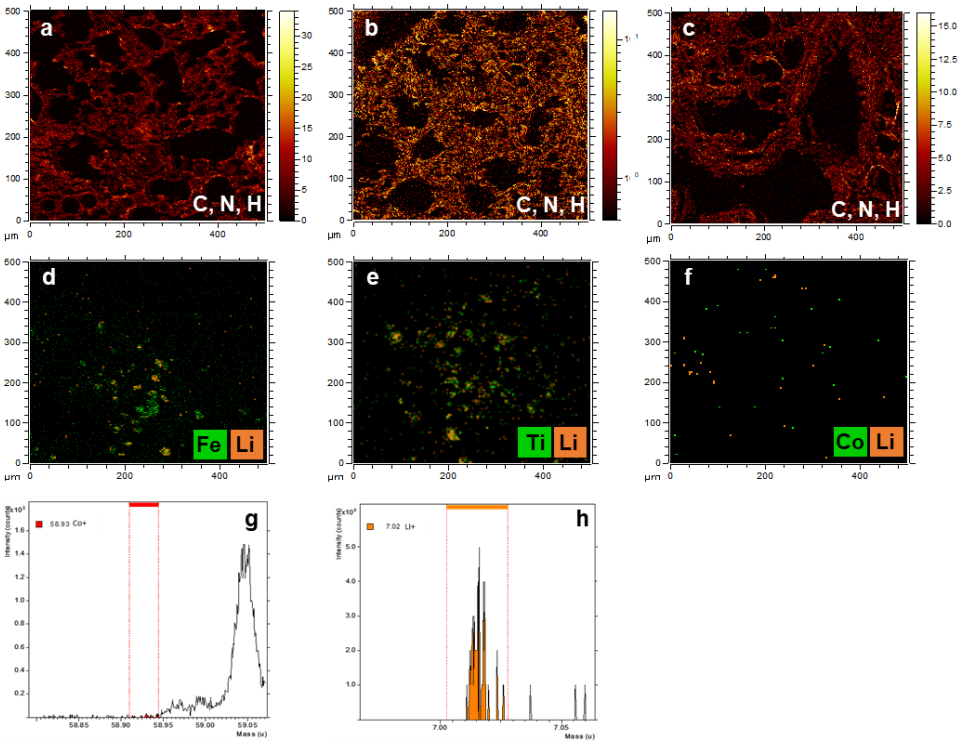

Figure S4: Localization of LIB particle elements in lung sections by ToF-SIMS after 2 months. Lung sections from mice exposed to 2 mg LFP, LTO or LCO were analyzed after 2 months by ToF-SIMS. ToF-SIMS maps show the distribution of Li and Fe in LFP- **(d)**, Li and Ti in LTO- **(e)** and Li and Co (background signal, see below) in LCO-treated lungs **(f)**. C, N, H distributions represent the lung matrix **(a-c)**. Spectra show the detection of Co **(g)** and Li **(h)** in LCO lungs. Co spectrum corresponds to the background noise while Li spectrum reveals the presence of Li in LCO lungs.

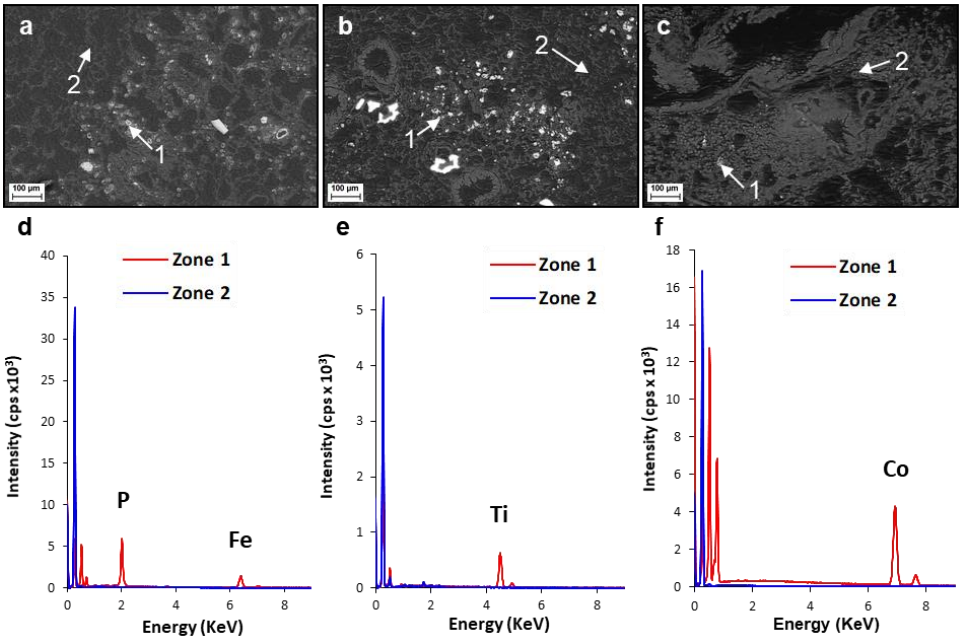

Figure S5: Detection of elements by SEM-EDX in lung sections after 2 months. Lung sections of mice exposed to 2 mg LFP **(a, d)**, LTO **(b, e)** or LCO **(c, f)** were analyzed after 2 months. Lung sections were scanned by SEM **(a-c)** and analyzed by EDX **(d-f)**. Lungs contain brilliant spots attributed to the presence of LIB particles. EDX spectra for zones 1 (brilliant spots) and 2 (lung matrix) are shown **(d-f)**.

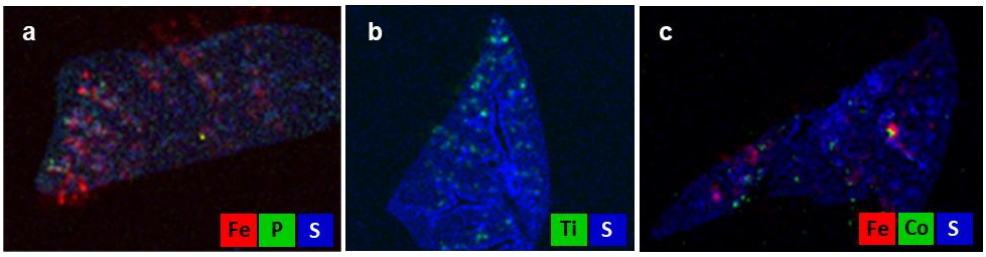

Figure S6: Detection of elements in lungs by x-ray micro fluorescence (µ-XRF). Paraffin-embedded lungs of mice exposed to 2 mg LFP **(a)**, LTO **(b)** and LCO **(c)** were analyzed after 2 months by µ-XRF. µ-XRF maps show the distribution of Fe and P **(a)** in LFP-, Ti **(b)** in LTO- and Fe and Co **(c)** in LCO-treated lungs. S distribution represents the lung matrix **(a-c)**. 1 px = 76 µm.

Supplementary data: publication 2

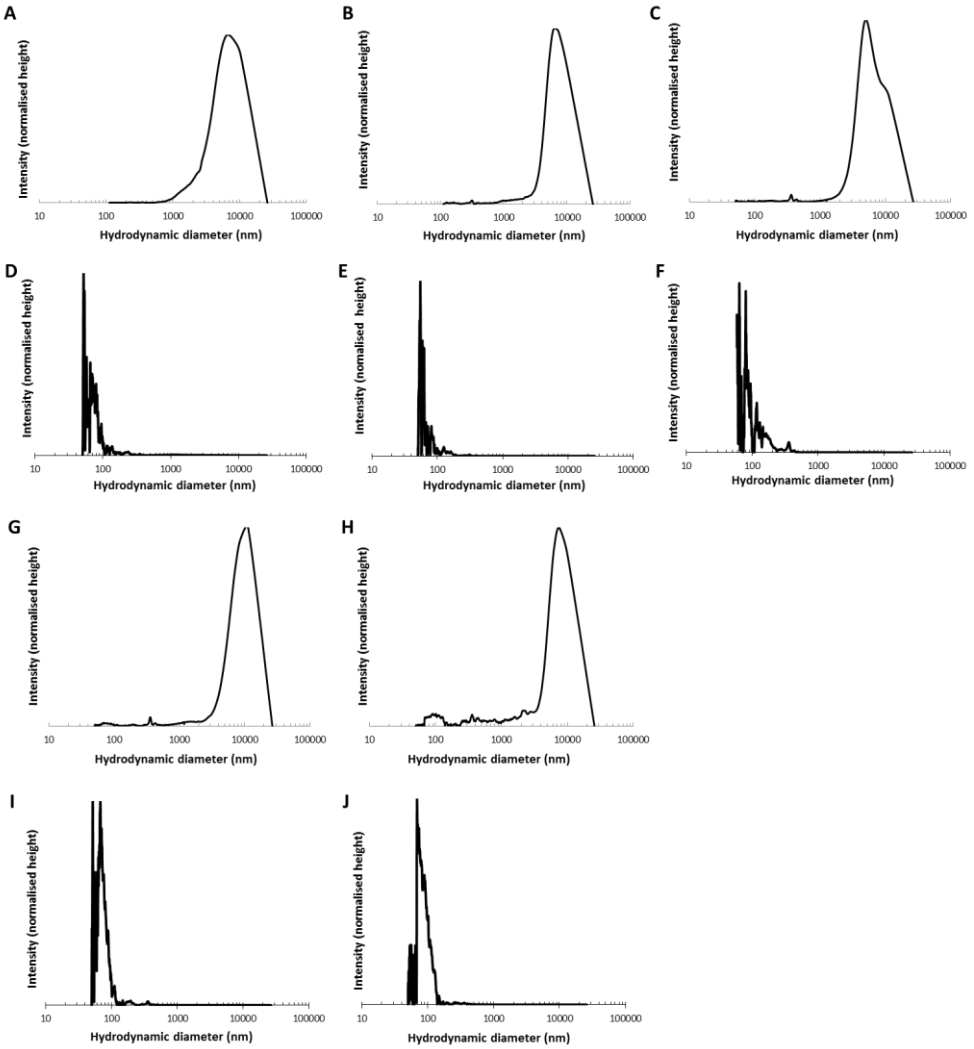

Figure S7: Particle size distributions. LCO **(a, d)**, NCA **(b, e)**, NMC 1:1:1 **(c, f)**, NMC 6:2:2 **(g, i)** and NMC 8:1:1 **(h, j)** size distributions (weight based distributions **(a-c, g-h)** and number based distributions **(d-f, i-j)**) assessed by centrifugal liquid sedimentation.

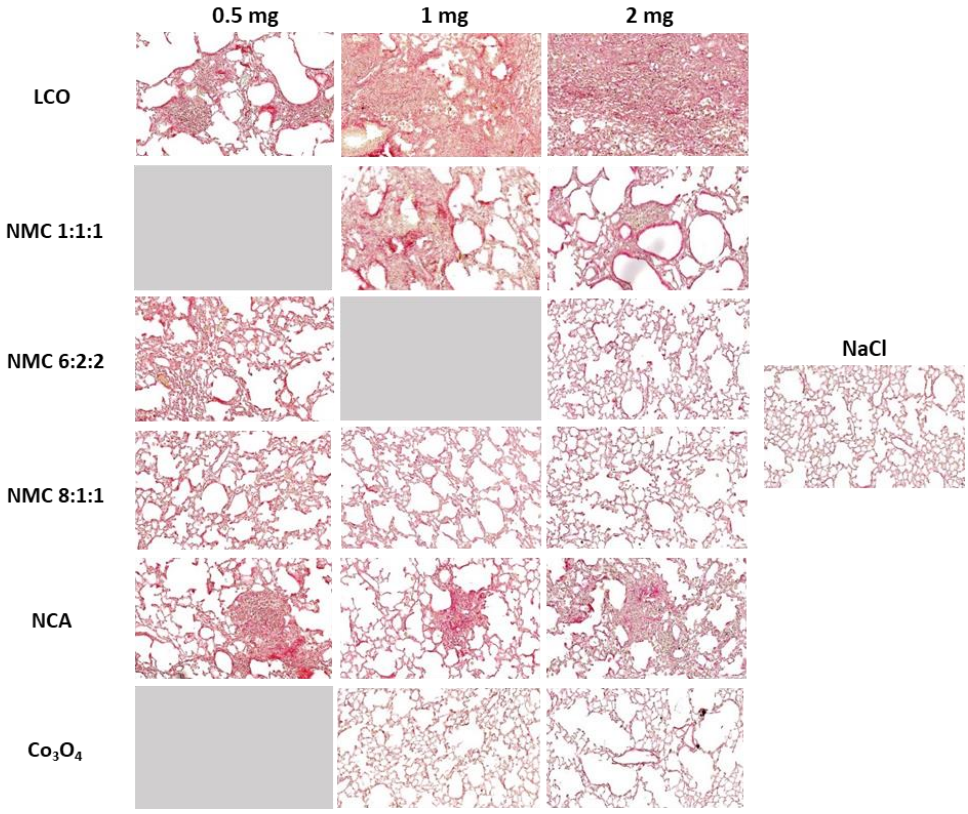

Figure S8: Lung sections of mice 2 months after treatment with LIB particles. C57BL/6Jrj mice were treated with an oro-pharyngeal aspiration of NaCl (control), 0.5, 1 or 2 mg LCO, NMC 1:1:1, NMC 6:2:2, NMC 8:1:1, NCA or Co_3O_4. Lung sections were stained with Sirius red (magnification 200x).

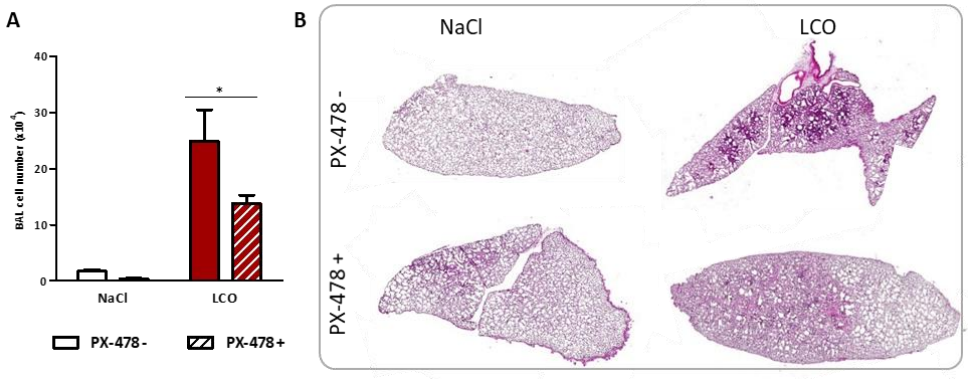

Figure S9: HIF-1α drives lung inflammation induced by LCO. C57BL/6Jrj mice were treated with an oro-pharyngeal aspiration of NaCl (control) or 2 mg LCO. Mice were treated with i.p. injections of 20 mg/kg bw/d PX-478 or with the vehicle (saline solution with 10 % DMSO) at day -1, 1 and 2. Mice were euthanized after 3 days. Inflammatory cell infiltration was assessed in the BAL **(a)**. Lung sections were stained with HE (magnification 10x) **(b)**. *P < 0.05, **P < 0.01 and ***P < 0.001 (t-test between PX-478 - and + mice for each condition, N = 1, n = 5, means ± SEM).

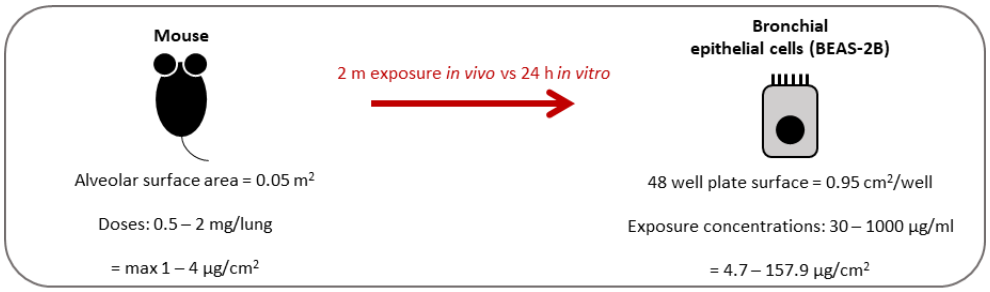

Figure S10: Comparison of *in vivo* and *in vitro* dose

Supplementary data: publication 3

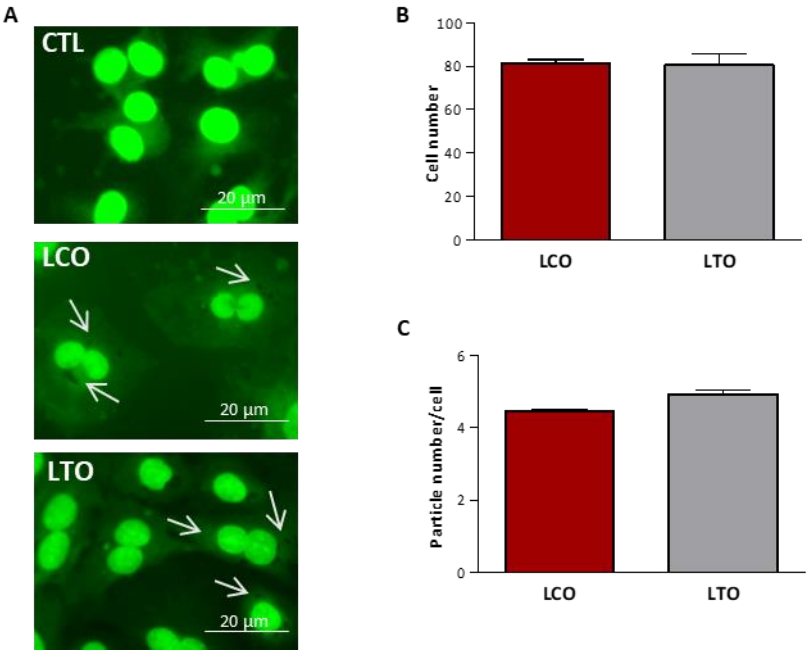

Figure S11: LCO and LTO particle endocytosis by RLE cells. Rat lung epithelial cells (RLE) were exposed to NaCl or 50 µg/ml of LCO or LTO and treated with cytochalasin B 4 h after particle exposure. Endocytosis was assessed 24 h after particle exposure. Images of binucleated cells after treatment. White arrows designate some particles **(a)**. 100 binucleated cells were scored to determine the proportion of cells containing particles **(b)** as well as the number of endocytosed particles per cell **(c)**. Bars represent means ± SEM (N = 1, n = 2).

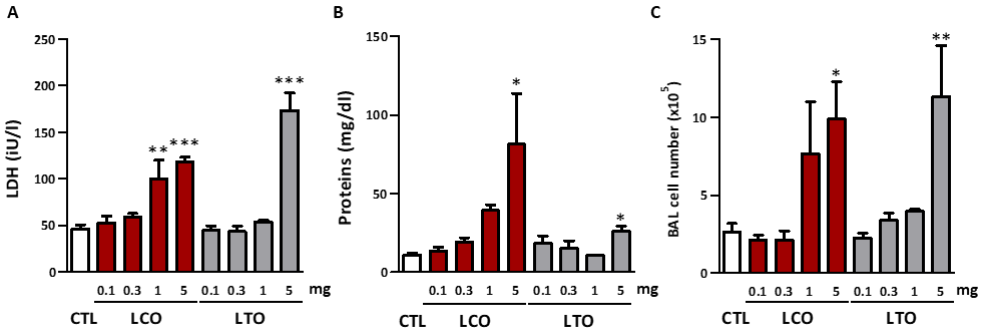

Figure S12: Inflammatory dose-response to LCO and LTO particles. Wistar rats were treated with an oro-pharyngeal aspiration of NaCl (control, CTL), 0.1, 0.3, 1 or 5 mg LCO or LTO particles. Inflammation was assessed after 3 days. LDH activity **(a)** and proteins **(b)** were measured in the BALF, recruited inflammatory cells in the BAL **(c)**. Bars represent means ± SEM. *P < 0.05, **P < 0.01 and ***P < 0.001 relative to CTL mice (one-way ANOVA followed by a Dunnett's multiple comparison, N = 1, n = 4).

REFERENCES

1. Roselin LS, Juang RS, Hsieh CT, Sagadevan S, Umar A, Selvin R, Hegazy HH. Recent Advances and Perspectives of Carbon-Based Nanostructures as Anode Materials for Li-ion Batteries. Materials. 2019;12(8).
2. Tarascon JM. Key challenges in future Li-battery research. Phil Trans R Soc A. 2010;368(1923):3227-3241.
3. Li M, Lu J, Chen Z, Amine K. 30 Years of Lithium-Ion Batteries. Adv Mater. 2018:e1800561.
4. Wu X, Wang J, Ding F, Chen X, Nasybulin E, Zhang Y, Zhang J-G. Lithium metal anodes for rechargeable batteries. Energy and environmental science. 2014;7(2):513-537.
5. Nitta N, Wu F, Lee JT, Yushin G. Li-ion battery materials: present and future. Mater today. 2015;18:252-264.
6. Tarascon JM, Armand M. Issues and challenges facing rechargeable lithium batteries. Nature. 2001;414(6861):359-367.
7. Garche J. Advanced battery systems — the end of the lead–acid battery? Physical Chemistry Chemical Physics. 2001;3(3):356-367.
8. Cairns EJ, Albertus P. Batteries for electric and hybrid-electric vehicles. Annu Rev Chem Biomol Eng. 2010;1:299-320.
9. Zhang H, Zhao H, Khan MA, Zou W, Xu J, Zhang L, Zhang J. Recent progress in advanced electrode materials, separators and electrolytes for lithium batteries. Journal of Materials Chemistry A. 2018;6(42):20564-20620.
10. Goodenough JB. Evolution of strategies for modern rechargeable batteries. Acc Chem Res. 2013;46(5):1053-1061.
11. Pagliaro M, Meneguzzo F. Lithium battery reusing and recycling: A circular economy insight. Heliyon. 2019;5(6):e01866.
12. Godshall NA, Raistrick ID, Huggins RA. Thermodynamic investigations of ternary lithium-transition metal-oxygen cathode materials. Materials Research Bulletin. 1980;15(5):561-570.

13. Ozawa K. Lithium-ion rechargeable batteries with LiCoO2 and carbon electrodes: the LiCoO2/C system. Solid state ionics. 1994;69(3-4):212-221.
14. Vertruyen B, Eshraghi N, Piffet C, Bodart J, Mahmoud A, Boschini F. Spray-Drying of Electrode Materials for Lithium- and Sodium-Ion Batteries. Materials. 2018;11(7).
15. Kim SH, Choi KH, Cho SJ, Choi S, Park S, Lee SY. Printable solid-state lithium-ion batteries: a new route toward shape-conformable power sources with aesthetic versatility for flexible electronics. Nano Lett. 2015;15(8):5168-5177.
16. Cheng M, Jiang Y, Yao W, Yuan Y, Deivanayagam R, Foroozan T, Huang Z, Song B, Rojaee R, Shokuhfar T, Pan Y, Lu J, Shahbazian-Yassar R. Elevated-Temperature 3D Printing of Hybrid Solid-State Electrolyte for Li-Ion Batteries. Adv Mater. 2018;30(39):e1800615.
17. Singh N, Galande C, Miranda A, Mathkar A, Gao W, Reddy AL, Vlad A, Ajayan PM. Paintable battery. Sci Rep. 2012;2:481.
18. De B, Yadav A, Khan S, Kar KK. A facile methodology for the development of a printable and flexible all-solid-state rechargeable battery. ACS Appl Mater Interfaces. 2017;9(23):19870-19880.
19. Koike S, Tatsumi K. Preparation and performances of highly porous layered LiCoO2 films for lithium batteries. Journal of Power Sources. 2007;174:976-980.
20. Lee SH, Li K, Huang C, Evans JD, Grant PS. Spray-Printed and Self-Assembled Honeycomb Electrodes of Silicon-Decorated Carbon Nanofibers for Li-Ion Batteries. ACS Appl Mater Interfaces. 2019;11(1):603-612.
21. Parikh VP, Ahmadi A, Parekh MH, Sadeghi F, Pol VG. Upcycling of Spent Lithium Cobalt Oxide Cathodes from Discarded Lithium-Ion Batteries as Solid Lubricant Additive. Environ Sci Technol. 2019;53(7):3757-3763.
22. Liu J, Ludwig B, Liu Y, Pan H, Wang Y. Strengthening the Electrodes for Li-Ion Batteries with a Porous Adhesive Interlayer through Dry-Spraying Manufacturing. ACS Appl Mater Interfaces. 2019;11(28):25081-25089.
23. Région Wallone. Projets de recherche financés par le département des programmes de recherche de la DGO6: BATWAL (2013), online source:

http://recherche-technologie.wallonie.be/projets/index.html?IDD=25074, consulted the 13/05/16.

24. Flexer V, Baspineiro CF, Galli CI. Lithium recovery from brines: A vital raw material for green energies with a potential environmental impact in its mining and processing. Sci Total Environ. 2018;639:1188-1204.
25. Yu Y, Chen B, Huang K, Wang X, Wang D. Environmental impact assessment and end-of-life treatment policy analysis for Li-ion batteries and Ni-MH batteries. Int J Environ Res Public Health. 2014;11(3):3185-3198.
26. Kang DH, Chen M, Ogunseitan OA. Potential environmental and human health impacts of rechargeable lithium batteries in electronic waste. Environ Sci Technol. 2013;47(10):5495-5503.
27. Cusenza MA, Bobba S, Ardente F, Cellura M, Di PF. Energy and environmental assessment of a traction lithium-ion battery pack for plug-in hybrid electric vehicles. J Clean Prod. 2019;215:634-649.
28. Bozich J, Hang M, Hamers R, Klaper R. Core chemistry influences the toxicity of multicomponent metal oxide nanomaterials, lithium nickel manganese cobalt oxide, and lithium cobalt oxide to Daphnia magna. Environ Toxicol Chem. 2017;9999:1-10.
29. Hang MN, Gunsolus IL, Wayland H, Melby ES, Mensch AC, Hurley KR, Pedersen JA, Haynes CL, Hamers RJ. Impact of Nanoscale Lithium Nickel Manganese Cobalt Oxide (NMC) on the Bacterium Shewanella oneidensis MR-1. Chemistry of materials. 2016;28:1092-1100.
30. Dogangun M, Hang MN, Troiano JM, McGeachy AC, Melby ES, Pedersen JA, Hamers RJ, Geiger FM. Alteration of Membrane Compositional Asymmetry by LiCoO2 Nanosheets. ACS Nano. 2015;9(9):8755-8765.
31. Larsson F, Andersson P, Blomqvist P, Mellander BE. Toxic fluoride gas emissions from lithium-ion battery fires. Sci Rep. 2017;7(1):10018.
32. Strehlau J, Weber T, Lurenbaum C, Bornhorst J, Galla HJ, Schwerdtle T, Winter M, Nowak S. Towards quantification of toxicity of lithium ion battery electrolytes - development and validation of a liquid-liquid extraction GC-MS method for the determination of organic carbonates in cell culture materials. Anal Bioanal Chem. 2017;409(26):6123-6131.

33. Brog JP, Crochet A, Seydoux J, Clift MJD, Baichette B, Maharajan S, Barosova H, Brodard P, Spodaryk M, Zuttel A, Rothen-Rutishauser B, Kwon NH, Fromm KM. Characteristics and properties of nano-LiCoO2 synthesized by pre-organized single source precursors: Li-ion diffusivity, electrochemistry and biological assessment. J Nanobiotechnology. 2017;15(1):58.
34. Yokota K, Johyama Y, Kunitani Y, Michitsuji H, Yamada S. Urinary elimination of nickel and cobalt in relation to airborne nickel and cobalt exposures in a battery plant. Int Arch Occup Environ Health. 2007;80(6):527-531.
35. OberdÖRster G. Significance of Particle Parameters in the Evaluation of Exposure-Dose Response Relationships of Inhaled Particles. Particulate Science and Technology. 1996;14(2):135-151.
36. Heppleston AG. Pathegenesis of mineral pneumoconioses. In: Parkes WR, editor. Occupational lung disorders; 1994. p. 100-134.
37. Lauwerys RH, V.; Hoet,P.; Lison,D. Exposition admissible aux substances chimiques en milieu professionnel. In. Toxicologie industrielle et intoxications professionnelles 5th edition; 2007. p. 89-105.
38. Lauwerys RH, V.; Hoet,P.; Lison,D. Principes généraux des méthodes de prévention des intoxications professionnelles. In. Toxicologue industrielle et intoxications professionnelles 5th edition; 2007. p. 1226-1235.
39. Recommendation from the Scientific Committee on Occupational Exposure Limits for Silica, Crystalline (respirable dust). In: SCOEL, editor.SUM/94; 2003.
40. Oberdorster G, Graham U. Predicting EMP hazard: Lessons from studies with inhaled fibrous and non-fibrous nano- and micro-particles. Toxicol Appl Pharmacol. 2018;361:50-61.
41. GBD 2017 Risk Factors Collaborators. Global, regional, and national comparative risk assessment of 84 behavioural, environmental and occupational, and metabolic risks or clusters of risks for 195 countries and territories, 1990-2017: a systematic analysis for the Global Burden of Disease Study 2017. Lancet. 2018;392(10159):1923-1994.
42. Farzaneh MR, Jamshidiha F, Kowsarian S. Inhalational lung disease. Int J Occup Environ Med. 2010;1(1):11-20.

43. Racanelli AC, Kikkers SA, Choi AMK, Cloonan SM. Autophagy and inflammation in chronic respiratory disease. Autophagy. 2018;14(2):221-232.
44. Losacco C, Perillo A. Particulate matter air pollution and respiratory impact on humans and animals. Environ Sci Pollut Res Int. 2018;25(34):33901-33910.
45. Bierkandt FS, Leibrock L, Wagener S, Laux P, Luch A. The impact of nanomaterial characteristics on inhalation toxicity. Toxicol Res. 2018;7(3):321-346.
46. Alfaro-Moreno E, Nawrot TS, Nemmar A, Nemery B. Particulate matter in the environment: pulmonary and cardiovascular effects. Curr Opin Pulm Med. 2007;13(2):98-106.
47. Sayan M, Mossman BT. The NLRP3 inflammasome in pathogenic particle and fibre-associated lung inflammation and diseases. Part Fibre Toxicol. 2016;13(51).
48. Barkauskas CE, Noble PW. Cellular mechanisms of tissue fibrosis: New insights into the cellular mechanisms of pulmonary fibrosis. Am J Physiol Cell Physiol. 2014;306(11):C987-996.
49. Wu JZ, Ge DD, Zhou LF, Hou LY, Zhou Y, Li QY. Effects of particulate matter on allergic respiratory diseases. Chronic Dis Transl Med. 2018;4(2):95-102.
50. Munoz X, Barreiro E, Bustamante V, Lopez-Campos JL, Gonzalez-Barcala FJ, Cruz MJ. Diesel exhausts particles: Their role in increasing the incidence of asthma. Reviewing the evidence of a causal link. Sci Total Environ. 2019;652:1129-1138.
51. Guarnieri M, Balmes JR. Outdoor air pollution and asthma. The Lancet. 2014;383(9928):1581-1592.
52. Li N, Hao M, Phalen RF, Hinds WC, Nel AE. Particulate air pollutants and asthma. A paradigm for the role of oxidative stress in PM-induced adverse health effects. Clin Immunol. 2003;109(3):250-265.
53. Baldacci S, Maio S, Cerrai S, Sarno G, Baiz N, Simoni M, Annesi-Maesano I, Viegi G, Study H. Allergy and asthma: Effects of the exposure to particulate matter and biological allergens. Respir Med. 2015;109(9):1089-1104.

54. Keet CA, Keller JP, Peng RD. Long-Term Coarse Particulate Matter Exposure Is Associated with Asthma among Children in Medicaid. Am J Respir Crit Care Med. 2018;197(6):737-746.
55. Tarlo SM, Lemiere C. Occupational asthma. N Engl J Med. 2014;370(7):640-649.
56. Lauwerys RH, V.; Hoet,P.; Lison,D. Asthmes et rhinites professionnels. In. Toxicolgie industrielle et intoxications professionelles 5th edition; 2007. p. 957-968.
57. Antonini JM, Taylor MD, Zimmer AT, Roberts JR. Pulmonary responses to welding fumes: role of metal constituents. J Toxicol Environ Health A. 2004;67(3):233-249.
58. Peden D, Reed CE. Environmental and occupational allergies. J Allergy Clin Immunol. 2010;125(2 Suppl 2):S150-160.
59. Hoet P, Desvallees L, Lison D. Do current OELs for silica protect from obstructive lung impairment? A critical review of epidemiological data. Crit Rev Toxicol. 2017;47(8):650-677.
60. International Agency for research on Cancer (IARC). IARC Monographs on the Identification of Carcinogenic Hazards to Humans: list of classifications. 23/09/2019. Available from: https://monographs.iarc.fr/list-of-classifications.
61. Leung CC, Yu IT, Chen W. Silicosis. Lancet. 2012;379(9830):2008-2018.
62. Heintz NH, Janssen-Heininger YM, Mossman BT. Asbestos, lung cancers, and mesotheliomas: from molecular approaches to targeting tumor survival pathways. Am J Respir Cell Mol Biol. 2010;42(2):133-139.
63. Lauwerys RH, V.; Hoet,P.; Lison,D. Poussières. In. Toxicologie industrielle et intoxications professionnelles 5th edition; 2007. p. 879-956.
64. Jaurand MC, Renier A, Daubriac J. Mesothelioma: Do asbestos and carbon nanotubes pose the same health risk? Part Fibre Toxicol. 2009;6(16).
65. Huaux F, d'Ursel de Bousies V, Parent MA, Orsi M, Uwambayinema F, Devosse R, Ibouraadaten S, Yakoub Y, Panin N, Palmai-Pallag M, van der Bruggen P, Bailly C, Marega R, Marbaix E, Lison D. Mesothelioma response to carbon nanotubes is associated with an early and selective accumulation of immunosuppressive monocytic cells. Part Fibre Toxicol. 2016;13(46).

66. Stone KC, Mercer RR, Gehr P, Stockstill B, Crapo JD. Allometric relationships of cell numbers and size in the mammalian lung. Am J Respir Cell Mol Biol. 1992;6(2):235-243.
67. Dimakakou E, Johnston HJ, Streftaris G, Cherrie JW. Exposure to Environmental and Occupational Particulate Air Pollution as a Potential Contributor to Neurodegeneration and Diabetes: A Systematic Review of Epidemiological Research. Int J Environ Res Public Health. 2018;15(8).
68. Yang W, Peters JI, Williams RO, III. Inhaled nanoparticles--a current review. Int J Pharm. 2008;356(1-2):239-247.
69. Beamish LA, Osornio-Vargas AR, Wine E. Air pollution: An environmental factor contributing to intestinal disease. J Crohns Colitis. 2011;5(4):279-286.
70. Pietroiusti A, Bergamaschi E, Campagna M, Campagnolo L, De Palma G, Iavicoli S, Leso V, Magrini A, Miragoli M, Pedata P, Palombi L, Iavicoli I. The unrecognized occupational relevance of the interaction between engineered nanomaterials and the gastro-intestinal tract: a consensus paper from a multidisciplinary working group. Part Fibre Toxicol. 2017;14(47).
71. van den Brule S, Ambroise J, Lecloux H, Levard C, Soulas R, De Temmerman PJ, Palmai-Pallag M, Marbaix E, Lison D. Dietary silver nanoparticles can disturb the gut microbiota in mice. Part Fibre Toxicol. 2016;13(38).
72. Kaplan GG, Hubbard J, Korzenik J, Sands BE, Panaccione R, Ghosh S, Wheeler AJ, Villeneuve PJ. The inflammatory bowel diseases and ambient air pollution: a novel association. Am J Gastroenterol. 2010;105(11):2412-2419.
73. van den Brule S, Ambroise J, Lecloux H, Levard C, Soulas R, De Temmerman PJ, Palmai-Pallag M, Marbaix E, Lison D. Dietary silver nanoparticles can disturb the gut microbiota in mice. Part Fibre Toxicol. 2016;13(38).
74. Kaplan GG, Dixon E, Panaccione R, Fong A, Chen L, Szyszkowicz M, Wheeler A, MacLean A, Buie WD, Leung T, Heitman SJ, Villeneuve PJ. Effect of ambient air pollution on the incidence of appendicitis. CMAJ. 2009;181(9):591-597.

75. Bell ML, Davis DL. Reassessment of the lethal London fog of 1952: novel indicators of acute and chronic consequences of acute exposure to air pollution. Environ Health Perspect. 2001;109 Suppl 3:389-394.
76. Miller MR, Shaw CA, Langrish JP. From particles to patients: oxidative stress and the cardiovascular effects of air pollution. Future Cardiol. 2012;8(4):577-602.
77. Kendall M, Holgate S. Health impact and toxicological effects of nanomaterials in the lung. Respirology. 2012;17(5):743-758.
78. Bostan HB, Rezaee R, Valokala MG, Tsarouhas K, Golokhvast K, Tsatsakis AM, Karimi G. Cardiotoxicity of nano-particles. Life Sci. 2016;165:91-99.
79. Oberdorster G, Castranova V, Asgharian B, Sayre P. Inhalation Exposure to Carbon Nanotubes (CNT) and Carbon Nanofibers (CNF): Methodology and Dosimetry. J Toxicol Environ Health B Crit Rev. 2015;18(3-4):121-212.
80. Christophersen DV, Jacobsen NR, Andersen MH, Connell SP, Barfod KK, Thomsen MB, Miller MR, Duffin R, Lykkesfeldt J, Vogel U, Wallin H, Loft S, Roursgaard M, Moller P. Cardiovascular health effects of oral and pulmonary exposure to multi-walled carbon nanotubes in ApoE-deficient mice. Toxicology. 2016;371:29-40.
81. Stone V, Miller MR, Clift MJD, Elder A, Mills NL, Moller P, Schins RPF, Vogel U, Kreyling WG, Alstrup Jensen K, Kuhlbusch TAJ, Schwarze PE, Hoet P, Pietroiusti A, De Vizcaya-Ruiz A, Baeza-Squiban A, Teixeira JP, Tran CL, Cassee FR. Nanomaterials Versus Ambient Ultrafine Particles: An Opportunity to Exchange Toxicology Knowledge. Environ Health Perspect. 2017;125(10).
82. Allen JL, Oberdorster G, Morris-Schaffer K, Wong C, Klocke C, Sobolewski M, Conrad K, Mayer-Proschel M, Cory-Slechta DA. Developmental neurotoxicity of inhaled ambient ultrafine particle air pollution: Parallels with neuropathological and behavioral features of autism and other neurodevelopmental disorders. Neurotoxicology. 2017;59:140-154.
83. Arnoldussen YJ, Kringlen Ervik T, Baarnes Eriksen M, Kero I, Skaug V, Zienolddiny S. Cellular Responses of Industrially Relevant Silica Dust on Human Glial Cells In Vitro. Int J Mol Sci. 2019;20(2).

84. Wu T, Tang M. The inflammatory response to silver and titanium dioxide nanoparticles in the central nervous system. Nanomedicine 2018;13(2):233-249.
85. Carre J, Gatimel N, Moreau J, Parinaud J, Leandri R. Does air pollution play a role in infertility?: a systematic review. Environ Health. 2017;16(1):82.
86. Zhang J, Liu J, Ren L, Wei J, Duan J, Zhang L, Zhou X, Sun Z. PM2.5 induces male reproductive toxicity via mitochondrial dysfunction, DNA damage and RIPK1 mediated apoptotic signaling pathway. Sci Total Environ. 2018;634:1435-1444.
87. Fleischer NL, Merialdi M, van Donkelaar A, Vadillo-Ortega F, Martin RV, Betran AP, Souza JP. Outdoor air pollution, preterm birth, and low birth weight: analysis of the world health organization global survey on maternal and perinatal health. Environ Health Perspect. 2014;122(4):425-430.
88. Shi H, Magaye R, Castranova V, Zhao J. Titanium dioxide nanoparticles: a review of current toxicological data. Part Fibre Toxicol. 2013;10(15).
89. Nordberg GF, Nogawa K, Nordberg M. Cadmium. In: Nordberg GF, Fowler BA, Nordberg M, editors. Handbook on the toxicology of metals; 2015. p. 668-708.
90. Skerfving SB, I. Lead. In: Nordberg GF, Fowler BA, Nordberg M, editors. Hanbook on toxicology of metals; 2015. p. 911-956.
91. Loxham M, Nieuwenhuijsen MJ. Health effects of particulate matter air pollution in underground railway systems - a critical review of the evidence. Part Fibre Toxicol. 2019;16(12).
92. Sah D, Verma PK, Kumari KM, Lakhani A. Chemical partitioning of fine particle-bound As, Cd, Cr, Ni, Co, Pb and assessment of associated cancer risk due to inhalation, ingestion and dermal exposure. Inhal Toxicol. 2017;29(11):483-493.
93. ICRP publication 66. Human respiratory tract model for radiological protection; 1994;24.
94. Parkes WR. Aerosols: their deposition and clearance. In: Parkes WR, editor. Occupational lung disorders; 1994. p. 35-49.
95. Kreyling W, Möller W, Semmler-Behnke M, Oberdörster G. Particle dosimetry: deposition and clearance from the respiratory tract and

translocation towards extra-pulmonary sites. In: Donaldson K, Borm P, editors. Particle toxicology; 2007. p. 47-74.

96. Utembe W, Potgieter K, Stefaniak AB, Gulumian M. Dissolution and biodurability: Important parameters needed for risk assessment of nanomaterials. Part Fibre Toxicol. 2015;12(11).
97. Köbrich R, Rudolf G, Stahlhofen W. A Mathematical Model of Mass Deposition in Man. The Annals of Occupational Hygiene. 1994;38(inhaled_particles_VII):15-23.
98. Donaldson K, MacNee W, Li XY. Ultrafine (nanometre) particle mediated lung injury. Journal of aerosol science. 1998;29:553-560.
99. Riediker M, Zink D, Kreyling W, Oberdorster G, Elder A, Graham U, Lynch I, Duschl A, Ichihara G, Ichihara S, Kobayashi T, Hisanaga N, Umezawa M, Cheng TJ, Handy R, Gulumian M, Tinkle S, Cassee F. Particle toxicology and health - where are we? Part Fibre Toxicol. 2019;16(19).
100. Hillaireau H, Couvreur P. Nanocarriers' entry into the cell: relevance to drug delivery. Cell Mol Life Sci. 2009;66(17):2873-2896.
101. Luyts K, Napierska D, Nemery B, Hoet PHM. How physico-chemical characteristics of nanoparticles cause their toxicity: complex and unresolved interrelations. Environ Sci: Processes Impacts. 2013;15(1):23-38.
102. Hussain S, Sangtian S, Anderson SM, Snyder RJ, Marshburn JD, Rice AB, Bonner JC, Garantziotis S. Inflammasome activation in airway epithelial cells after multi-walled carbon nanotube exposure mediates a profibrotic response in lung fibroblasts. Part Fibre Toxicol. 2014;11(28).
103. Oberdorster G, Ferin J, Lehnert BE. Correlation between particle size, in vivo particle persistence, and lung injury. Environ Health Perspect. 1994;102 Suppl 5:173-179.
104. Rabolli V, Lison D, Huaux F. The complex cascade of cellular events governing inflammasome activation and IL-1beta processing in response to inhaled particles. Part Fibre Toxicol. 2016;13(1):40.
105. Liu Y, Hardie J, Zhang X, Rotello VM. Effects of engineered nanoparticles on the innate immune system. Semin Immunol. 2017;34:25-32.

106. Huaux F. Innate immunity to inhaled particles: A new paradigm of collective recognition. Current Opinion in Toxicology. 2018;10:84-90.
107. Huaux F. Emerging Role of Immunosuppression in Diseases Induced by Micro- and Nano-Particles: Time to Revisit the Exclusive Inflammatory Scenario. Front Immunol. 2018;9:2364.
108. Mercer BA, Lemaitre V, Powell CA, D'Armiento J. The Epithelial Cell in Lung Health and Emphysema Pathogenesis. Curr Respir Med Rev. 2006;2(2):101-142.
109. Schroder K, Tschopp J. The inflammasomes. Cell. 2010;140(6):821-832.
110. Bauernfeind F, Bartok E, Rieger A, Franchi L, Nunez G, Hornung V. Cutting edge: reactive oxygen species inhibitors block priming, but not activation, of the NLRP3 inflammasome. J Immunol. 2011;187(2):613-617.
111. Gasse P, Mary C, Guenon I, Noulin N, Charron S, Schnyder-Candrian S, Schnyder B, Akira S, Quesniaux VF, Lagente V, Ryffel B, Couillin I. IL-1R1/MyD88 signaling and the inflammasome are essential in pulmonary inflammation and fibrosis in mice. J Clin Invest. 2007;117(12):3786-3799.
112. Guo J, Gu N, Chen J, Shi T, Zhou Y, Rong Y, Zhou T, Yang W, Cui X, Chen W. Neutralization of interleukin-1 beta attenuates silica-induced lung inflammation and fibrosis in C57BL/6 mice. Arch Toxicol. 2013;87(11):1963-1973.
113. Hosseinian N, Cho Y, Lockey RF, Kolliputi N. The role of the NLRP3 inflammasome in pulmonary diseases. Ther Adv Respir Dis. 2015;9(4):188-197.
114. Lo Re S, Giordano G, Yakoub Y, Devosse R, Uwambayinema F, Couillin I, Ryffel B, Marbaix E, Lison D, Huaux F. Uncoupling between inflammatory and fibrotic responses to silica: evidence from MyD88 knockout mice. PLoS One. 2014;9(7).
115. Cassel SL, Eisenbarth SC, Iyer SS, Sadler JJ, Colegio OR, Tephly LA, Carter AB, Rothman PB, Flavell RA, Sutterwala FS. The Nalp3 inflammasome is essential for the development of silicosis. Proc Natl Acad Sci U S A. 2008;105(26):9035-9040.
116. Vince JE, Silke J. The intersection of cell death and inflammasome activation. Cell Mol Life Sci. 2016;73(11-12):2349-2367.

117. Nikota J, Banville A, Goodwin LR, Wu D, Williams A, Yauk CL, Wallin H, Vogel U, Halappanavar S. Stat-6 signaling pathway and not Interleukin-1 mediates multi-walled carbon nanotube-induced lung fibrosis in mice: insights from an adverse outcome pathway framework. Part Fibre Toxicol. 2017;14(37).
118. Dong J, Ma Q. Type 2 Immune Mechanisms in Carbon Nanotube-Induced Lung Fibrosis. Front Immunol. 2018;9.
119. Shull MM, Ormsby I, Kier AB, Pawlowski S, Diebold RJ, Yin M, Allen R, Sidman C, Proetzel G, Calvin D, et al. Targeted disruption of the mouse transforming growth factor-beta 1 gene results in multifocal inflammatory disease. Nature. 1992;359(6397):693-699.
120. Vallyathan V, Shi X, Castranova V. Reactive oxygen species: their relation to pneumoconiosis and carcinogenesis. Environ Health Perspect. 1998;106 Suppl 5:1151-1155.
121. Abdal Dayem A, Hossain MK, Lee SB, Kim K, Saha SK, Yang GM, Choi HY, Cho SG. The Role of Reactive Oxygen Species (ROS) in the Biological Activities of Metallic Nanoparticles. Int J Mol Sci. 2017;18(1).
122. Fubini B, Hubbard A. Reactive oxygen species (ROS) and reactive nitrogen species (RNS) generation by silica in inflammation and fibrosis. Free Radic Biol Med. 2003;34(12):1507-1516.
123. Donaldson K, Poland CA, Schins RP. Possible genotoxic mechanisms of nanoparticles: criteria for improved test strategies. Nanotoxicology. 2010;4:414-420.
124. van Berlo D, Hullmann M, Schins RP. Toxicology of ambient particulate matter. Exp Suppl. 2012;101:165-217.
125. Mittal M, Siddiqui MR, Tran K, Reddy SP, Malik AB. Reactive oxygen species in inflammation and tissue injury. Antioxid Redox Signal. 2014;20(7):1126-1167.
126. Valavanidis A, Vlachogianni T, Fiotakis K, Loridas S. Pulmonary oxidative stress, inflammation and cancer: respirable particulate matter, fibrous dusts and ozone as major causes of lung carcinogenesis through reactive oxygen species mechanisms. Int J Environ Res Public Health. 2013;10(9):3886-3907.

127. Schins RP, Knaapen AM. Genotoxicity of poorly soluble particles. Inhal Toxicol. 2007;19 Suppl 1:189-198.
128. Knaapen AM, Borm PJ, Albrecht C, Schins RP. Inhaled particles and lung cancer. Part A: Mechanisms. Int J Cancer. 2004;109(6):799-809.
129. Schins RP. Mechanisms of genotoxicity of particles and fibers. Inhal Toxicol. 2002;14(1):57-78.
130. Schins RPFH, T.K. Genotoxic effects of particles. In: Donaldson KB, P., editor. Particle toxicology; 2007. p. 285-298.
131. Fu PP, Xia Q, Hwang HM, Ray PC, Yu H. Mechanisms of nanotoxicity: generation of reactive oxygen species. J Food Drug Anal. 2014;22(1):64-75.
132. Baird WM, Hooven LA, Mahadevan B. Carcinogenic polycyclic aromatic hydrocarbon-DNA adducts and mechanism of action. Environ Mol Mutagen. 2005;45(2-3):106-114.
133. Gonzalez L, Lison D, Kirsch-Volders M. Genotoxicity of engineered nanomaterials: A critical review. Nanotoxicology. 2009;2(4):252-273.
134. Ruthenborg RJ, Ban JJ, Wazir A, Takeda N, Kim JW. Regulation of wound healing and fibrosis by hypoxia and hypoxia-inducible factor-1. Mol Cells. 2014;37(9):637-643.
135. Majmundar AJ, Wong WJ, Simon MC. Hypoxia-inducible factors and the response to hypoxic stress. Mol Cell. 2010;40(2):294-309.
136. Epstein AC, Gleadle JM, McNeill LA, Hewitson KS, O'Rourke J, Mole DR, Mukherji M, Metzen E, Wilson MI, Dhanda A, Tian YM, Masson N, Hamilton DL, Jaakkola P, Barstead R, Hodgkin J, Maxwell PH, Pugh CW, Schofield CJ, Ratcliffe PJ. C. elegans EGL-9 and mammalian homologs define a family of dioxygenases that regulate HIF by prolyl hydroxylation. Cell. 2001;107(1):43-54.
137. Yuan Y, Hilliard G, Ferguson T, Millhorn DE. Cobalt inhibits the interaction between hypoxia-inducible factor-alpha and von Hippel-Lindau protein by direct binding to hypoxia-inducible factor-alpha. J Biol Chem. 2003;278(18):15911-15916.
138. Klein C, Costa M. Nickel. In: Nordberg G, Fowler B, Nordberg M, editors. Handbook on the toxicology of metals; 2015. p. 1091-1111.

139. Kaelin WG, Jr. ROS: really involved in oxygen sensing. Cell Metab. 2005;1(6):357-358.
140. Jochmanova I, Yang C, Zhuang Z, Pacak K. Hypoxia-inducible factor signaling in pheochromocytoma: turning the rudder in the right direction. J Natl Cancer Inst. 2013;105(17):1270-1283.
141. Carmeliet P, Dor Y, Herbert JM, Fukumura D, Brusselmans K, Dewerchin M, Neeman M, Bono F, Abramovitch R, Maxwell P, Koch CJ, Ratcliffe P, Moons L, Jain RK, Collen D, Keshert E. Role of HIF-1alpha in hypoxia-mediated apoptosis, cell proliferation and tumour angiogenesis. Nature. 1998;394(6692):485-490.
142. Nizet V, Johnson RS. Interdependence of hypoxic and innate immune responses. Nat Rev Immunol. 2009;9(9):609-617.
143. Tannahill GM, Curtis AM, Adamik J, Palsson-McDermott EM, McGettrick AF, Goel G, Frezza C, Bernard NJ, Kelly B, Foley NH, Zheng L, Gardet A, Tong Z, Jany SS, Corr SC, Haneklaus M, Caffrey BE, Pierce K, Walmsley S, Beasley FC, Cummins E, Nizet V, Whyte M, Taylor CT, Lin H, Masters SL, Gottlieb E, Kelly VP, Clish C, Auron PE, Xavier RJ, O'Neill LA. Succinate is an inflammatory signal that induces IL-1beta through HIF-1alpha. Nature. 2013;496(7444):238-242.
144. Rius J, Guma M, Schachtrup C, Akassoglou K, Zinkernagel AS, Nizet V, Johnson RS, Haddad GG, Karin M. NF-kappaB links innate immunity to the hypoxic response through transcriptional regulation of HIF-1alpha. Nature. 2008;453(7196):807-811.
145. Higgins DF, Kimura K, Bernhardt WM, Shrimanker N, Akai Y, Hohenstein B, Saito Y, Johnson RS, Kretzler M, Cohen CD, Eckardt KU, Iwano M, Haase VH. Hypoxia promotes fibrogenesis in vivo via HIF-1 stimulation of epithelial-to-mesenchymal transition. J Clin Invest. 2007;117(12):3810-3820.
146. Warbrick I, Rabkin SW. Hypoxia-inducible factor 1-alpha (HIF-1alpha) as a factor mediating the relationship between obesity and heart failure with preserved ejection fraction. Obes Rev. 2019;20(5):701-712.
147. Zhu Y, Tan J, Xie H, Wang J, Meng X, Wang R. HIF-1alpha regulates EMT via the Snail and beta-catenin pathways in paraquat poisoning-induced early pulmonary fibrosis. J Cell Mol Med. 2016;20(4):688-697.

148. Tzouvelekis A, Harokopos V, Paparountas T, Oikonomou N, Chatziioannou A, Vilaras G, Tsiambas E, Karameris A, Bouros D, Aidinis V. Comparative expression profiling in pulmonary fibrosis suggests a role of hypoxia-inducible factor-1alpha in disease pathogenesis. Am J Respir Crit Care Med. 2007;176(11):1108-1119.
149. Stegen S, Laperre K, Eelen G, Rinaldi G, Fraisl P, Torrekens S, Van Looveren R, Loopmans S, Bultynck G, Vinckier S, Meersman F, Maxwell PH, Rai J, Weis M, Eyre DR, Ghesquiere B, Fendt SM, Carmeliet P, Carmeliet G. HIF-1alpha metabolically controls collagen synthesis and modification in chondrocytes. Nature. 2019;565(7740):511-515.
150. Zhou G, Dada LA, Wu M, Kelly A, Trejo H, Zhou Q, Varga J, Sznajder JI. Hypoxia-induced alveolar epithelial-mesenchymal transition requires mitochondrial ROS and hypoxia-inducible factor 1. Am J Physiol Lung Cell Mol Physiol. 2009;297(6):L1120-L1130.
151. Zhao B, Guan H, Liu JQ, Zheng Z, Zhou Q, Zhang J, Su LL, Hu DH. Hypoxia drives the transition of human dermal fibroblasts to a myofibroblast-like phenotype via the TGF-beta1/Smad3 pathway. Int J Mol Med. 2017;39(1):153-159.
152. Aral H, Vecchio-Sadus A. Toxicity of lithium to humans and the environment--a literature review. Ecotoxicol Environ Saf. 2008;70(3):349-356.
153. Shahzad B, Mughal MN, Tanveer M, Gupta D, Abbas G. Is lithium biologically an important or toxic element to living organisms? An overview. Environ Sci Pollut Res Int. 2017;24(1):103-115.
154. Bernard A. Lithium. In: Nordberg G, Fowler B, Nordberg M, editors. Handbook on the toxicology of metals; 2014. p. 969-974.
155. Timmer RT, Sands JM. Lithium intoxication. J Am Soc Nephrol. 1999;10(3):666-674.
156. Schrauzer GN. Lithium: occurrence, dietary intakes, nutritional essentiality. J Am Coll Nutr. 2002;21(1):14-21.
157. McKnight RF, Adida M, Budge K, Stockton S, Goodwin GM, Geddes JR. Lithium toxicity profile: a systematic review and meta-analysis. Lancet. 2012;379(9817):721-728.

158. Nassar A, Azab AN. Effects of Lithium on Inflammation. ACS Chem Neurosci. 2014;5:451-458.
159. Li H, Li Q, Du X, Sun Y, Wang X, Kroemer G, Blomgren K, Zhu C. Lithium-mediated long-term neuroprotection in neonatal rat hypoxia-ischemia is associated with antiinflammatory effects and enhanced proliferation and survival of neural stem/progenitor cells. J Cereb Blood Flow Metab. 2011;31(10):2106-2115.
160. Rebar AH, Greenspan BJ, Allen MD. Acute inhalation toxicopathology of lithium combustion aerosols in rats. Fundam Appl Toxicol. 1986;7(1):58-67.
161. Sahin O, Sulak O, Yavuz Y, Uz E, Eren I, Ramazan YH, Malas MA, Altuntas I, Songur A. Lithium-induced lung toxicity in rats: the effect of caffeic acid phenethyl ester (CAPE). Pathology. 2006;38(1):58-62.
162. Johansson A, Camner P, Curstedt T, Jarstrand C, Robertson B, Urban T. Rabbit lung after inhalation of lithium chloride. J Appl Toxicol. 1988;8(5):373-375.
163. Barceloux DG. Cobalt. J Toxicol Clin Toxicol. 1999;37(2):201-206.
164. Donaldson JD, Clarck SJ, Grimes SM. Cobalt in chemicals: the monograph series. London: The Cobalt development institute; 1986.
165. Lison D. Cobalt. In: Nordberg GF, Fowler BA, Nordberg M, editors. Handbook on the toxicology of metals; 2015. p. 743-763.
166. Leyssens L, Vinck B, Van Der Straeten C, Wuyts F, Maes L. Cobalt toxicity in humans-A review of the potential sources and systemic health effects. Toxicology. 2017;387:43-56.
167. Lison D, van den Brule S, Van Maele-Fabry G. Cobalt and its compounds: update on genotoxic and carcinogenic activities. Crit Rev Toxicol. 2018:1-18.
168. Simonsen LO, Harbak H, Bennekou P. Cobalt metabolism and toxicology--a brief update. Sci Total Environ. 2012;432:210-215.
169. Leggett RW. The biokinetics of inorganic cobalt in the human body. Sci Total Environ. 2008;389(2-3):259-269.
170. Ortega R, Bresson C, Darolles C, Gautier C, Roudeau S, Perrin L, Janin M, Floriani M, Aloin V, Carmona A, Malard V. Low-solubility particles and a

Trojan-horse type mechanism of toxicity: the case of cobalt oxide on human lung cells. Part Fibre Toxicol. 2014;11(14).

171. Simonsen LO, Harbak H, Bennekou P. Passive transport pathways for Ca(2+) and Co(2+) in human red blood cells. (57)Co(2+) as a tracer for Ca(2+) influx. Blood Cells Mol Dis. 2011;47(4):214-225.
172. Yamada K. Cobalt: its role in health and disease. Met Ions Life Sci. 2013;13:295-320.
173. Lauwerys RH, V.; Hoet,P.; Lison,D. Cobalt. In. Toxicologie industrielle et intoxications professionnelles 5th edition; 2007. p. 260-271.
174. Paustenbach DJ, Tvermoes BE, Unice KM, Finley BL, Kerger BD. A review of the health hazards posed by cobalt. Crit Rev Toxicol. 2013;43(4):316-362.
175. Jomova K, Valko M. Advances in metal-induced oxidative stress and human disease. Toxicology. 2011;283(2-3):65-87.
176. Schaumloffel D. Nickel species: analysis and toxic effects. J Trace Elem Med Biol. 2012;26(1):1-6.
177. Das KK, Reddy RC, Bagoji IB, Das S, Bagali S, Mullur L, Khodnapur JP, Biradar MS. Primary concept of nickel toxicity - an overview. J Basic Clin Physiol Pharmacol. 2018;30(2):141-152.
178. Das KK, Das SN, Dhundasi SA. Nickel, its adverse health effects & oxidative stress. Indian J Med Res. 2008;128(4):412-425.
179. Lauwerys RH, V.; Hoet,P.; Lison,D. Nickel. In. Toxicologie industrielle et intoxications professionnelles 5th edition; 2007. p. 363-379.
180. Samet JmG, A.J. Particle-associated metals and oxidative stress in signaling. In: Donaldson KB, P., editor. Particle toxicology; 2007. p. 161-181.
181. Denkhaus E, Salnikow K. Nickel essentiality, toxicity, and carcinogenicity. Crit Rev Oncol Hematol. 2002;42(1):35-56.
182. Zambelli B, Uversky VN, Ciurli S. Nickel impact on human health: An intrinsic disorder perspective. Biochim Biophys Acta. 2016;1864(12):1714-1731.
183. Rendall RE, Phillips JI, Renton KA. Death following exposure to fine particulate nickel from a metal arc process. Ann Occup Hyg. 1994;38(6):921-930.

184. Eid R, Arab NT, Greenwood MT. Iron mediated toxicity and programmed cell death: A review and a re-examination of existing paradigms. Biochim Biophys Acta Mol Cell Res. 2017;1864(2):399-430.
185. Coffey R, Ganz T. Iron homeostasis: An anthropocentric perspective. J Biol Chem. 2017;292(31):12727-12734.
186. Ponka P, Tenenbein M, Eaton JW. Iron. In: Nordberg G, Fowler BA, Nordberg M, editors. Handbook on the toxicology of metals; 2015. p. 879-902.
187. Fanning EW, Froines JR, Utell MJ, Lippmann M, Oberdorster G, Frampton M, Godleski J, Larson TV. Particulate matter (PM) research centers (1999-2005) and the role of interdisciplinary center-based research. Environ Health Perspect. 2009;117(2):167-174.
188. Papanikolaou G, Pantopoulos K. Iron metabolism and toxicity. Toxicol Appl Pharmacol. 2005;202(2):199-211.
189. Dev S, Babitt JL. Overview of iron metabolism in health and disease. Hemodial Int. 2017;21 Suppl 1:S6-S20.
190. Eaton JW, Qian M. Molecular bases of cellular iron toxicity. Free Radic Biol Med. 2002;32(9):833-840.
191. Winterbourn CC. Toxicity of iron and hydrogen peroxide: the Fenton reaction. Toxicol Lett. 1995;82-83:969-974.
192. Jin T, Berlin M. Titanium. In: Nordberg G, Fowler B, Nordberg M, editors. Handbook on the toxicology of metals; 2014. p. 1287-1296.
193. Fage SW, Muris J, Jakobsen SS, Thyssen JP. Titanium: a review on exposure, release, penetration, allergy, epidemiology, and clinical reactivity. Contact Dermatitis. 2016;74(6):323-345.
194. Kim KT, Eo MY, Nguyen TTH, Kim SM. General review of titanium toxicity. Int J Implant Dent. 2019;5(10).
195. Bos PMJ, Gosens I, Geraets L, Delmaar C, Cassee FR. Pulmonary toxicity in rats following inhalation exposure to poorly soluble particles: The issue of impaired clearance and the relevance for human health hazard and risk assessment. Regul Toxicol Pharmacol. 2019;109:104498.

196. Borm PJA, Driscoll KE. The hazards and risks of inhaled poorly soluble particles - where do we stand after 30 years of research? Part Fibre Toxicol. 2019;16(11).
197. Wang J, Fan Y. Lung injury induced by TiO2 nanoparticles depends on their structural features: size, shape, crystal phases, and surface coating. Int J Mol Sci. 2014;15(12):22258-22278.
198. Lucchini RG, Aschner M, Kim Y, Saric M. Manganese. In: Nordberg GF, Folwer BA, Nordberg M, editors. Handbook on the toxicology of metals; 2015. p. 975-1011.
199. Chen P, Bornhorst J, Aschner M. Manganese metabolism in humans. Front Biosci (Landmark Ed). 2018;23:1655-1679.
200. Horning KJ, Caito SW, Tipps KG, Bowman AB, Aschner M. Manganese Is Essential for Neuronal Health. Annu Rev Nutr. 2015;35:71-108.
201. O'Neal SL, Zheng W. Manganese Toxicity Upon Overexposure: a Decade in Review. Curr Environ Health Rep. 2015;2(3):315-328.
202. Chen P, Culbreth M, Aschner M. Exposure, epidemiology, and mechanism of the environmental toxicant manganese. Environ Sci Pollut Res Int. 2016;23(14):13802-13810.
203. Nemery B. Metal toxicity and the respiratory tract. Eur Respir J. 1990;3(2):202-219.
204. Lauwerys RH, V.; Hoet,P.; Lison,D. Manganèse. In. Toxicologie industrielle et intoxications professionnelles 5th edition; 2007. p. 285-308.
205. Sjögren B, Iregren A, Montelius J, Yokel RA. Aluminum. In: Nordberg GF, Fowler BA, Nordberg M, editors. Handbook on the toxicology of metals; 2015. p. 549-564.
206. Krewski D, Yokel RA, Nieboer E, Borchelt D, Cohen J, Harry J, Kacew S, Lindsay J, Mahfouz AM, Rondeau V. Human health risk assessment for aluminium, aluminium oxide, and aluminium hydroxide. J Toxicol Environ Health B Crit Rev. 2007;10 Suppl 1:1-269.
207. Willhite CC, Karyakina NA, Yokel RA, Yenugadhati N, Wisniewski TM, Arnold IM, Momoli F, Krewski D. Systematic review of potential health risks posed by pharmaceutical, occupational and consumer exposures to metallic and

nanoscale aluminum, aluminum oxides, aluminum hydroxide and its soluble salts. Crit Rev Toxicol. 2014;44 Suppl 4:1-80.

208. Wilhelm M, Jager DE, Ohnesorge FK. Aluminium toxicokinetics. Pharmacol Toxicol. 1990;66(1):4-9.
209. Alfrey AC. Aluminum toxicity. Bull N Y Acad Med. 1984;60(2):210-212.
210. Kongerud J, Soyseth V. Respiratory disorders in aluminum smelter workers. J Occup Environ Med. 2014;56(5 Suppl):S60-S70.
211. Klotz K, Weistenhofer W, Neff F, Hartwig A, van TC, Drexler H. The Health Effects of Aluminum Exposure. Dtsch Arztebl Int. 2017;114(39):653-659.
212. Limonciel A. The Past, Present, and Future of Chemical Risk Assessment. In. In Vitro Toxicology Systems; 2014. p. 3-23.
213. Furuya S, Chimed-Ochir O, Takahashi K, David A, Takala J. Global Asbestos Disaster. Int J Environ Res Public Health. 2018;15(5).
214. Banares MA, Haase A, Tran L, Lobaskin V, Oberdorster G, Rallo R, Leszczynski J, Hoet P, Korenstein R, Hardy B, Puzyn T. CompNanoTox2015: novel perspectives from a European conference on computational nanotoxicology on predictive nanotoxicology. Nanotoxicology. 2017;11(7):839-845.
215. The European parliament and the council of the European Union. Directive 2010/63/EU on the protection of animals used for scientific purposes. Official Journal of the European Union. 2010:33-79.
216. OECD. Animal welfare: OECD considers Animal Welfare in the Development of Test Guidelines. 2019 03/10/2019. Available from: https://www.oecd.org/chemicalsafety/testing/animal-welfare.htm.
217. Tornqvist E, Annas A, Granath B, Jalkesten E, Cotgreave I, Oberg M. Strategic focus on 3R principles reveals major reductions in the use of animals in pharmaceutical toxicity testing. PLoS One. 2014;9(7).
218. Braakhuis HM, Oomen AG, Cassee FR. Grouping nanomaterials to predict their potential to induce pulmonary inflammation. Toxicol Appl Pharmacol. 2016;299:3-7.
219. Arts JH, Hadi M, Irfan MA, Keene AM, Kreiling R, Lyon D, Maier M, Michel K, Petry T, Sauer UG, Warheit D, Wiench K, Wohlleben W, Landsiedel R. A

decision-making framework for the grouping and testing of nanomaterials (DF4nanoGrouping). Regul Toxicol Pharmacol. 2015;71(2 Suppl):S1-27.

220. Landsiedel R. Concern-driven integrated approaches for the grouping, testing and assessment of nanomaterials. Environ Pollut. 2016;218:1376-1380.

221. Walser T, Studer C. Sameness: The regulatory crux with nanomaterial identity and grouping schemes for hazard assessment. Regul Toxicol Pharmacol. 2015;72(3):569-571.

222. Nel A, Xia T, Meng H, Wang X, Lin S, Ji Z, Zhang H. Nanomaterial toxicity testing in the 21st century: use of a predictive toxicological approach and high-throughput screening. Acc Chem Res. 2013;46(3):607-621.

223. Godwin H, Nameth C, Avery D, Bergeson LL, Bernard D, Beryt E, Boyes W, Brown S, Clippinger AJ, Cohen Y, Doa M, Hendren CO, Holden P, Houck K, Kane AB, Klaessig F, Kodas T, Landsiedel R, Lynch I, Malloy T, Miller MB, Muller J, Oberdorster G, Petersen EJ, Pleus RC, Sayre P, Stone V, Sullivan KM, Tentschert J, Wallis P, Nel AE. Nanomaterial categorization for assessing risk potential to facilitate regulatory decision-making. ACS Nano. 2015;9(4):3409-3417.

224. Zhang L, McHale CM, Greene N, Snyder RD, Rich IN, Aardema MJ, Roy S, Pfuhler S, Venkatactahalam S. Emerging approaches in predictive toxicology. Environ Mol Mutagen. 2014;55(9):679-688.

225. Villeneuve DL, Angrish MM, Fortin MC, Katsiadaki I, Leonard M, Margiotta-Casaluci L, Munn S, O'Brien JM, Pollesch NL, Smith LC, Zhang X, Knapen D. Adverse outcome pathway networks II: Network analytics. Environ Toxicol Chem. 2018;37(6):1734-1748.

226. Leist M, Ghallab A, Graepel R, Marchan R, Hassan R, Bennekou SH, Limonciel A, Vinken M, Schildknecht S, Waldmann T, Danen E, van Ravenzwaay B, Kamp H, Gardner I, Godoy P, Bois FY, Braeuning A, Reif R, Oesch F, Drasdo D, Hohme S, Schwarz M, Hartung T, Braunbeck T, Beltman J, Vrieling H, Sanz F, Forsby A, Gadaleta D, Fisher C, Kelm J, Fluri D, Ecker G, Zdrazil B, Terron A, Jennings P, van der Burg B, Dooley S, Meijer AH, Willighagen E, Martens M, Evelo C, Mombelli E, Taboureau O, Mantovani A, Hardy B, Koch B, Escher S, van Thriel C, Cadenas C, Kroese D, van de

Water B, Hengstler JG. Adverse outcome pathways: opportunities, limitations and open questions. Arch Toxicol. 2017;91(11):3477-3505.

227. Ankley GT, Bennett RS, Erickson RJ, Hoff DJ, Hornung MW, Johnson RD, Mount DR, Nichols JW, Russom CL, Schmieder PK, Serrrano JA, Tietge JE, Villeneuve DL. Adverse outcome pathways: a conceptual framework to support ecotoxicology research and risk assessment. Environ Toxicol Chem. 2010;29(3):730-741.
228. Bal-Price A, Meek MEB. Adverse outcome pathways: Application to enhance mechanistic understanding of neurotoxicity. Pharmacol Ther. 2017;179:84-95.
229. Vietti G, Lison D, van den Brule S. Mechanisms of lung fibrosis induced by carbon nanotubes: towards an Adverse Outcome Pathway (AOP). Part Fibre Toxicol. 2016;13(11).
230. Rabolli V, Badissi AA, Devosse R, Uwambayinema F, Yakoub Y, Palmai-Pallag M, Lebrun A, De G, V, Couillin I, Ryffel B, Marbaix E, Lison D, Huaux F. The alarmin IL-1alpha is a master cytokine in acute lung inflammation induced by silica micro- and nanoparticles. Part Fibre Toxicol. 2014;11(69).
231. Arras M, Huaux F, Vink A, Delos M, Coutelier JP, Many MC, Barbarin V, Renauld JC, Lison D. Interleukin-9 reduces lung fibrosis and type 2 immune polarization induced by silica particles in a murine model. Am J Respir Cell Mol Biol. 2001;24(4):368-375.
232. Guo JL, Cui XQ, Rong Y, Zhou T, Zhou Y, Zhang ZH, Gu NL, Chen WH. [The role of interleukin-1beta on the pulmonary fibrosis in mice exposed to crystalline silica]. Zhonghua Lao Dong Wei Sheng Zhi Ye Bing Za Zhi. 2013;31(7):481-486.
233. Xiang GA, Zhang YD, Su CC, Ma YQ, Li YM, Zhou X, Wei LQ, Ji WJ. Dynamic changes of mononuclear phagocytes in circulating, pulmonary alveolar and interstitial compartments in a mouse model of experimental silicosis. Inhal Toxicol. 2016;28(9):393-402.
234. Goriparti S, Miele E, De Angelis F, Di Fabrizio E, Zaccaria R, Capiglia C. Review on recent progress of nanostructured anode materials for Li-ion batteries. J Power Sources. 2014;257:421-443.

235. Norbet C, Joseph A, Rossi SS, Bhalla S, Gutierrez FR. Asbestos-related lung disease: a pictorial review. Curr Probl Diagn Radiol. 2015;44(4):371-382.
236. Greenspan BJ, Allen MD, Rebar AH. Inhalation toxicity of lithium combustion aerosols in rats. J Toxicol Environ Health. 1986;18(4):627-637.
237. Emerit J, Beaumont C, Trivin F. Iron metabolism, free radicals, and oxidative injury. Biomed Pharmacother. 2001;55(6):333-339.
238. Demedts M, Gheysens B, Nagels J, Verbeken E, Lauweryns J, van den Eeckhout A, Lahaye D, Gyselen A. Cobalt lung in diamond polishers. Am Rev Respir Dis. 1984;130(1):130-135.
239. Kinaret P, Ilves M, Fortino V, Rydman E, Karisola P, Lahde A, Koivisto J, Jokiniemi J, Wolff H, Savolainen K, Greco D, Alenius H. Inhalation and oropharyngeal aspiration exposure to rod-like carbon nanotubes induce similar airway inflammation and biological responses in mouse lungs. ACS Nano. 2017;11(1):291-303.
240. Mercer RR, Scabilloni JF, Hubbs AF, Battelli LA, McKinney W, Friend S, Wolfarth MG, Andrew M, Castranova V, Porter DW. Distribution and fibrotic response following inhalation exposure to multi-walled carbon nanotubes. Part Fibre Toxicol. 2013;10(33).
241. Biondi PA, Chiesa LM, Storelli MR, Renon P. A new procedure for the specific high-performance liquid chromatographic determination of hydroxyproline. J Chromatogr Sci. 1997;35(11):509-512.
242. Ibouraadaten S, van den Brule S, Lison D. Does carbonation of steel slag particles reduce their toxicity? An in vitro approach. Toxicol In Vitro. 2015;29(4):722-726.
243. Bosquillon C, Lombry C, Preat V, Vanbever R. Comparison of particle sizing techniques in the case of inhalation dry powders. J Pharm Sci. 2001;90(12):2032-2041.
244. Vanbever R, Mintzes JD, Wang J, Nice J, Chen D, Batycky R, Langer R, Edwards DA. Formulation and physical characterization of large porous particles for inhalation. Pharm Res. 1999;16(11):1735-1742.
245. Pharmacopea E. Preparations for inhalation: Aerodynamic assessment of fine particles, section 2.9.18. In. European Pharmacopeia; 2008. p. 309-320.

246. Devoy J, Brun E, Cosnefroy A, Disdier C, Melczer M, Antoine G, Chalansonnet M, Mabonzo A. Mineralization of TiO_2 Nanoparticles for the Determination of Titanium in Rat Tissues. J Anal Chem. 2016;71(4):418-425.
247. Nitti M, Piras S, Marinari UM, Moretta L, Pronzato MA, Furfaro AL. HO-1 Induction in Cancer Progression: A Matter of Cell Adaptation. Antioxidants. 2017;6(29).
248. Ghio AJ, Funkhouser W, Pugh CB, Winters S, Stonehuerner JG, Mahar AM, Roggli VL. Pulmonary fibrosis and ferruginous bodies associated with exposure to synthetic fibers. Toxicol Pathol. 2006;34(6):723-729.
249. Pardo A, Selman M. Molecular mechanisms of pulmonary fibrosis. Front Biosci. 2002;7:d1743-d1761.
250. Han SW, Ryu JH, Jeong J, Yoon DH. Solid-state synthesis of Li4Ti5O12 for high power lithium ion battery applications. J Alloys comp. 2013;570:144-149.
251. Yoshiura Y, Izumi H, Oyabu T, Hashiba M, Kambara T, Mizuguchi Y, Lee BW, Okada T, Tomonaga T, Myojo T, Yamamoto K, Kitajima S, Horie M, Kuroda E, Morimoto Y. Pulmonary toxicity of well-dispersed titanium dioxide nanoparticles following intratracheal instillation. J Nanopart Res. 2015;17(241).
252. Gazzano E, Turci F, Foresti E, Putzu MG, Aldieri E, Silvagno F, Lesci IG, Tomatis M, Riganti C, Romano C, Fubini B, Roveri N, Ghigo D. Iron-loaded synthetic chrysotile: a new model solid for studying the role of iron in asbestos toxicity. Chem Res Toxicol. 2007;20(3):380-387.
253. Lasfargues G, Lison D, Maldague P, Lauwerys R. Comparative study of the acute lung toxicity of pure cobalt powder and cobalt-tungsten carbide mixture in rat. Toxicol Appl Pharmacol. 1992;112(1):41-50.
254. Ghio AJ, Churg A, Roggli VL. Ferruginous bodies: implications in the mechanism of fiber and particle toxicity. Toxicol Pathol. 2004;32(6):643-649.
255. Pascolo L, Zabucchi G, Gianoncelli A, Kourousias G, Trevisan E, Pascotto E, Casarsa C, Ryan C, Lucattelli M, Lungarella G, Cavarra E, Bartalesi B, Zweyer M, Cammisuli F, Melato M, Borelli V. Synchrotron X-ray microscopy reveals

early calcium and iron interaction with crocidolite fibers in the lung of exposed mice. Toxicol Lett. 2016;241:111-120.

256. Fahmy M, Young SP. Modulation of iron metabolism in monocyte cell line U937 by inflammatory cytokines: changes in transferrin uptake, iron handling and ferritin mRNA. Biochem J. 1993;296 (Pt 1):175-181.
257. Ganz T, Nemeth E. Iron homeostasis in host defence and inflammation. Nat Rev Immunol. 2015;15(8):500-510.
258. Fubini B. Surface reactivity in the pathogenic response to particulates. Environ Health Perspect. 1997;105 Suppl 5:1013-1020.
259. Weidemann A, Johnson RS. Biology of HIF-1alpha. Cell Death Differ. 2008;15(4):621-627.
260. Sironval V, Reylandt L, Chaurand P, Ibouraadaten S, Palmai-Pallag M, Yakoub Y, Ucakar B, Rose J, Poleunis C, Vanbever R, Marbaix E, Lison D, van den Brule S. Respiratory hazard of Li-ion battery components: elective toxicity of lithium cobalt oxide (LiCoO2) particles in a mouse bioassay. Arch Toxicol. 2018;92(5):1673-1684.
261. Jiang BH, Zheng JZ, Leung SW, Roe R, Semenza GL. Transactivation and inhibitory domains of hypoxia-inducible factor 1alpha. Modulation of transcriptional activity by oxygen tension. J Biol Chem. 1997;272(31):19253-19260.
262. Salnikow K, Davidson T, Zhang Q, Chen LC, Su W, Costa M. The involvement of hypoxia-inducible transcription factor-1-dependent pathway in nickel carcinogenesis. Cancer Res. 2003;63(13):3524-3530.
263. Driscoll KE, Carter JM, Howard BW, Hassenbein DG, Pepelko W, Baggs RB, Oberdorster G. Pulmonary inflammatory, chemokine, and mutagenic responses in rats after subchronic inhalation of carbon black. Toxicol Appl Pharmacol. 1996;136(2):372-380.
264. Sabaitis CP, Leong BK, Rop DA, Aaron CS. Validation of intratracheal instillation as an alternative for aerosol inhalation toxicity testing. J Appl Toxicol. 1999;19(2):133-140.
265. Hubner RH, Gitter W, El Mokhtari NE, Mathiak M, Both M, Bolte H, Freitag-Wolf S, Bewig B. Standardized quantification of pulmonary fibrosis in histological samples. Biotechniques. 2008;44(4):507-507.

266. Kung AL, Zabludoff SD, France DS, Freedman SJ, Tanner EA, Vieira A, Cornell-Kennon S, Lee J, Wang B, Wang J, Memmert K, Naegeli HU, Petersen F, Eck MJ, Bair KW, Wood AW, Livingston DM. Small molecule blockade of transcriptional coactivation of the hypoxia-inducible factor pathway. Cancer Cell. 2004;6(1):33-43.

267. Koh MY, Spivak-Kroizman T, Venturini S, Welsh S, Williams RR, Kirkpatrick DL, Powis G. Molecular mechanisms for the activity of PX-478, an antitumor inhibitor of the hypoxia-inducible factor-1alpha. Mol Cancer Ther. 2008;7(1):90-100.

268. Kheshtchin N, Arab S, Ajami M, Mirzaei R, Ashourpour M, Mousavi N, Khosravianfar N, Jadidi-Niaragh F, Namdar A, Noorbakhsh F, Hadjati J. Inhibition of HIF-1alpha enhances anti-tumor effects of dendritic cell-based vaccination in a mouse model of breast cancer. Cancer Immunol Immunother. 2016;65(10):1159-1167.

269. Welsh S, Williams R, Kirkpatrick L, Paine-Murrieta G, Powis G. Antitumor activity and pharmacodynamic properties of PX-478, an inhibitor of hypoxia-inducible factor-1alpha. Mol Cancer Ther. 2004;3(3):233-244.

270. Saini Y, Greenwood KK, Merrill C, Kim KY, Patial S, Parameswaran N, Harkema JR, LaPres JJ. Acute cobalt-induced lung injury and the role of hypoxia-inducible factor 1alpha in modulating inflammation. Toxicol Sci. 2010;116(2):673-681.

271. Prows DR, Leikauf GD. Quantitative trait analysis of nickel-induced acute lung injury in mice. Am J Respir Cell Mol Biol. 2001;24(6):740-746.

272. Wesselkamper SC, Prows DR, Biswas P, Willeke K, Bingham E, Leikauf GD. Genetic susceptibility to irritant-induced acute lung injury in mice. Am J Physiol Lung Cell Mol Physiol. 2000;279(3):L575-L582.

273. Cummins EP, Berra E, Comerford KM, Ginouves A, Fitzgerald KT, Seeballuck F, Godson C, Nielsen JE, Moynagh P, Pouyssegur J, Taylor CT. Prolyl hydroxylase-1 negatively regulates IkappaB kinase-beta, giving insight into hypoxia-induced NFkappaB activity. Proc Natl Acad Sci U S A. 2006;103(48):18154-18159.

274. Goebeler M, Roth J, Brocker EB, Sorg C, Schulze-Osthoff K. Activation of nuclear factor-kappa B and gene expression in human endothelial cells by

the common haptens nickel and cobalt. J Immunol. 1995;155(5):2459-2467.

275. Reece KM, Richardson ED, Cook KM, Campbell TJ, Pisle ST, Holly AJ, Venzon DJ, Liewehr DJ, Chau CH, Price DK, Figg WD. Epidithiodiketopiperazines (ETPs) exhibit in vitro antiangiogenic and in vivo antitumor activity by disrupting the HIF-1alpha/p300 complex in a preclinical model of prostate cancer. Mol Cancer. 2014;13(91).
276. Courcot E, Leclerc J, Lafitte JJ, Mensier E, Jaillard S, Gosset P, Shirali P, Pottier N, Broly F, Lo-Guidice JM. Xenobiotic metabolism and disposition in human lung cell models: comparison with in vivo expression profiles. Drug Metab Dispos. 2012;40(10):1953-1965.
277. Uboldi C, Orsiere T, Darolles C, Aloin V, Tassistro V, George I, Malard V. Poorly soluble cobalt oxide particles trigger genotoxicity via multiple pathways. Part Fibre Toxicol. 2016;13(5).
278. Smith MT, Guyton KZ, Gibbons CF, Fritz JM, Portier CJ, Rusyn I, DeMarini DM, Caldwell JC, Kavlock RJ, Lambert PF, Hecht SS, Bucher JR, Stewart BW, Baan RA, Cogliano VJ, Straif K. Key Characteristics of Carcinogens as a Basis for Organizing Data on Mechanisms of Carcinogenesis. Environ Health Perspect. 2016;124(6):713-721.
279. Sironval V, Palmai-Pallag M, Vanbever R, Huaux F, Mejia J, Lucas S, Lison D, van den Brule S. HIF-1α is a key mediator of the lung inflammatory potential of lithium-ion battery particles. Particle and Fibre Toxicology. 2019;16(35).
280. Kasprzak KS, Sunderman FW, Jr., Salnikow K. Nickel carcinogenesis. Mutat Res. 2003;533(1-2):67-97.
281. Patil A, Patil V, Shin DW, Choi JW, Paik DS, Yoon SJ. Issue and challenges facing rechargeable thin film lithium batteries. Mater Res Bull. 2008;43:1913-1942.
282. Borm PJA, Fowler P, Kirkland D. An updated review of the genotoxicity of respirable crystalline silica. Part Fibre Toxicol. 2018;15(23).
283. Bonassi S, Milic M, Neri M. Frequency of micronuclei and other biomarkers of DNA damage in populations exposed to dusts, asbestos and other fibers. A systematic review. Mutat Res. 2016;770(Pt A):106-118.

284. International Agency for research of cancer (IARC), Cobalt in hard metals and cobalt sulfate, gallium arsenide, indium phosphide and vanadium pentoxide. In.: World Health Organization; 2006.
285. Driscoll KE, Carter JM, Iype PT, Kumari HL, Crosby LL, Aardema MJ, Isfort RJ, Cody D, Chestnut MH, Burns JL, et al. Establishment of immortalized alveolar type II epithelial cell lines from adult rats. In Vitro Cell Dev Biol Anim. 1995;31(7):516-527.
286. Kirsch-Volders M, Sofuni T, Aardema M, Albertini S, Eastmond D, Fenech M, Ishidate M, Jr., Kirchner S, Lorge E, Morita T, Norppa H, Surralles J, Vanhauwaert A, Wakata A. Report from the in vitro micronucleus assay working group. Mutat Res. 2003;540(2):153-163.
287. Surralles J, Carbonell E, Marcos R, Degrassi F, Antoccia A, Tanzarella C. A collaborative study on the improvement of the micronucleus test in cultured human lymphocytes. Mutagenesis. 1992;7(6):407-410.
288. Fenech M. The in vitro micronucleus technique. Mutat Res. 2000;455(1-2):81-95.
289. van den Brule S, Beckers E, Chaurand P, Liu W, Ibouraadaten S, Palmai-Pallag M, Uwambayinema F, Yakoub Y, Avellan A, Levard C, Haufroid V, Marbaix E, Thill A, Lison D, Rose J. Nanometer-long Ge-imogolite nanotubes cause sustained lung inflammation and fibrosis in rats. Part Fibre Toxicol. 2014;11(67).
290. Wallace WT, Taylor LA, Liu Y, Cooper BL, Mckay DS, Chen B, Jeevarajan AS. Lunar dust and lunar simulant activation' and monitoring. Meteorit Planet Sci. 2009;44(7):961-970.
291. Collins AR. The comet assay for DNA damage and repair: principles, applications, and limitations. Mol Biotechnol. 2004;26(3):249-261.
292. European parliament and the council of the European Union. Regulation (EC) No 1907/2006 concerning the Registration, Evaluation, Authorisation and Restriction of Chemicals (REACH), establishing a European Chemicals Agency, amending Directive 1999/45/EC and repealing Council Regulation (EEC) No 793/93 and Commission Regulation (EC) No 1488/94 as well as Council Directive 76/769/EEC and Commission Directives 91/155/EEC,

93/67/EEC, 93/105/EC and 2000/21/EC. Official Journal of the European Union. 2006:1-849.

293. De Boek M, Hoet P, Lombaert N, Nemery B, Kirsch-Volders M, Lison D. In vivo genotoxicity of hard metal dust: induction of micronuclei in rat type II epithelial lung cells. Carcinogenesis. 2003;24(11):1793-1800.
294. Kauffman SL. Cell proliferation in the mammalian lung. Int Rev Exp Pathol. 1980;22:131-191.
295. De Boek M, Lison D, Kirsch-Volders M. Evaluation of the in vitro direct and indirect genotoxic effects of cobalt compounds using the alkaline comet assay. Influence of interdonor and interexperimental variability. Carcinogenesis. 1998;19(11):2021-2029.
296. Lison D, Carbonnelle P, Mollo L, Lauwerys R, Fubini B. Physicochemical mechanism of the interaction between cobalt metal and carbide particles to generate toxic activated oxygen species. Chem Res Toxicol. 1995;8(4):600-606.
297. Bonassi S, Znaor A, Ceppi M, Lando C, Chang WP, Holland N, Kirsch-Volders M, Zeiger E, Ban S, Barale R, Bigatti MP, Bolognesi C, Cebulska-Wasilewska A, Fabianova E, Fucic A, Hagmar L, Joksic G, Martelli A, Migliore L, Mirkova E, Scarfi MR, Zijno A, Norppa H, Fenech M. An increased micronucleus frequency in peripheral blood lymphocytes predicts the risk of cancer in humans. Carcinogenesis. 2007;28(3):625-631.
298. Deshpande A, Narayanan PK, Lehnert BE. Silica-induced generation of extracellular factor(s) increases reactive oxygen species in human bronchial epithelial cells. Toxicol Sci. 2002;67(2):275-283.
299. Kinnula VL, Everitt JI, Whorton AR, Crapo JD. Hydrogen peroxide production by alveolar type II cells, alveolar macrophages, and endothelial cells. Am J Physiol. 1991;261(L84):91.
300. Turci F, Corazzari I, Alberto G, Matra G, Fubini B. Free-radical chemistry as means to evaluate lunar dust health hazard in view of future missions to the moon. Astrobiology. 2015;15(5):371-380.
301. Han B, Qian D, Risch M, Chen H, Chi M, Meng YS, Shao-Horn Y. Role of $LiCoO_2$ Surface Terminations in Oxygen Reduction and Evolution Kinetics. The journal of physical chemistry letters. 2015;6:1357-1362.

302. Mu J, Zhang L, Zhao M, Wang Y. Co_3O_4 nanoparticles as an efficient catalase mimic: Properties, mechanism and its electrocatalytic sensing application for hydrogen peroxide. Journal of molecular catalysis A: Chemical. 2013;378:30-37.
303. Evans SJ, Clift MJ, Singh N, de Oliveira MJ, Burgum M, Wills JW, Wilkinson TS, Jenkins GJ, Doak SH. Critical review of the current and future challenges associated with advanced in vitro systems towards the study of nanoparticle (secondary) genotoxicity. Mutagenesis. 2017;32(1):233-241.
304. Lopez-Castejon G, Brough D. Understanding the mechanism of IL-1beta secretion. Cytokine Growth Factor Rev. 2011;22(4):189-195.
305. Munoz-Planillo R, Kuffa P, Martinez-Colon G, Smith BL, Rajendiran TM, Nunez G. K(+) efflux is the common trigger of NLRP3 inflammasome activation by bacterial toxins and particulate matter. Immunity. 2013;38(6):1142-1153.
306. Sironval V, Scagliarini V, Murugadoss S, Tomatis M, Yakoub Y, Turci F, Hoet P, Lison D, van den Brule S. LiCoO2 particles used in Li-ion batteries induce primary mutagenicity in lung cells via their capacity to generate hydroxyl radicals. Part Fibre Toxicol. 2020;17(6).
307. Nymark P, Rieswijk L, Ehrhart F, Jeliazkova N, Tsiliki G, Sarimveis H, Evelo CT, Hongisto V, Kohonen P, Willighagen E, Grafstrom RC. A Data Fusion Pipeline for Generating and Enriching Adverse Outcome Pathway Descriptions. Toxicol Sci. 2018;162(1):264-275.
308. Labib S, Williams A, Yauk CL, Nikota JK, Wallin H, Vogel U, Halappanavar S. Nano-risk Science: application of toxicogenomics in an adverse outcome pathway framework for risk assessment of multi-walled carbon nanotubes. Part Fibre Toxicol. 2016;13(15).
309. Halappanavar SS, M.; Wllin,H.; Vogel,U.; Sullivan,K.; Clippinger,A.J. AOP 173: Substance interaction with the lung resident cell membrane components leading to lung fibrosis. december 06, 2019. Available from: https://aopwiki.org/aops/173.
310. Piguet PF, Vesin C, Grau GE, Thompson RC. Interleukin 1 receptor antagonist (IL-1ra) prevents or cures pulmonary fibrosis elicited in mice by bleomycin or silica. Cytokine. 1993;5(1):57-61.

311. Girtsman TA, Beamer CA, Wu N, Buford M, Holian A. IL-1R signalling is critical for regulation of multi-walled carbon nanotubes-induced acute lung inflammation in C57Bl/6 mice. Nanotoxicology. 2014;8(1):17-27.
312. Higgins DF, Kimura K, Iwano M, Haase VH. Hypoxia-inducible factor signaling in the development of tissue fibrosis. Cell Cycle. 2008;7(9):1128-1132.
313. Goodwin J, Choi H, Hsieh MH, Neugent ML, Ahn JM, Hayenga HN, Singh PK, Shackelford DB, Lee IK, Shulaev V, Dhar S, Takeda N, Kim JW. Targeting Hypoxia-Inducible Factor-1alpha/Pyruvate Dehydrogenase Kinase 1 Axis by Dichloroacetate Suppresses Bleomycin-induced Pulmonary Fibrosis. Am J Respir Cell Mol Biol. 2018;58(2):216-231.